ChemComm

Accepted Manuscript

This article can be cited before page numbers have been issued, to do this please use: L. Cheng, H. Zhang, Y. Dong, Y. Zhao, Y. Yu and L. Cao, *Chem. Commun.*, 2019, DOI: 10.1039/C9CC00599D.

This is an Accepted Manuscript, which has been through the Royal Society of Chemistry peer review process and has been accepted for publication.

Accepted Manuscripts are published online shortly after acceptance, before technical editing, formatting and proof reading. Using this free service, authors can make their results available to the community, in citable form, before we publish the edited article. We will replace this Accepted Manuscript with the edited and formatted Advance Article as soon as it is available.

You can find more information about Accepted Manuscripts in the author guidelines.

Please note that technical editing may introduce minor changes to the text and/or graphics, which may alter content. The journal's standard Terms & Conditions and the ethical guidelines, outlined in our author and reviewer resource centre, still apply. In no event shall the Royal Society of Chemistry be held responsible for any errors or omissions in this Accepted Manuscript or any consequences arising from the use of any information it contains.

ROYAL SOCIETY OF CHEMISTRY

rsc.li/chemcomm

Chemical Communications Guidelines for reviewers

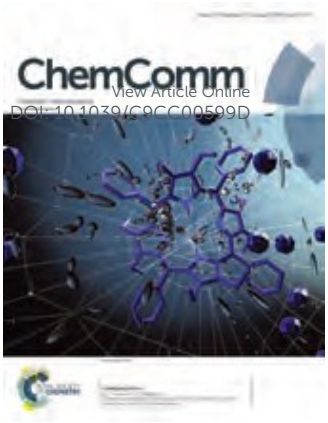

ChemComm is a forum for urgent high quality communications from across the chemical sciences.

Communications in *ChemComm* should be preliminary accounts of original and urgent work of significance to a general chemistry audience. The 2017 Impact Factor for *ChemComm* is **6.290**.

Only work within the top 25% of the field in terms of quality and interest should be recommended for publication. Acceptance should only be recommended if the content is of such urgency and significant general interest that rapid publication will be advantageous to the progress of chemical research.

Routine and incremental work – however competently researched and reported – should not be recommended for publication.

Articles which rely excessively on supplementary information should not be recommended for publication.

Thank you very much for your assistance in evaluating this manuscript.

General Guidance

Reviewers have the responsibility to treat the manuscript as confidential. Please be aware of our **Ethical Guidelines**, which contain full information on the responsibilities of reviewers and authors, and our **Refereeing Procedure and Policy**.

Supporting information and characterisation of new compounds
Experimental information must be provided to enable other researchers to reproduce the work accurately. It is the responsibility of authors to provide fully convincing evidence for the homogeneity, purity and identity of all compounds they claim as new. This evidence is required to establish that the properties and constants reported are those of the compound with the new structure claimed.

Please assess the evidence presented in support of the claims made by the authors and comment on whether adequate supporting information has been provided to address the above. Further details on the requirements for characterisation criteria can be found **here**.

When preparing your report, please:
- comment on the originality, significance, impact and scientific reliability of the work;
- state clearly whether you would like to see the article accepted or rejected and give detailed comments (with references, as appropriate) that will both help the Editor to make a decision on the article and the authors to improve it;
- it is the expectation that only work with two strong endorsements will be accepted for publication.

Please inform the Editor if:
- there is a conflict of interest;
- there is a significant part of the work which you are not able to referee with confidence;
- the work, or a significant part of the work, has previously been published;
- you believe the work, or a significant part of the work, is currently submitted elsewhere;
- the work represents part of an unduly fragmented investigation.

Submit your report at **http://mc.manuscriptcentral.com/chemcomm**

View Article Online
DOI: 10.1039/C9CC00599D

This manuscript is submitted on an exclusive basis:

Firstly, two new tetracationic cyclophanes **1-2** containing tetraphenylethene and bipyridinium moieties were synthesized via two-step S_N2 reaction

Secondly, the cyclic structure and cavity's size of cyclophanes **1**-**2** were further confirmed by single crystal X-ray analysis.

Thirdly, two cyclophanes showed fluorescence quenching effect on the fluorescence indicator HPTS through π-π and electrostatic interactions with strong affinity in aqueous media. More interestingly, **1** exhibited highly-selective recognition for tryptophan and ATP due to its proper size of cavity and good water-solubility. We firmly believe these two cyclophanes could offer new opportunities for detecting biological analytes (e.g. DNA) and constructing molecular knots in supramolecular chemistry.

We are proud, therefore, to offer this manuscript for publication in *Chemical Communications.*

View Article Online
DOI: 10.1039/C9CC00599D

Dear Dr Alexander Metherell:

Thank you for your email of Jan. 08, 2019 about our manuscript (CC-COM-12-2018-010009) detailed below.

Title: Tetraphenylethene-based tetracationic cyclophanes and their selective recognition for amino acids and adenosine derivatives in water

Authors: Lin Cheng, Haiyang Zhang, Yunhong Dong, Yanxia Zhao, Yang Yu, and Liping Cao*

Please find below a complete transcription of the comments of the reviewers and our response. We have carefully re-refined the X-ray files, and uploaded a version of the manuscript with the relevant scientific changes highlighted to aid your examination of the revisions. We very much hope that you'll find the paper in a suitable form for publication in *Chemical Communications.* Look forward to your reply.

Sincerely,
Liping Cao

Herein, we answer the questions and indicate the changes in the revised manuscript.

==========

Reviewer 1: Herein, Cao and co-authors reported synthesis of two new water-soluble tetracationic cyclophanes 1-2 containing tetraphenylethene and bipyridinium moieties. The water-soluble tetracationic cyclophanes show selective recognition for tryptophan and ATP via electrostatic and π-π interactions in water. It's an interesting work and the investigation contents are original and data enrichment. I recommend it to be published in Chemical Communications after minor revisions.

1.Sensitivity is an important feature for chemosensor. Author should supply the recognition sensitivity (i.e. LOD) of tetracationic cyclophane for ATP and Trp, respectively.

Response: *We have measured the sensitivity, and have rewritten the description about the recognition sensitivity of* ***1***•*4Cl*$^-$ *for ATP and Trp in the ESI, as follows: "* **The method of the recognition sensitivity:** The recognition sensitivity (i.e. the detection

View Article Online
DOI: 10.1039/C9CC00599D

limits) of host for guests were determined by UV-vis experiments in phosphate buffer (10 mmol, pH=7.4). With different concentrations of 2 μL guests (Trp and ATP) solution (0, 2, 4, 6, 8, 10 μmol) were added into 2.4 mL host (1•4Cl^-) while keeping the host concentration constant (10 μmol) in all the samples. And UV-vis absorption of host-guest solution was measured after mixing homogeneously. Next, the difference △A between the different host-guest mixtures and host of absorption values in a certain wavelength was taken, and the linear fitting between △A and the corresponding guest concentration can be conducted ([guest] as the x-axis, △A as the y-axis). When y=0, the obtained x value is the detection limits of guest that the lowest concentration of the guest can be detected by host. *(page S28) " The detection limit of **1**•4Cl^- for ATP (1.89 μmol) and Trp (0.36 μmol) were determined by UV-vis experiments (Figures S36 and S79) and calculated on the basis of the linear fitting between △A* (i.e. *the difference between the different host-guest mixtures and host of absorption values in a certain wavelength) and the corresponding guest concentration.*

*In text, we have added "Then, the limit of detection of the host **1** for Trp was calculated as 0.36 μmol by UV-vis experiments (Figure S36). (page 3, the second paragraph) "* and *"In addition, the limit of detection of the host **1** for ATP was calculated as 1.89 μmol (Figure S79). (page 4, the first paragraph)"*

2. Author investigated the recognition property of tetracationic cyclophane for ATP and Trp by ^{1}H NMR and ITC, how is it reflected in the fluorescence intensity? Some fluorescent spectra and photographs of tetracationic cyclophane with different amino acids or adenosine derivatives should be supplied.

Response: *In our case, **1-2** are non-emitted in water due to the photoinduced electron transfer (PET) from TPE to bipyridinium units, so we can't use fluorescence experiments to further verify the recognition properties of host and ATP or Trp.*

3. In order to make the results more realistic, the mass spectrum of the host-guest complex should be provided.

Response: *We performed the mass spectrum experiments of the host-guest complexes*

View Article Online
DOI: 10.1039/C9CC00599D

*in the ESI. (1) For the complex **1**•HPTS, the peaks at 626.1466 (calcd. for 626.1405) and 655.1273 (calcd. for 655.1198) were observed in the ESI-MS, which could be attributed to the $[1•HPTS\text{-}4Cl^{-}\text{-}2Na^{+}]^{2+}$ and $[\mathbf{1}•HPTS\text{-}3Cl^{-}\text{-}1Na^{+}]^{2+}$, respectively (Figure S25). (2) For the complex **2**•HPTS, the peaks at 753.7004 (calcd. for 753.6969) could be attributed to the $[\mathbf{2}•HPTS\text{-}4Cl^{-}\text{-}2Na^{+}]^{2+}$ (Figure S26). (3) For the complex **1**•Trp, the peaks at 337.8140 (calcd. for 337.8098) and 524.2022 (calcd. for 524.1994) could be attributed to the $[\mathbf{1}•Trp]^{3+}$ and $[\mathbf{1}•Trp]^{2+}$, respectively (Figure S35). (4) For the complex **1**•ATP, the peaks at 650.6692 (calcd. for 650.6666) and 679.6466 (calcd. for 679.6459) could be attributed to the $[\mathbf{1}•ATP\text{-}4Cl^{-}\text{-}1Na^{+}\text{-}1H^{+}]^{2+}$ and $[\mathbf{1}•ATP\text{-}3Cl^{-}\text{-}1H^{+}]^{2+}$, respectively (Figure S84). (5) For the complex **1**•ADP, the peaks at 610.6829 (calcd. for 610.6834), 628.6739 (calcd. for 628.6718) and 639.6767 (calcd. for 639.6627) could be attributed to the $[\mathbf{1}•ADP\text{-}4Cl^{-}\text{-}1Na^{+}\text{-}1H^{+}]^{2+}$, $[\mathbf{1}•ADP\text{-}3Cl^{-}\text{-}1Na^{+}]^{2+}$ and $[\mathbf{1}•ADP\text{-}3Cl^{-}\text{-}1H^{+}]^{2+}$, respectively (Figure S85). (6) For the complex **1**•AMP, the peaks at 559.7139 (calcd. for 559.7093) and 599.6963 (calcd. for 599.6796) could be attributed to the $[\mathbf{1}•AMP\text{-}4Cl^{-}\text{-}2Na^{+}]^{2+}$ and $[\mathbf{1}•AMP\text{-}3Cl^{-}\text{-}1H^{+}]^{2+}$, respectively (Figure S86).*

*In text, we have added (1) "In addition, electrospray ionization mass spectrometry (ESI-MS) confirmed the formation of 1:1 host-guest complex between **1-2** and HPTS, respectively (Figures S25-26). (page 4, the third paragraph)", (2) "Furthermore, ESI-MS also observed the two- and three-charged peaks ($[\mathbf{1}•Trp]^{3+}$ and $[\mathbf{1}•Trp]^{2+}$), which confirm the formation of 1:1 host-guest complex, respectively (Figure S35). (page 3, the second paragraph)" and (3) "All ESI-MS spectra of **1**•ATP, **1**•ADP and **1**•AMP showed the formation of 1:1 host-guest complexes, respectively (Figure S84-86). (page 4, the first paragraph)"*

4. Some related references on recognition of amino acids should be included: Macromolecules, 2017, 50, 7863; Chem. Eur. J., 2018, 24, 777; Soft Matter, 2018, 14, 8390.

***Response:** We have corrected reference [23] as follows: "Q. Lin, Y.-Q. Fan, P.-P. Mao, L. Liu, J. Liu, Y.-M. Zhang, H. Yao, and T.-B. Wei, Chem. Eur. J., 2018, **24**, 777-783."*

View Article Online
DOI: 10.1039/C9CC00599D

Reviewer 2: By using a two-step reaction starting from tetraphenylethene and bipyridine, cao and his tetracationic cyclophenes, and then they characterized and determined the X-ray single crystal structures for the two new cyclophene hosts. Furthermore, they studied host-guest interactions in water. The results revealed a selective recognition for amino acids and adenosine derivatives (ATP) etc. through electrostatic and π-π interactions in water. This work is well-done and the novel results deserve the publication in RSC journal chem. commun. as it stands.

Response: *No response.*

Reviewer 3: This submission has details of the structures of the two cyclophane compounds labelled by the authors as Cyclophane **1**•$4PF_6^-$ and Cyclophane **2**•$4PF_6^-$
None of these structures is well determined and while the gross non-H connectivities may have been established the crystallographic work is not of an acceptable quality (see below) and I cannot recommend acceptance in this present form. Rejection and perhaps resubmission to a different journal after significant revisions is recommended.

Cyclophane **1**•$4PF_6^-$

==========

1.1.1 We see from the CIF that the SQUEEZE program was used to remove the contributions of disordered solvent but we are nowhere told about this in text or ESI material, although the authors have appended the CIF format output from PLATON (generated as platon.sqf) to the CIF from which we see that the contributions of some 455 electrons were removed from the unit-cell contents.

Response: *We have re-refined the structures **1**•$4PF_6^-$ And **2**•$4PF_6^-$ with the version of OLEX2 1.2. and ShelXL-2018/3 respectively, and we used the SQUEEZE subroutine in the latest version (201118) of PLATON to remove severely disordered solvent molecules from structure model of compound **1**•$4PF_6^-$. Four CH_2Cl_2 and two $CHCl_3$ molecules co-crystallised in the unit cell of complex **1**•$4PF_6^-$, with the corresponding electron density removed using the SQUEEZE subroutine implemented within the*

View Article Online
DOI: 10.1039/C9CC00599D

*program PLATON (Ver. 201118). The above description has been added in the ESI, as follows: "**X-ray Crystal Structure Determination.** Diffraction data for the complexes **1**•4PF_6^- and **2**•4PF_6^- were performed on a Bruker D8 Venture photon II, at low temperature (153 K) with graphite-monochromated Mo Kα radiation (λ = 0.71073 Å). An empirical absorption correction using SADABS was applied for all data.[4] Both structures were solved and refined to convergence on F^2 for all independent reflections by the full-matrix least squares method using SHELXL-2018/3[5] in OLEX2 1.2.[6] All non-hydrogen atoms, including those in disordered parts, were refined anisotropically. All H-atoms were also included at calculated positions and refined as riders, with $U_{iso}(H)$ = 1.2 U_{eq}. In **1**•4PF_6^-, two PF_6^- anions were found to be disordered and were modelled with two orientations having relative occupancies of 0.54:0.46 and 0.57:0.43 for the two parts, separately. The geometries of the disordered parts were restrained to be similar. The anisotropic displacement parameters of the disordered molecules in the direction of the bonds were restrained to be equal with a standard uncertainty of 0.01 Å^2. They were also restrained to have the same U_{ij} components, with a standard uncertainty of 0.04 Å^2. In **1**•4PF_6^-, four CH_2Cl_2 and two $CHCl_3$ molecules co-crystallized in each unit cell of complex **1**•4PF_6^-, with the corresponding electron densities removed using the SQUEEZE subroutine implemented within the software program PLATON (Ver. 201118),[7] and the resulting .fab file was processed with OLEX2 1.2. using the ABIN instruction. Approximately 280 electron equivalents were removed from the unit cell. The total void volume was 1804 Å^3 indicated by PLATON, equivalent to 25.38 % of the unit cell's total volume. In **2**•4PF_6^-, the PF_6^- anion was found to be disordered and was modelled with two orientations having relative occupancy of 0.55:0.45. The geometries of the disordered parts were restrained to be similar. The anisotropic displacement parameters of the disordered molecules in the direction of the bonds were restrained to be equal with a standard uncertainty of 0.01 Å^2. They were also restrained to have the same U_{ij} components, with a standard uncertainty of 0.04 Å^2. There are 32 severely disordered Et_2O molecules in crystal **2**•4PF_6^-, They were also removed by by the SQUEEZE subroutine in PLATON (Ver.*

View Article Online
DOI: 10.1039/C9CC00599D

201118) and the resulting .fab file was processed with OLEX2 1.2. using the ABIN instruction. Approximately 1324 electron equivalents were removed from each unit cell. The total void volume was 4070 Å^3 indicated by PLATON, equivalent to 39.81 % of the unit cell's total volume. Crystallographic data and refinement details for ***1***•*4PF$_6^-$ and* ***2***•*4PF$_6^-$ are given in Table S1. CCDC 1870620 (****1***•*4PF$_6^-$) and 1870621 (****2***•*4PF$_6^-$). These data can be obtained free of charge from the Cambridge Crystallographic Data Centre www.ccdc.cam.ac.uk/data_request/cif.(page S7)"*

We have corrected reference [4-7] in the ESI, as follows:"4. G. M. Sheldrick, Program SADABS: Area-Detector Absorption Correction, ***1996****, University of Göttingen, Germany. 5. G. M. Sheldrick, Acta Crystallogr., Sect. C: Cryst. Struct. Chem.* ***2015****, C71, 3-8. 6. O. V. Dolomanov, L. J. Bourhis, R. J. Gildea, J. A. K. Howard and H. Puschmann, J. Appl. Cryst.* ***2009****, 42, 339-341. 7. A. L. Spek, Acta Cryst.* ***2015****, C71, 9–18. (page S8)"*

1.1.2 The contribution of any disordered solvent removed by the SQUEEZE process should have been included in the overall formula, formula weight, density, F(000), etc., calculations reported in the crystal-data text and in the CIF. This should now be done and we should also be explicitly told what (and the amount of) disordered solvent that was removed from the Formula unit by the SQUEEZE process in the _platon_squeeze_details text of the revised CIF. A reference to the SQUEEZE process should be in the reference list: - Spek, A. L. (2015). Acta Cryst. C71, 9–18

Response: *The disordered solvent removed by the SQUEEZE have been included in the overall formula, formula weight, density, F(000), etc. calculations reported in the crystal-data text and in the CIF. The details of SQUEEZE were included in the _platon_squeeze_details text of the revised CIF. A reference to the SQUEEZE has been added in the references list.*

In text, we have corrected reference [21] as follows: "*A. L. Spek, Acta Cryst. 2015, C****71****, 9-18."*

View Article Online
DOI: 10.1039/C9CC00599D

1.1.3 It is also clear from the submitted CIF that the authors did not carry out the post-squeeze refinement as required by the squeeze program. This is: - "Continue refinement in the presence of the three files name_sq.ins, name_sq.hkl & name_sq.fab" as produced by SQUEEZE.

Response: *The solvent contribution to the structure factors was re-calculated with the latest version of PLATON SQUEEZE (A. L. Spek, Acta Cryst. 2015, C71, 9–18.) and the resulting .fab file was processed with SHELXL using the ABIN instruction. We have submitted the full CIF files to the CCDC.*

1.1.4 Before this is done the authors must look very carefully at their pre-SQUEEZE shelxl.ins file and consider why they have some 52 OMIT commands in that file. [Note that it is usual to use the OMIT command only for very few low order reflections that may have been obscured by the beam stop and not all reflections with poor Fo/Fc agreements.]

Response: *Most omitted commands have been deleted. Only reflection -2 0 2 was omitted because it was obscured by the beam stop.*

1.1.5 If SQUEEZE had been correctly run there should have been no large positive residual density as is found in this post-squeeze refinement (_refine_diff_density_max 2.410).

Response: *After re-perform SQUEEZE, no large positive residual density is left (_refine_diff_density_max 0.880).*

Cyclophane **2**•$4PF_6^-$

==========

2.1 Routine PLATON checks indicate that the Cmc2~1~space group has been wrongly deduced and reports an excellent fit in the Cmca space group with some minor disorder and the various component molecules having significant crystallographically imposed symmetries about which we must be told. The refinement should be carefully redone in the Cmca space group and the text revised as appropriate.

Response: *The space group of compound* ***2***•$4PF_6^-$ *has been changed from Cmc2(1) to Cmca space group by PLATON. The refinement based on space group Cmca was*

View Article Online
DOI: 10.1039/C9CC00599D

redone. All disorder modeling and SQUEEZE operation details were included in the revised crystallographic description.

Due to the disorder of ether molecules in the cavity of ***2***•*4*PF_6^-*, we rerefined and deleted it. In text, (1) Because we have re-refined the structures* ***1***•*4*PF_6^-, the dihedral angle between two pyridinium rings in the bipyridinium moieties is converted from 44.3° to 44.4° *(page 3, the second paragraph).* (2) *we have deleted the following sentence :"in which a diethyl ether molecule as guest is encapsulated. (page 3, the second paragraph)" and the corresponding fig. 1(b) was modified. (3) In addition, we have rewritten in the text, as follows: "At the same time, solvent molecules (e.g. MeCN, acetone,* CH_2Cl_2*,* $CHCl_3$ *and* Et_2O*) and* PF_6^- *counter ions exist in the interspace of the framework structure. (page 3, the last sentence of the second paragraph)"*

Journal Name

View Article Online
DOI: 10.1039/C9CC00599D

COMMUNICATION

Tetraphenylethene-based tetracationic cyclophanes and their selective recognition for amino acids and adenosine derivatives in water†

Received 00th January 20xx,
Accepted 00th January 20xx

DOI: 10.1039/x0xx00000x

www.rsc.org/

Lin Cheng,[a,‡] Haiyang Zhang,[a,‡] Yunhong Dong,[a,b,‡] Yanxia Zhao,[a] Yang Yu,[a] and Liping Cao[a,*]

Two new tetracationic cyclophanes 1-2 containing tetraphenylethene and bipyridinium moieties were synthesized via two-step S_N2 reaction. These water-soluble cyclophanes with a cationic and hydrophobic cavity exhibited selective recognition for amino acids (e.g. tryptophan) and adenosine derivatives (e.g. ATP) via electrostatic and π-π interactions in water.

Synthesis, recognition and self-assembly of supramolecular hosts (e.g. clips, macrocycles, cages, and capsules) have played an important role in the development of supramolecular chemistry.[1] Several famous macrocyclic compounds, such as crown ether,[2] cyclodextrin,[3] calixarene,[4] cucurbituril,[5] cyclophane,[6] and pillararene,[7] have already attracted attention from chemical community to explore the nature of molecular interactions and construct supramolecular architectures/machines. Particularly, cationic cyclophanes with various sizes, shapes, and functional groups has been widely used, because of not only their unique electron-deficient cavity for selectively binding guest molecules, but also their reduction-oxidation property for electronic devices[8] (e.g. semiconductor) and molecular machine[9] (e.g. molecular shuttle and molecular pump). The most famous one is Stoddart's 'Blue Box', as a classic cationic cyclophane, which has milestone significance for the synthesis and development of the new cationic cyclophanes.[10] It and its derivatives can form stable complexes with a series of electron-rich guest molecules through non-covalent bonds for the construction of many complicated supramolecular structure, such as catenane,[11] rotaxane,[12] nano conductive material,[13] electrochemically switchable molecule,[14] metal–organic framework (MOF),[15] and so on.

Tetraphenylethene (TPE) as a typical aggregation-induced emission (AIE) luminogen has been widely applied to fabricate and construct fluorescent systems with carbohydrates, lipids, amino acids, proteins, enzymes, nucleic acids, and others.[16] In supramolecular chemistry, TPE derivatives have been also used as building block for the design and synthesis of macrocyclic compounds or assemblies.[17-19] For example, Zheng and co-workers reported a series of TPE-based macrocycles and cages with AIE effect for functional applications, such as chiral recognition,[17a] self-assembly,[17b] gas sorption,[17c] and TNT detection.[17d] Stang and co-workers developed a series of pyridyl TPE-based platinum(II) metallacycles[18] and metallacages,[19] which exhibited a high emission based on their AIE properties in various solvents. Although several cationic cyclophane derivatives have been effectively utilized for host–guest complexation, the synthesis and host-guest study of water-soluble cyclophanes that retain the recognition ability in aqueous media still has been a huge challenge.[20] Here we report the synthesis and characterization of two cationic cyclophanes (**1-2**) containing tetraphenylethene (TPE) and bipyridinium (BP) moieties, which have a suitable cavity for selectively recognizing amino acids (e.g. tryptophan) and adenosine derivatives (e.g. ATP) in water.

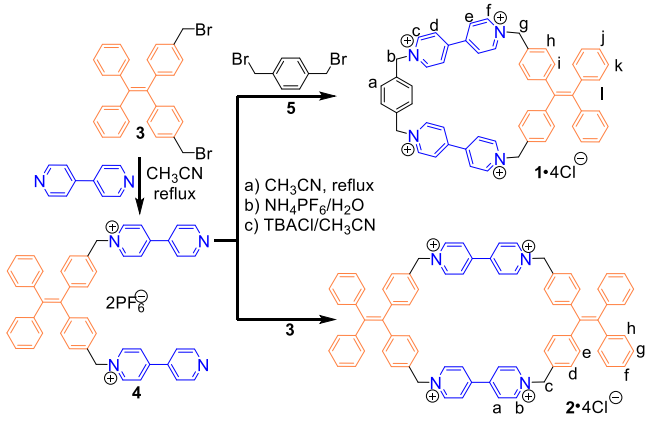

Scheme 1. Synthesis of the cationic cyclophane derivatives **1** and **2**.

[a]*Key Laboratory of Synthetic and Natural Functional Molecule Chemistry of the Ministry of Education,* [b]*National Demonstration Center for Experimental Chemistry Education, College of Chemistry and Materials Science, Northwest University, Xi'an, 710069, P. R. China. E-mail: chcaoliping@nwu.edu.cn*

†Electronic Supplementary Information (ESI) available: Experimental details, including synthesis, ITC, NMR, UV/vis, fluorescence, and crystal data in the cif format (CCDC 1870620-1870621). For ESI and crystallographic data in CIF or other electronic format see DOI: 10.1039/x0xx00000x

‡These authors contributed equally.

Cationic cyclophanes (**1-2**) were synthesized via two-step S_N2 reactions as shown in Scheme 1 (see the Supporting Information): 1) the first-step S_N2 reaction between **3** and dipyridine gives a C-shaped compound (**4**) in 97% yield; 2) the second-step S_N2 reaction between **4** and corresponding dibromide compounds (**3** or **5**) achives a cyclic formation to give **1-2** with PF_6^- as counterions in 35% and 42% yeild without chromatography, respectively. Finally, **1-2** were transferred to their Cl^- form by adding excess amount of tetrabutylammonium chloride in 90% and 85% yield, respectivley. **1-2** with Cl^- as counterions showed a good solubility of ~49.0 mM and ~3.4 mM in D_2O determined by NMR, indicating their potential application for molecular recognition in water (Figures S15-S16).

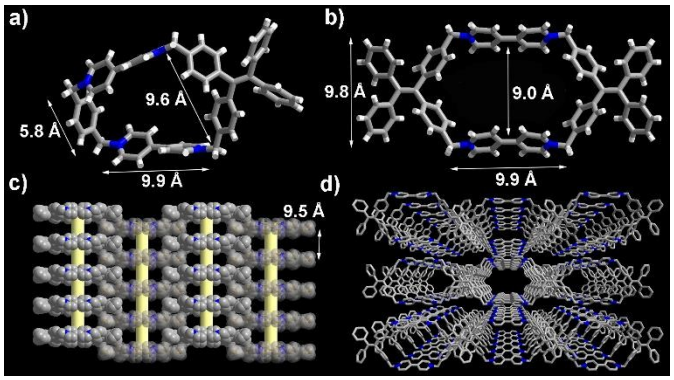

Fig. 1 The single-crystal X-ray structures of (a) a single molecule of **1**•4PF_6^-; (b) a single molecule, (c) side view of the 2D nanotubular layer from the *c* axis, and (d) perspective view of the 3D framework of **2**•4PF_6^- from the *b* axis, respectively. Colour code: C, grey; N, blue; H, white; O, red. Counter ions and solvent molecules have been omitted for clarity; the atom-to-atom distances are showed here.

The cyclic structure and cavity's size of cyclophanes **1-2** were further confirmed by single crystal X-ray analysis (Figure 1). The X-ray-quality single crystals of cyclophane **1**•4PF_6^- were obtained by slow vapour diffusion of dichloromethane into an acetone solution of **1**•4PF_6^- at room temperature. Cationic cyclophane **1** was found to crystallise in monoclinic crystal system. The dihedral angle between two pyridinium rings is about 44.4° in the bipyridinium moieties. Interestingly, **1** possesses a trapezoid-like cavity with up, down, and side lengths of about 5.8 Å, 9.6 Å, and 9.9 Å, respectively (Figures 1a and S17). Furthermore, **1** exhibits a head-to-head and tail-to-tail stacking pattern to form supramolecular framework structure (Figure S17). On the other hand, X-ray-quality single crystals of **2**•4PF_6^- were also obtained by slow vapour diffusion of diethyl ether into a solution of **2**•4PF_6^- in acetonitrile/acetone at room temperature. Cationic cyclophane **2** was crystallized in orthorhombic crystal system. Because the middle part of bipyridinium units bent into the inside of the cavity, **2** possesses a flat rectangle-like cavity with a length of about 9.9 Å and widths of ~9.8 Å at two sides and ~9.0 Å at the center (Figure 1b). Beyond the intriguing macrocyclic cavity described above, a 3D nanotubular framework stacked by **2** molecules is revealed, that features 1D intrinsic nanotubes constructed by the cavities of **2** along the *b* axis (Figure 1c-d). Firstly, **2** molecules are aligned parallelly to form a 1D intrinsic nanotube, in which each **2** molecules are in register to one another to extend through a lattice translation (~9.5 Å repeat) along the *b* axis. Secondly, neighboring 1D nanotubes formed from **2** with a parallel arrangement form a 2D nanotubular layer in the alternate pattern (Figure 1c). Close inspection of this 2D nanotubular layer, neighboring **2** molecules from two 1D nanotubes contact with each other through C–H•••π interactions (Figure S18). Finally, neighboring 2D nanotubular layers are stacked parallelly to form a 3D nanotubular framework (Figure 1d). At the same time, solvent molecules (e.g. MeCN, acetone, CH_2Cl_2, $CHCl_3$ and Et_2O) and PF_6^- counter ions exist in the interspace of the framework structure.[21]

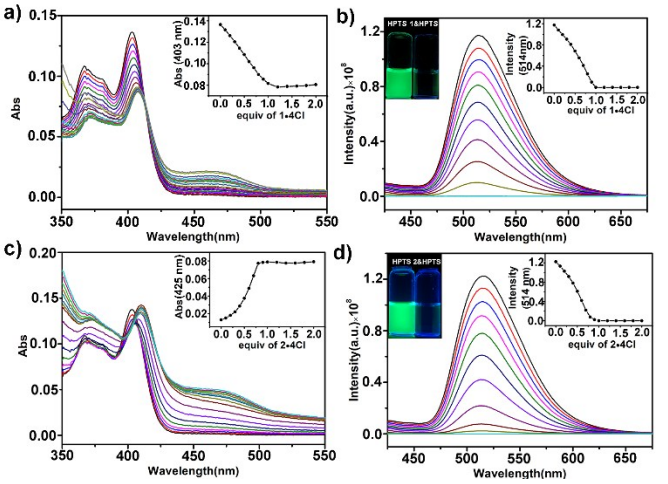

Fig. 2 (a) UV-vis and (b) fluorescence titration (λ_{ex}= 365 nm) of HPTS (5μmol) with gradual addition of **1**•4Cl^- in water at 298K. The insets show a plot of absorbance intensity at 403 nm and emission intensity at 514 nm versus the equivalent of **1**•4Cl^-. (c) UV-vis and (d) fluorescence titration (λ_{ex}= 365 nm) of HPTS (5μmol) with gradual addition of **2**•4Cl^- in water at 298K. The insets show a plot of absorbance intensity at 403 nm and emission intensity at 514 nm versus the equivalent of **2**•4Cl^-.

To explore the recognition ability of these cationic cyclophanes as hosts, ^{1}H NMR experiments between cyclophanes (**1-2**) and 8-hydroxy-1,3,6-pyrene trisulfonate (HPTS) were first performed in D_2O or DMSO-d_6. The host-guest recognition between **1-2** and HPTS was presented more clearly in DMSO-d_6 than in D_2O, because strong electrostatic interactions between sulfonate groups and pyridinium ring make the host-guest complex a poor solubility in water (Figures S19-S23). As a result, NMR titration of **1-2** and HPTS confirmed the formation of 1:1 host-guest complexes in DMSO-d_6. For example, when HPTS was added to the solution of **2**, upfield shifts of the pyrene resonances for HPTS were observed, indicating that the pyrene unit of HPTS is totally encapsulated by the cavity of **2**. Simultaneously, all resonances (H_{a-e}) of **2** located around HPTS in the host-guest complex exhibited upfield shifts, because of the shielding effect of π-electron-rich HPTS. In addition, the COSY and NOESY spectra showed a $H_{2'}$-$H_{b'}$ inter-correlation between guest and host, indicating the inclusion complex between **2** and HPTS in the DMSO-d_6 (Figure S24). In addition, electrospray ionization mass spectrometry (ESI-MS) confirmed the formation of 1:1 host-guest complex between **1-2** and HPTS, respectively (Figures S25-26).

Subsequently, the photophysical properties of HPTS and **1-2** were analysed in water by fluorescence and UV-vis experiments. Like Ramaih's anthracene-based cyclophane, **1-2** are non-emitted in water due to the photoinduced electron transfer (PET) from TPE to bipyridinium units.[22] As shown in Figure 2a, when **1** was successively added to HPTS in water, the absorbance maxima at 403 nm decreased and moved to 408 nm, indicating that the formation of the host-guest complex. And there was a new peak at 430-510nm which may be

caused by the charge-transfer interaction between HPTS and the bipyridinium units. As a result, a dramatic fluorescence quenching of HPTS at 514 nm happened when 1.0 equiv. of **1** was added, which could be contributed to the PET from HPTS to **1** based on the formation of host-guest complex (Figure 2b). In addition, UV-vis and fluorescence titration experiments between **1** and HPTS gave a 1:1 stoichiometry for the complex **1**•HPTS. Similarly, UV-vis and fluorescence titration experiments of HPTS with **2** also established a 1:1 stoichiometry of the host-guest complex **2**•HPTS (Figure 2c-d). Job plot using the UV-vis spectroscopy displayed a maximum at about 0.5, which supports a 1:1 binding stoichiometry for both complexes (Figure S28). Furthermore, isothermal titration calorimetry (ITC) data also confirmed that a 1:1 binding stoichiometry and the strong binding ($K_{\mathbf{1}\cdot HPTS} = 4.88 \times 10^8\ M^{-1}$ and $K_{\mathbf{2}\cdot HPTS} = 1.42 \times 10^9\ M^{-1}$) facilitates these stable host-guest complexes in water (Figure S29). Because of the proper size of cavity, **2** exhibited a stronger binding affinity for HPTS through π-π and electrostatic interactions. However, the utility of the host-guest complexes (**1**•HPTS and **2**•HPTS) as an on-off-on fluorescent sensor is limited due to the too high binding constants between **1-2** and HPTS.[22]

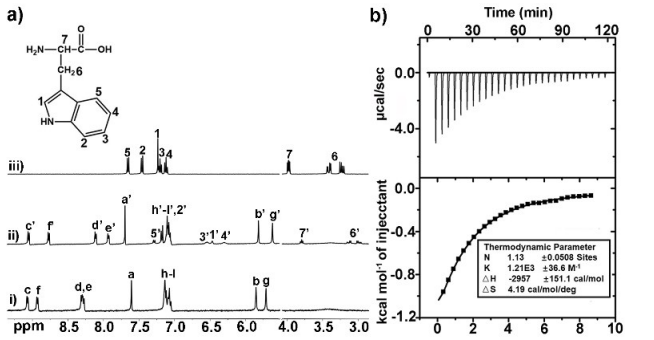

Fig. 3 a) ^{1}H NMR spectra (400MHz, 298 K, D_2O, 10 mM phosphate buffer, pH = 7.4) recorded for: i) **1**•4Cl$^-$ (0.4 mM); ii) **1**•4Cl$^-$ (0.4 mM) and Trp (0.4 mM); iii) tryptophan (0.4 pmM) at 298K. b) ITC data for the titration of **1**•4Cl$^-$ (0.40 mM) in the cell with a solution of Trp (16.0 mM) in the syringe in phosphate buffer (10 mM, pH = 7.4) at 298 K. **1**•4Cl$^-$: tryptophan = 1:1. Here, primes (') denote resonances within the host-guest complexes.

To further explore the host-guest recognition of **1-2** in aqueous media, we decided to investigate the recognition ability of **1-2** for amino acids and nucleotides (e.g. ATP, ADP, and AMP). Initially, the recognition between **1-2** and amino acids was screened by ^{1}H NMR in D_2O with phosphate buffer (Figures S30-S75). Interestingly, **1** exhibited a highly-selective recognition toward tryptophan (Trp), compared to other amino acids (Figures 3 and S30). NMR spectra of the 1:1 mixture of **1** and Trp showed that all proton resonances ($H_{1'}$-$H_{7'}$) of Trp underwent upfield shifts (Δδ = 0.14-0.79 ppm), indicating Trp molecule is fully encapsulated into the cavity of **1**. At the same time, partial protons ($H_{d'}$-$H_{g'}$) of **1** displayed upfield shifts (Δδ = 0.04-0.33 ppm), which could be caused by π-electron shielding of the face-to-face oriented aromatic rings between the π-electron-rich indole moiety of Trp and π-electron-deficient bipyridinium unit of **1**.[15] Remarkably, compared with that of protons near the p-xylylene ring, the chemical shifts of the proton ($H_{d'}$-$H_{g'}$) near the TPE unit in **1** was larger, which indicated that Trp molecule was closer to the TPE unit in the cavity of **1**. Job plot by ^{1}H NMR in D_2O (phosphate buffer, pH = 7.4) determined a 1:1 stoichiometry of the host-guest complex **1**•Trp with a moderate binding constant ($K_{\mathbf{1}\cdot Trp} = 2.67 \times 10^3\ M^{-1}$) in the solution (Figures S29-S34). In addition, binding constant ($K_{\mathbf{1}\cdot Trp} = 1.21 \times 10^3\ M^{-1}$) and 1:1 stoichiometry of **1**•Trp were also confirmed by ITC experiments (Figure 3b and Table 1). Furthermore, ESI-MS also observed the two- and three-charged peaks ([**1**•Trp]$^{3+}$ and [**1**•Trp]$^{2+}$), which confirmed the formation of 1:1 host-guest complex, respectively (Figure S35). Then, the limit of detection of the host **1** for Trp was calculated as 0.36 μmol by UV-vis experiments (Figure S36).[23] Similar but weak recognition behaviours were observed in the case of tyrosine, phenylalanine, aspartic acid, and cysteine with **1**, however, their association constants are too weak to be calculated by NMR or ITC (Figures S37-S41). In contrast, **2** showed weaker interactions with all the amino acids on account of its too large cavity (Figures S56-S75). For arginine (Asn) and lysine (Leu) as basic amino acids, the *α*- and *β*-protons ($H_{1'}$-$H_{2'}$) of Asn/Leu with **1-2** showed downfield shifts, indicating only electrostatic interactions between the deprotonated carboxyl groups and positive pyridinium groups played a main role (Figures S42-S43 and S62-S63).

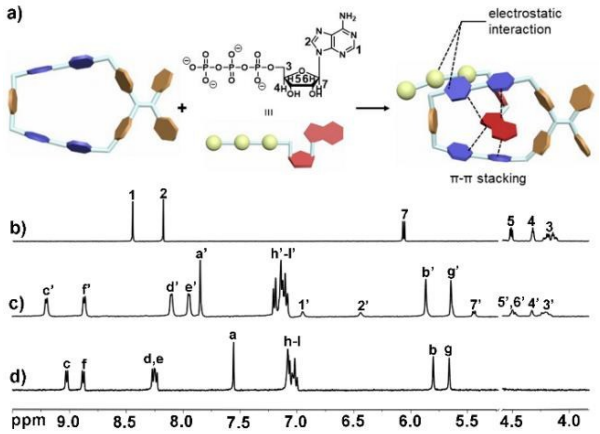

Fig. 4 a) schematic representation of **1**•ATP; ^{1}H NMR spectra (400MHz, 298 K, D_2O, 10 mM phosphate buffer, pH = 7.4) recorded for: b) ATP (0.4 mM); c) **1**•4Cl$^-$ (0.4 mM) and ATP (0.4 mM); d) **1**•4Cl$^-$ (0.4 mM). Here, primes (') denote resonances within the host-guest complexes.

Next, adenosine derivatives (e.g. ATP, ADP, and AMP) as guests were investigated for **1-2** as hosts by NMR and ITC. In the ^{1}H NMR spectrum of **1** with 1.0 equiv. of ATP in D_2O (phosphate buffer, pH = 7.4), proton resonances ($H_{1'}$-$H_{2'}$ and $H_{6'}$-$H_{7'}$) for adenine ($\Delta\delta_{H1'} = 1.50$ ppm and $\Delta\delta_{H2'} = 1.74$ ppm) and ribose moieties ($\Delta\delta_{H7'} = 0.62$ ppm) of ATP were obviously shifted to upfield, compared to free ATP, indicating that whole adenine and part of ribose moieties resided in the cavity of **1** (Figure 4). In addition, NOESY spectra showed a $H_{1'}$-$H_{h'\text{-}l'}$ inter-correlation between adenine moiety of ATP and the TPE unit of **1**, indicating adenine moiety of ATP was closer to the TPE unit in the cavity of **1**. The π-π interaction between adenine moiety of ATP and bipyridinium units of **1** also results in a shielding effect for proton resonances ($H_{d'}$-$H_{e'}$) for the bipyridinium unit in **1**. At the same time, proton resonances for the *p*-xylylene ($H_{a'}$), bridged CH_2 ($H_{b'}$) and neighboring pyridinium ($H_{c'}$) units in **1** were significant downshifted (Δδ = 0.29 ppm, 0.06 ppm, and 0.18 ppm, respectively), which probably were caused by the electrostatic interactions between the

triphosphate unit of ATP and the pyridinium near the *p*-xylylene ring in **1** (Figure 4). Based on the above NMR data, the adenine moiety of ATP molecule is closed to TPE in the cavity of **1**, while triphosphate unit prefers to *p*-xylylene and neighboring pyridinium rings, which is consistent with the result of NOESY spectra (Figure S77). On the other hand, the 1:1 host-guest stoichiometry and binding constant (K_a = 1.17 × 10^4 M^{-1}) were determined by ITC (Figure S78). In addition, the limit of detection of the host **1** for ATP was calculated as 1.89 μmol (Figure S79). Similarly, ADP and AMP were quantitatively accommodated within cyclophane **1** to give 1:1 host-guest complexes by the ^{1}H NMR and ITC. ADP and AMP were bound by **1** with moderate binding constants of 5.07 × 10^3 M^{-1} and 1.09 ×10^3 M^{-1}, respectively (Figures S80-S83). Compared the host-guest interactions of three nucleotides with **1**, their binding ability gradually strengthen, accompanying with the increase of the number of phosphate (Tables 1 and S2). All ESI-MS spectra of **1**•ATP, **1**•ADP and **1**•AMP showed the formation of 1:1 host-guest complexes, respectively (Figure S84-86). The results indicated that cyclophane **1** can selectively recognize ATP molecule through both electrostatic and π-π interactions. However, the weak binding behavior between **2** and adenosine derivatives was confirmed by the ^{1}H NMR and UV-vis (Figures S87-S92), probably because the large cavity of **2** is not fit with adenine ring.

Table 1. Binding constants between **1-2** and guests.[a]

Host	Guest	Binding Constant (K_a, M^{-1})
1	HPTS	(4.88 ± 1.95) × 10^8
2	HPTS	(1.42 ± 0.98) × 10^9
1	Trp	(1.21 ± 0.04) × 10^3
1	ATP	(1.17 ± 0.12) × 10^4
1	ADP	(5.07 ± 0.28) × 10^3
1	AMP	(1.09 ± 0.16) × 10^3

[a]Determined by ITC.

In conclusion, we have designed and synthesized two new cationic cyclophanes (**1**-**2**) containing tetraphenylethene and bipyridinium moieties. Determined by their X-ray crystal structures, asymmetrical cyclophane **1** possesses a trapezoid-like and smaller cavity whereas symmetrical cyclophane **2** possesses a flat rectangle-like and larger cavity. Their host-guest behaviours have been investigated by ^{1}H NMR, UV-vis, fluorescence and ITC experiments. In aqueous media, two cyclophanes have fluorescence quenching effect on the fluorescence indicator HPTS when forming 1:1 host-guest complexes through π-π and electrostatic interactions with strong affinity (10^8~10^9 M^{-1}). More interestingly, **1** exhibited a highly-selective recognition for tryptophan and ATP (~2 times to ADP, ~10 times to AMP) due to its proper size of cavity and good water-solubility. We anticipate that this kind of cationic cyclophane can also be synthesized and modified with other functional linkers, affording the ability to tune the cavity, host-guest and photophysical properties of these cationic macrocycles, which may find utility in applications such as not only biosensor for detecting biological analytes (e.g. DNA) but also supramolecular building blocks for constructing molecular knots in near future.

This work was supported by National Natural Science Foundation of China (21771145 and 21472149 to L.C., 21402151 to Y.Z.).

Notes and references

View Article Online
DOI: 10.1039/C9CC00599D

1 F. Diederich, P. J. Stang and R. R. Tykwinski, Modern Supramolecular Chemistry: Strategies for Macrocycle Synthesis. Wiley-VCH Verlag GmbH & Co. KGaA, Weinheim, **2008**.
2 G. W. Gokel, W. M. Leevy and M. E. Weber, *Chem. Rev.*, 2004, **104**, 2723-2750.
3 G. Chen and M. Jiang, *Chem. Soc. Rev.*, 2011, **40**, 2254-2266.
4 D.-S. Guo and Y. Liu, *Chem. Soc. Rev.*, 2012, **41**, 5907-5921.
5 J. Lagona, P. Mukhopadhyay, S. Chakrabarti and L. Isaacs, *Angew. Chem. Int. Ed.*, 2005, **44**, 4844-4870.
6 Z. Liu, S. K. M. Nalluri and J. F. Stoddart, *Chem. Soc. Rev.*, 2017, **46**, 2459-2478.
7 M. Xue, Y. Yang, X. Chi, Z. Zhang and F. Huang, *Acc. Chem. Res.*, 2012, **45**, 1294-1308.
8 (a) M. T. Nguyen, M. D. Krzyaniak, M. Owczarek, D. P. Ferris, M. R. Wasielewski and F. J. Stoddart, *Angew. Chem. Int. Ed.*, 2017, **56**, 5795-5800; (b) W. W. Porter, T. P. Vaid and A. L. Rheingold, *J. Am. Chem. Soc.*, 2005, **127**, 16559-16566.
9 C. Cheng, P. R. McGonigal, S. T. Schneebeli, H. Li, N. A. Vermeulen, C. Ke and J. F. Stoddart, *Nat. Nanotech.*, 2015, **10**, 547-553.
10 (a) E. J. Dale, N. A. Vermeulen, M. Juríček, J. C. Barnes, R. M. Young, M. R. Wasielewski and J. F. Stoddart, *Acc. Chem. Res.*, 2016, **49**, 262-273; (b) H. Y. Gong, B. M. Rambo, E. Karnas, V. M. Lynch and J. L. Sessler, *Nat Chem*, 2010, **2**, 406-409; (c) H. Y. Gong, B. M. Rambo, E. Karnas, V. M. Lynch, K. M. Keller and J. L. Sessler, *J. Am. Chem. Soc.*, 2011, **133**, 1526-1533.
11 J. Sun, Z. Liu, W. G. Liu, Y. Wu, Y. Wang, J. C. Barnes, K. R. Hermann, W. A. Goddard, III, M. R. Wasielewski and J. F. Stoddart, *J. Am. Chem. Soc.*, 2017, **139**, 12704-12709.
12 A. Trabolsi, A. C. Fahrenbach, S. K. Dey, A. I. Share, D. C. Friedman, S. Basu, T. B. Gasa, N. M. Khashab, S. Saha, I. Aprahamian, H. A. Khatib, A. H. Flood and J. F. Stoddart, *Chem. Commun.*, 2010, **46**, 871-873.
13 J. C. Barnes, E. J. Dale, A. Prokofjevs, A. Narayanan, I. C. Gibbs-Hall, M. Juríček, C. L. Stern, A. A. Sarjeant, Y. Y. Botros, S. I. Stupp and J. F. Stoddart, *J. Am. Chem. Soc.*, 2015, **137**, 2392-2399.
14 C. Cheng, P. R. McGonigal, S. T. Schneebeli, H. Li, N. A. Vermeulen, C. Ke and J. F. Stoddart, *Nat. Nanotech.*, 2015, **10**, 547-553.
15 Q. Chen, J. Sun, P. Li, I. Hod, P. Z. Moghadam, Z. S. Kean, R. Q. Snurr, J. T. Hupp, O. K. Farha and J. F. Stoddart, *J. Am. Chem. Soc.*, 2016, **138**, 14242-14245.
16 J. Mei, N. L. C. Leung, R. T. K. Kwok, J. W. Y. Lam and B. Z. Tang, *Chem. Rev.*, 2015, **115**, 11718-11940.
17 (a) J. B. Xiong, H. T. Feng, J. P. Sun, W. Z. Xie, D. Yang, M. H. Liu and Y. S. Zheng, *J. Am. Chem. Soc.*, 2016, **138**, 11469-11472; (b) S. Song and Y. S. Zheng, *Org. Lett.*, 2013, **15**, 820-823; (c) C. Zhang, Z. Wang, L. X. Tan, T. L. Zhai, S. Wang, B. Tan, Y. S. Zheng, X. L. Yang and H. B. Xu, *Angew. Chem., Int. Ed.*, 2015, **54**, 9244-9248.
18 X. Yan, H. Wang, C. E. Hauke, T. R. Cook, M. Wang, M. L. Saha, Z. Zhou, M. Zhang, X. Li, F. Huang and P. J. Stang, *J. Am. Chem. Soc.*, 2015, **137**, 15276-15286
19 X. Yan, T. R. Cook, P. Wang, F. Huang and P. J. Stang, *Nat. Chem.*, 2015, **7**, 342-348.
20 E. Persch, O. Dumele and F. Diederich, *Angew. Chem., Int. Ed.*, 2015, **54**, 3290-3327.
21 A. L. Spek, Acta Cryst. 2015, C**71**, 9-18.
22 P. P. Neelakandan, M. Hariharan and D. Ramaiah, *J. Am. Chem. Soc.*, 2006, **128**, 11334-11335.
23 Q. Lin, Y.-Q. Fan, P.-P. Mao, L. Liu, J. Liu, Y.-M. Zhang, H. Yao, and T.-B. Wei, *Chem. Eur. J.*, 2018, **24**, 777-783.

ROYAL SOCIETY OF CHEMISTRY View Article Online
DOI: 10.1039/C9CC00599D

Journal Name

COMMUNICATION

TOC:

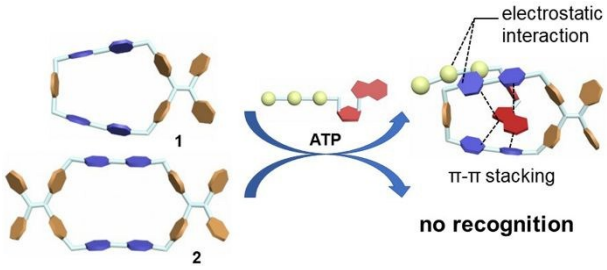

Tetracationic cyclophane **1** with a trapezoid-like cavity exhibited a highly-selective recognition for tryptophan and ATP through electrostatic and π-π interaction in water.

View Article Online
DOI: 10.1039/C9CC00599D

Tetraphenylethene-based tetracationic cyclophanes and their selective recognition for amino acids and adenosine derivatives in water

Lin Cheng,[a,‡] Haiyang Zhang,[a,‡] Yunhong Dong,[a,b,‡] Yanxia Zhao,[a] Yang Yu,[a] and Liping Cao[a,*]

[a]*Key Laboratory of Synthetic and Natural Functional Molecule Chemistry of the Ministry of Education,* [b]*National Demonstration Center for Experimental Chemistry Education, College of Chemistry and Materials Science, Northwest University, Xi'an, 710069, P. R. China. E-mail: chcaoliping@nwu.edu.cn*

Table of Contents **Pages**

View Article Online
DOI: 10.1039/C9CC00599D

General Experimental Details.

Starting materials were purchased from commercial suppliers were used without further purification. **SI3**[1], **SI6**[2], and **3**[3] was prepared according to the published procedure. Melting points were determined using XT-4 apparatus. IR spectra were recorded on a Bruker IFS 120HR spectrometer and were reported in cm^{-1}. ^{1}H and ^{13}C NMR spectra were done on a Bruker ascend spectrometer at 400MHz. UV-Vis spectra were measured using an Agilent Cary-100 spectrophotometer. Fluorescence spectra were recorded on a Horiba Fluorolog-3 spectrometer. Fluorescence decay profiles were recorded on a Flsp920. Electron Spray Ionization (ESI) mass spectra were acquired by using a UltiMate3000 electrospray instrument. Isothermal titration calorimetry (ITC) was carried out using a VP-ITC (Malvern) at 25 ˚C, and computer fitting of the data were performed using the VP-ITC analyze software. X-ray Crystal Structure was performed on a Bruker D8 Venture photon II.

View Article Online
DOI: 10.1039/C9CC00599D

Synthetic Procedures and Characterization Data.

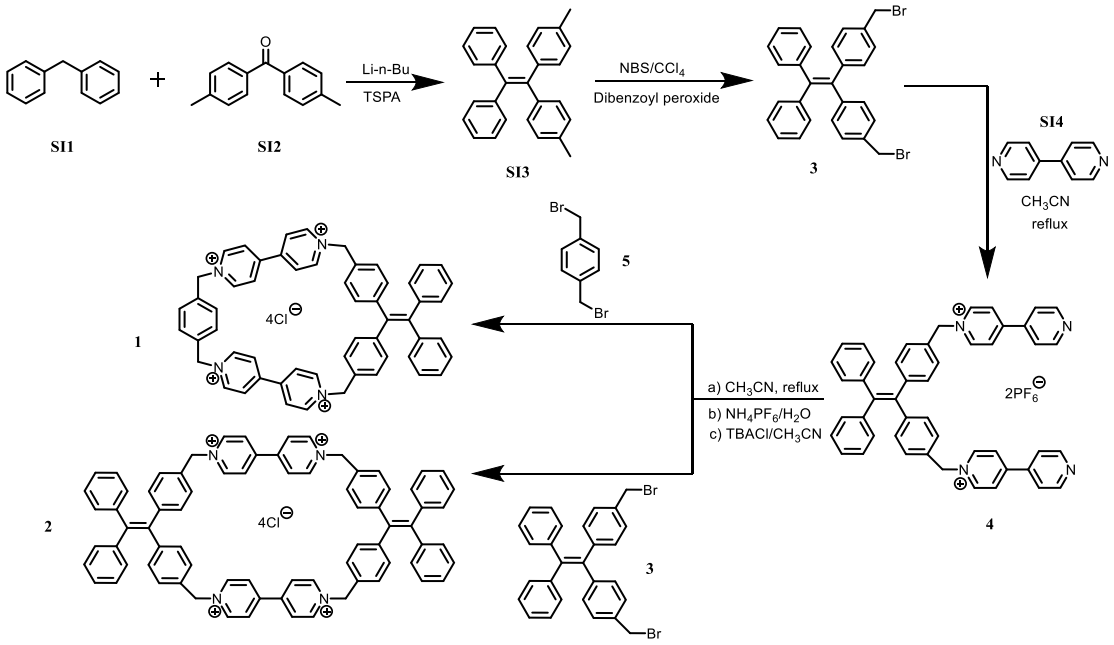

Compound SI3. To a solution of **SI2** (2.02 g, 12 mmol) in dry THF (20 mL) was added 6.2 mL of a 1.6 M solution of *n*-butyllithium in hexane at 0℃ under a N_2 atmosphere. The resulting orange-red solution was stirred for 30 min at that temperature. Next**,** **SI1** was dissolved in appropriate dry THF. This solution was added to the above mixture slowly with a dropping funnel, and the reaction mixture was allowed to warm to room temperature with stirring for 6 h. The reaction was quenched with addition of an aqueous solution of saturated ammonium chloride and the organic layer was extracted with CH_2Cl_2 (3 × 50 mL) and the combined organic layers were washed with saturated brine solution and dried over anhydrous $MgSO_4$. The solvent was evaporated and the resulting crude alcohol (containing excess **SI2**) was subjected to acid catalyzed dehydration as follows.

The crude alcohol was dissolved in about 80 mL of toluene in a 100 mL round flask with the 4Å molecular sieve dehydration unit. A catalytic amount of *p*-toluenesulphonic acid (342 mg, 1.8 mmol) was added and the mixture was refluxed for 5 h and cooled to room temperature. The toluene layer was washed with 10% aqueous $NaHCO_3$ solution (3 × 25 mL) and dried over anhydrous $MgSO_4$ and evaporated to afford the crude **SI3**. The crude product was purified by a silica gel column chromatography using petroleum

View Article Online
DOI: 10.1039/C9CC00599D

ether as eluent, and white solid of pure **SI3** was obtained. The ^{1}H NMR matches that reported in the reported literature.[1]

Compound 3. Under a N_2 atmosphere, compound **SI3** (1.08 g, 3.0 mmol), NBS (1.18 g, 8.4 mmol) and dibenzoyl peroxide (36 mg, 0.15 mmol) were added to CCl_4 (20 mL). The solution was heated to reflux for another 12 h. The mixture was cooled to room temperature and filtered to remove suspension. Next, CH_2Cl_2 (20 mL) was added to the filtrate and then the solution was washed with water and brine, respectively, for three times, it was dried over anhydrous Na_2SO_4, filtered and evaporated under vacuum to dryness. The residue was purified by a silica gel column chromatography using petroleum/dichloromethane ether as eluent, and white solid of pure compound **3** was obtained. The ^{1}H NMR matches that reported in the reported literature.[3]

Compound 4. 4,4'-bipyridine (603 mg, 3.86 mmol) was dissolved in 20 mL of CH_3CN in a 50 mL round flask and the solution was brought to reflux. Next, compound **3** (200 mg, 0.39 mmol) was dissolved in 5 mL of acetonitrile. This solution was added to the bipyridine refluxing solution slowly with a dropping funnel. Then the mixture was refluxed for an additional 48 h. The precipitate formed was filtered and washed with acetonitrile (3 × 35 mL), and compound **4** (yield: 97%) was obtained by dried in high vacuum. M.p. 170-171 °C. IR (KBr, cm^{-1}): 3128w, 3059w, 1637s, 1598w, 1404m, 1216w, 1153w, 841s, 700w, 560s. ^{1}H NMR (400 MHz, CD_3CN): 8.85 (d, J = 5.7, 4H), 8.72 (d, J = 6.6, 4H), 8.29 (d, J = 6.6, 4H), 7.77 (d, J = 5.7, 4H), 7.22 (d, J = 8.1, 4H), 7.20-7.10 (m, 10H), 7.05-6.95 (m, 4H), 5.63 (s, 4H). ^{13}C NMR (100 MHz, CD_3CN): 155.5, 152.1, 145.8, 145.7, 144.1, 143.8, 142.0, 139.7, 132.9, 132.0, 131.7, 129.6, 128.8, 127.9, 127.1, 122.7, 64.6. MS (ESI): m/z 335.1552 ([**4** - $2PF_6^-$]$^{2+}$, calcd. for 335.1543) and m/z 815.2676 ([**4** - PF_6^-]$^+$, calcd. for 815.2733).

Compound 1. **(Approach 1)** To a solution of compound **4** (200 mg, 0.28 mmol), **5** (55 mg, 0.28 mmol), and tetrabutylammonium iodide (TBAI, 21 mg, 0.20 mmol) in dry

MeCN (100 mL) was heated at 85 °C for 72 h. Then the crude product was obtained by centrifuge and was dried in high vacuum. The crude product was purified by anion conversion in water. Next, pale yellow solid of pure **1**·4PF_6^- (yield: 35%) was obtained by addition of an excess of NH_4PF_6. M.p. 233 -234 °C. IR (KBr, cm^{-1}): 3129w, 3058w, 2925w, 2848w, 1636s, 1559w, 1504w, 1441m, 1216w, 1153m, 832vs, 700w, 637w, 559s. ^{1}H NMR (100 MHz, CD_3CN): 8.92 (d, *J* = 7.0, 4H), 8.84 (d, *J* = 7.0, 4H), 8.24 (d, *J* = 7.0, 4H), 8.23 (d, *J* = 7.0, 4H), 7.63 (s, 4H), 7.20-7.10 (m, 6H), 7.09 (s, 8H), 7.05-7.00 (m, 4H), 5.79 (s, 4H), 5.67 (s, 4H). ^{13}C NMR (100 MHz, CD_3CN): 150.8, 146.5, 146.2, 145.4, 144.3, 143.8, 139.7, 136.7, 132.5, 132.4, 131.7, 131.5, 131.5, 129.0, 128.8, 128.5, 128.4, 127.8, 65.4, 65.2. MS (ESI): *m*/*z* 532.1521 ([**1**•4PF_6^- - 2PF_6^-]$^{2+}$, calcd. for 532.1498). An excess of TBACl (205.66mg, 0.74mmol) was added to the acetonitrile solution of **1**•4Cl^- (100mg, 0.074 mmol) and stirred overnight at room temperature. Then the mixture was centrifuged and washed twice with acetonitrile. Pure **1**•4Cl^- (61 mg, yield: 90%) was obtained by dried in high vacuum. M.p. 221-222 °C. IR (KBr, cm^{-1}): 3118w, 3041m, 1629s, 1551w, 1497w, 1443m, 1217w, 1156m, 791m, 759w, 691w, 628w. ^{1}H NMR (400 MHz, D_2O): 9.14 (d, *J* = 6.3, 4H), 9.00 (d, *J* = 6.3, 4H), 8.37 (d, *J* = 6.3, 4H), 8.35 (d, *J* = 6.3, 4H), 7.67 (s, 4H), 7.25-7.05 (m, 18H), 5.92 (s, 4H), 5.78 (s, 4H). ^{13}C NMR (100 MHz, CD_3OD): 151.2, 151.1, 147.2, 146.7, 146.1, 144.7, 143.9, 140.1, 137.3, 133.0, 132.0, 131.9, 129.2, 128.9, 128.8, 128.5, 128.0, 65.5, 65.4 (only 19 of the 20 resonances expected were observed).

Compound 2. To a solution of compound **4** (200 mg, 0.21 mmol), compound **3** (109 mg, 0.21 mmol), and tetrabutylammonium iodide (TBAI, 15.5 mg, 0.042 mmol) in dry MeCN (100 mL) was heated at 85 °C for 72 h. Then the crude product was obtained by centrifuge and was dried in high vacuum. The crude product was purified by anion conversion in water. Next, light yellow solid of pure **2**•4PF_6^- (yield: 42%) was obtained by addition of an excess of NH_4PF_6. M.p. 252-253 °C. IR (KBr, cm^{-1}): 3121w, 3056w, 2917w, 2856w, 1629s, 1559w, 1497w, 1443m, 1216w, 1153w, 838vs, 700m, 629w, 559s. ^{1}H NMR (400 MHz, CD_3CN): 8.86 (d, *J* = 6.6, 8H), 8.29 (d, *J* = 6.6, 8H),

7.25-7.10 (m, 28H), 7.10-7.00 (m, 8H), 5.69 (s, 8H). ^{13}C NMR (100 MHz, CD_3CN): 151.1, 146.3, 145.8, 144.3, 143.9, 139.7, 132.8, 131.6, 129.5, 128.8, 128.3, 127.9, 65.1 (only 13 of the 14 resonances expected were observed). MS (ESI): *m*/*z* 659.2058 ([**2**•4PF_6^-- 2PF_6^-]$^{2+}$, calcd. for 659.2045). An excess of TBACl (172.31mg, 0.62mmol) was added to the acetonitrile solution of **2**•4PF_6^- (100mg, 0.062 mmol) and stirred overnight at room temperature. Then the mixture was centrifuged and washed twice with acetonitrile. Pure **2**•4Cl^- (62mg, yield: 85%) was obtained by dried in high vacuum. M.p. 275-276 °C. IR (KBr, cm^{-1}): 3118w, 3025w, 2917w, 2855w, 1628s, 1559w, 1497w, 1442s, 1210w, 1155w, 790m, 759m, 698s, 628w. ^{1}H NMR (400 MHz, CD_3OD): 9.01 (d, *J* = 6.9, 8H), 8.40 (d, *J* = 6.9, 8H), 7.25-7.15 (m, 28H), 7.15-7.05 (m, 8H), 5.76 (s, 8H). ^{13}C NMR (100 MHz, CD_3OD): 151.6, 146.9, 146.6, 144.8, 144.0, 140.0, 133.4, 132.5, 132.1, 129.9, 129.0, 128.6, 128.1, 65.6.

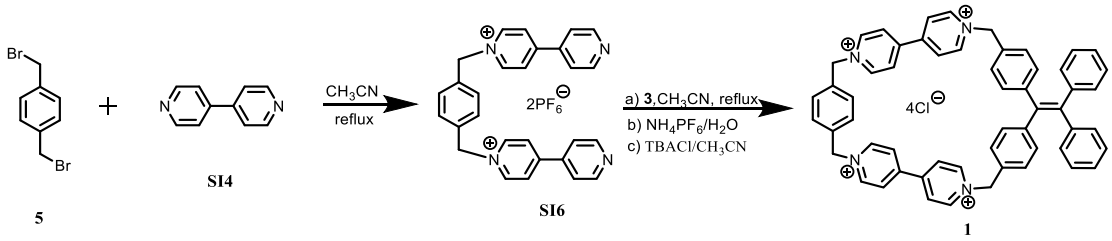

Compound SI6. 4,4'-bipyridine (592 mg, 3.79 mmol) was dissolved in 10 mL of CH_3CN in a 50 mL round flask and the solution was brought to reflux. Next, p-bis-(bromo-methyl) benzene (100 mg, 0.38 mmol) was dissolved in 5 mL of acetonitrile. This solution was added to the bipyridine refluxing solution slowly with a dropping funnel. Then the mixture was refluxed for an additional 24 h. The precipitate formed was filtered and washed with acetonitrile (3 × 35 mL), and dried in high vacuum. The ^{1}H NMR matches that reported in the literature.[2]

Compound 1. **(Approach 2)** To a solution of **SI6** (200 mg, 0.28 mmol), **3** (55 mg, 0.28 mmol), and tetrabutylammonium iodide (TBAI, 21 mg, 0.20 mmol) in dry MeCN (100 mL) was heated at 85 °C for 72 h. Then the crude product was obtained by centrifuge and was dried in high vacuum. The crude product was purified by anion

conversion in water. Next, yellow solid of pure **1**•4PF_6^- (yield: 30%) was obtained by a silica gel column chromatography using CH_2Cl_2/saturated NH_4PF_6 solution (5:1) as eluent.

X-ray Crystal Structure Determination. Diffraction data for the complexes **1**•4PF_6^- and **2**•4PF_6^- were performed on a Bruker D8 Venture photon II, at low temperature (153 K) with graphite-monochromated Mo Kα radiation (λ = 0.71073 Å). An empirical absorption correction using SADABS was applied for all data.[4] Both structures were solved and refined to convergence on F^2 for all independent reflections by the full-matrix least squares method using SHELXL-2018/3[5] in OLEX2 1.2.[6] All non-hydrogen atoms, including those in disordered parts, were refined anisotropically. All H-atoms were also included at calculated positions and refined as riders, with U_{iso}(H) = 1.2 U_{eq}. In **1**•4PF_6^-, two PF_6^- anions were found to be disordered and were modelled with two orientations having relative occupancies of 0.54:0.46 and 0.57:0.43 for the two parts, separately. The geometries of the disordered parts were restrained to be similar. The anisotropic displacement parameters of the disordered molecules in the direction of the bonds were restrained to be equal with a standard uncertainty of 0.01 Å^2. They were also restrained to have the same U_{ij} components, with a standard uncertainty of 0.04 Å^2. In **1**•4PF_6^-, four CH_2Cl_2 and two $CHCl_3$ molecules co-crystallized in each unit cell of complex **1**•4PF_6^-, with the corresponding electron densities removed using the SQUEEZE subroutine implemented within the software program PLATON (Ver. 201118),[7] and the resulting *.fab* file was processed with OLEX2 1.2. using the ABIN instruction. Approximately 280 electron equivalents were removed from the unit cell. The total void volume was 1804 Å^3 indicated by PLATON, equivalent to 25.38 % of the unit cell's total volume. In **2**•4PF_6^-, the PF_6^- anion was found to be disordered and was modelled with two orientations having relative occupancy of 0.55:0.45. The geometries of the disordered parts were restrained to be similar. The anisotropic displacement parameters of the disordered molecules in the direction of the bonds were restrained to be equal with a standard uncertainty of 0.01 Å^2. They were also restrained

to have the same U_{ij} components, with a standard uncertainty of 0.04 Å^2. There are 32 severely disordered Et_2O molecules in crystal **2**•4PF_6^-, They were also removed by by the SQUEEZE subroutine in PLATON (Ver. 201118) and the resulting *.fab* file was processed with OLEX2 1.2. using the ABIN instruction. Approximately 1324 electron equivalents were removed from each unit cell. The total void volume was 4070 Å^3 indicated by PLATON, equivalent to 39.81 % of the unit cell's total volume. Crystallographic data and refinement details for **1**•4PF_6^- and **2**•4PF_6^- are given in Table S1. CCDC 1870620 (**1**•4PF_6^-) and 1870621 (**2**•4PF_6^-). These data can be obtained free of charge from the Cambridge Crystallographic Data Centre www.ccdc.cam.ac.uk/data_request/cif.

References

1. Moloy Banerjee, Susanna J. Emond, Sergey V. Lindeman, and Rajendra Rathore, *J. Org. Chem.* **2007,** *72*, 8054-8061.

2. Wolfram Geuder, Sibgfried Hunig, Adolf Suchy, *Tetrahedron*, **1986,** *42*, 1665-1677.

3. Jin-Hua Wang, Hai-Tao Feng and Yan-Song Zheng, *Chem. Commun.* **2014,** *50*, 11407-11410.

4. G. M. Sheldrick, Program SADABS: Area-Detector Absorption Correction, **1996**, University of Göttingen, Germany.

5. G. M. Sheldrick, *Acta Crystallogr., Sect. C: Cryst. Struct. Chem*. **2015**, *C71*, 3–8.

6. O. V. Dolomanov, L. J. Bourhis, R. J. Gildea, J. A. K. Howard and H. Puschmann, *J. Appl. Cryst.* **2009**, *42*, 339–341.

7. A. L. Spek, *Acta Cryst.* **2015**, *C71*, 9–18.

View Article Online
DOI: 10.1039/C9CC00599D

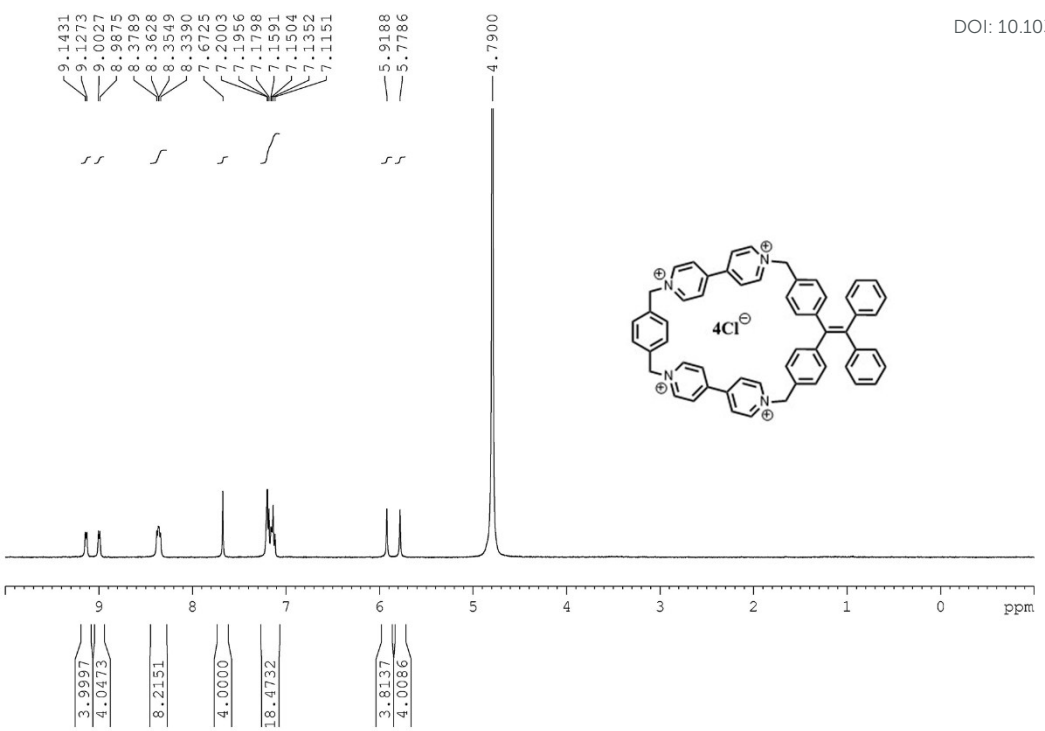

Figure S1. ^{1}H NMR spectrum recorded (400 MHz, D_2O, RT) for **1**•4Cl$^-$.

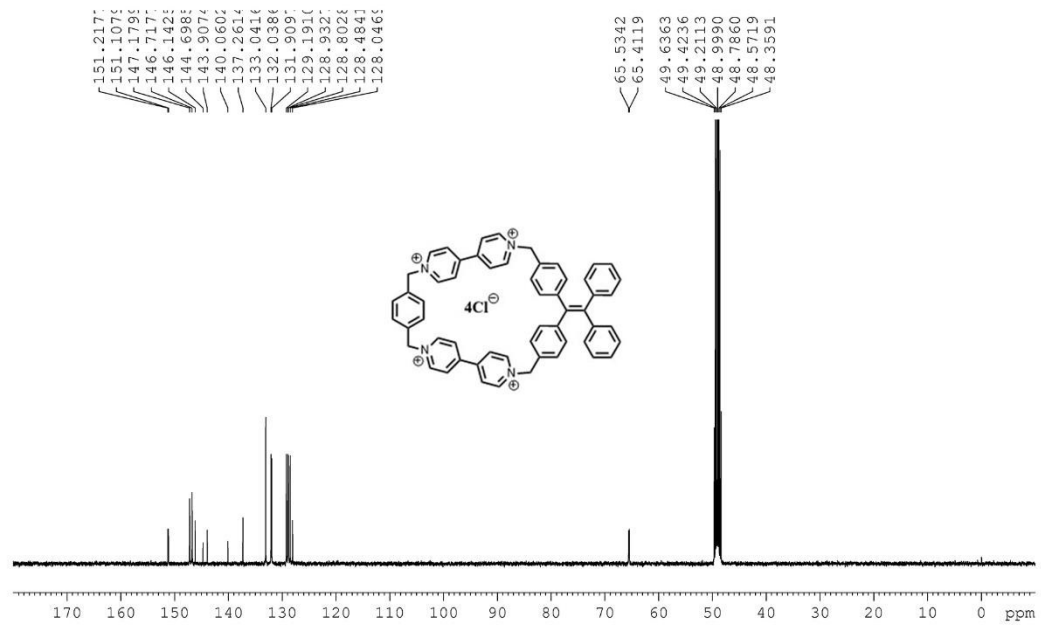

Figure S2. ^{13}C NMR spectrum recorded (400 MHz, CD_3OD, RT) for **1**•4Cl$^-$.

View Article Online
DOI: 10.1039/C9CC00599D

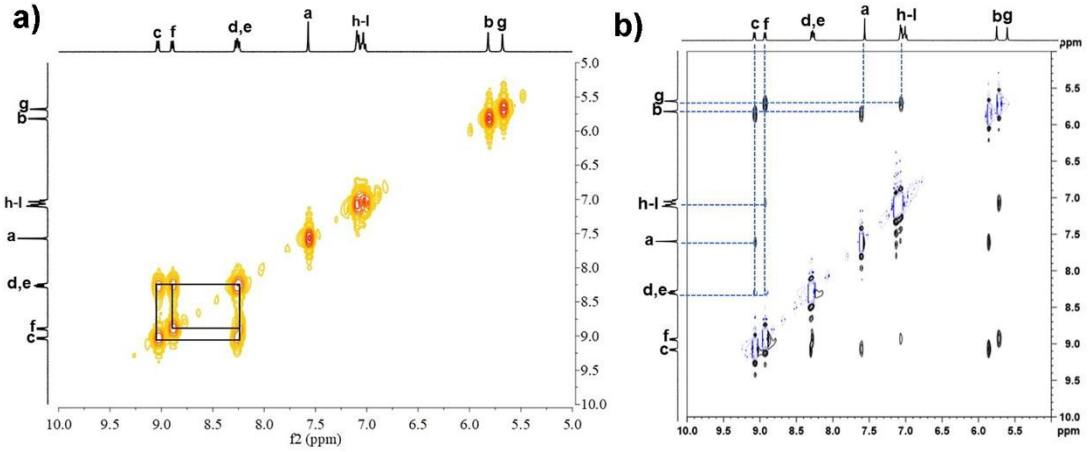

Figure S3. a) COSY and b) NOESY ^{1}H NMR spectrum recorded (400 MHz, D_2O, 298 K) for **1**•4Cl^- (2.0 mM).

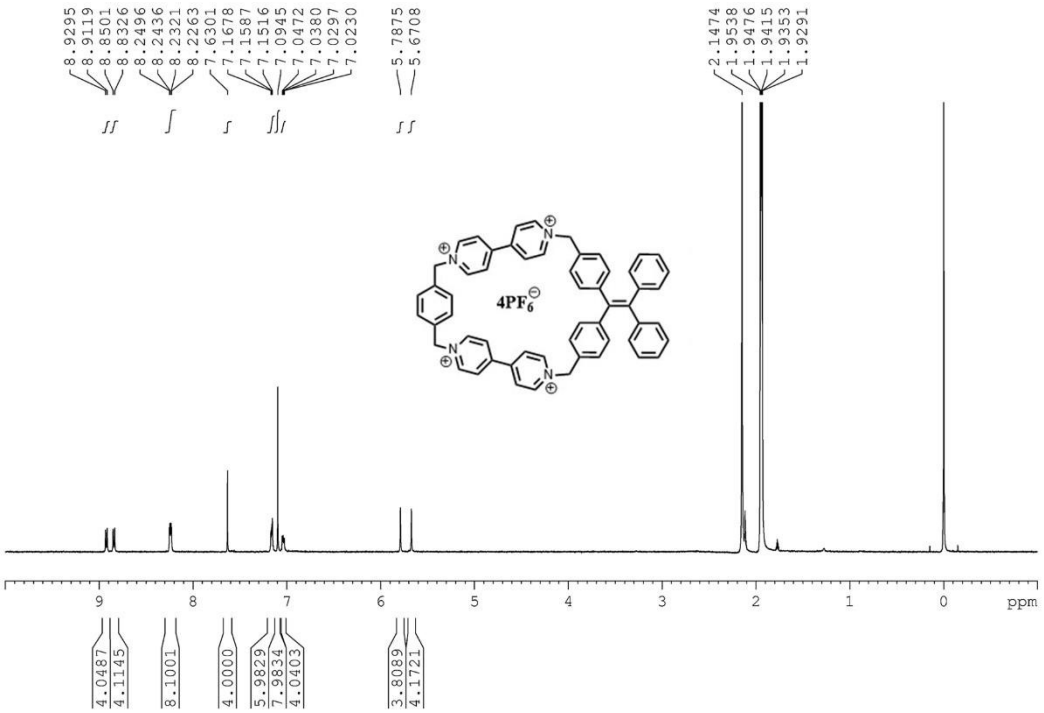

Figure S4. ^{1}H NMR spectrum recorded (400 MHz, CD_3CN, RT) for **1**•4PF_6^-.

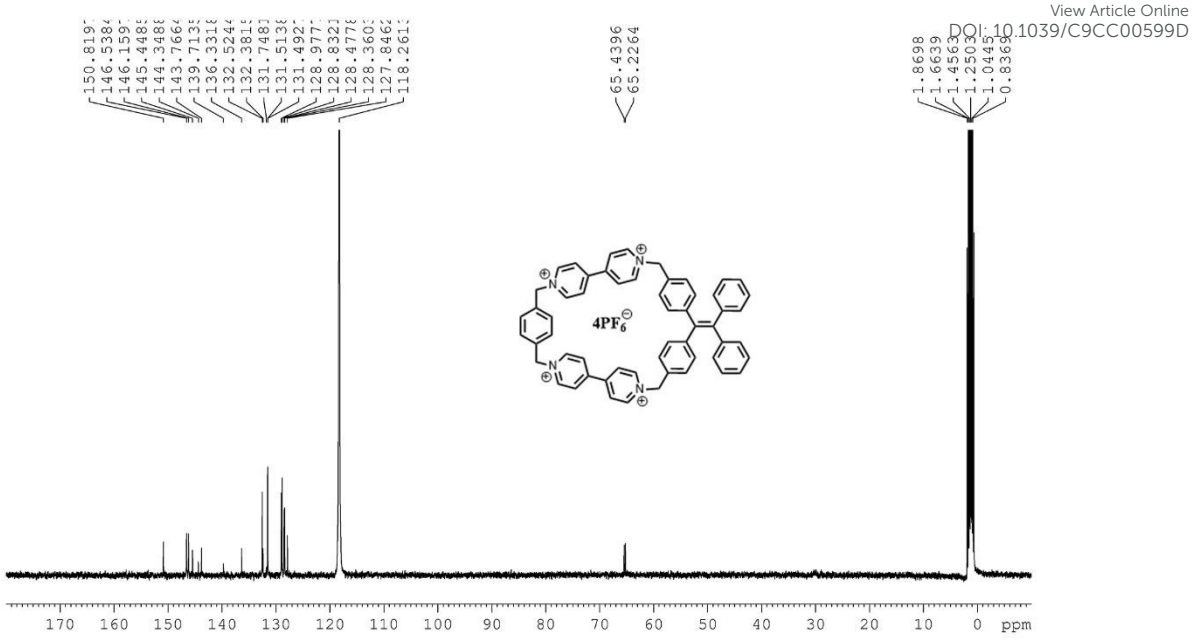

Figure S5. ^{13}C NMR spectrum recorded (100 MHz, CD_3CN, RT) for **1**•$4PF_6^-$.

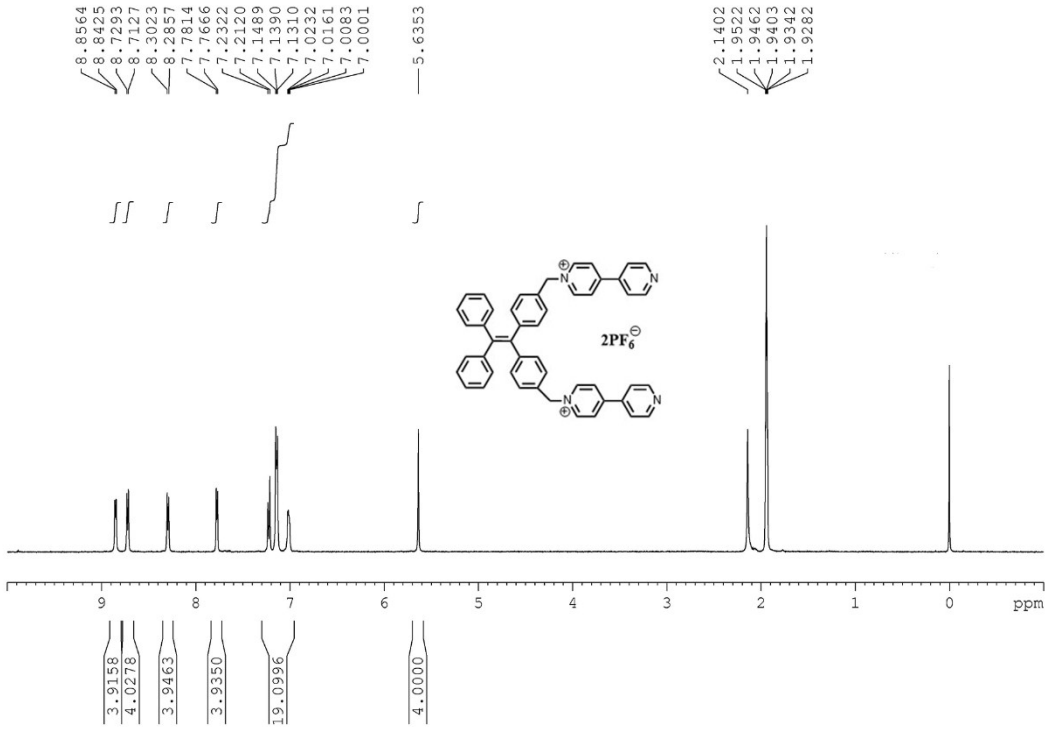

Figure S6. ^{1}H NMR spectrum recorded (400 MHz, CD_3CN, RT) for **4**•$2PF_6^-$.

View Article Online
DOI: 10.1039/C9CC00599D

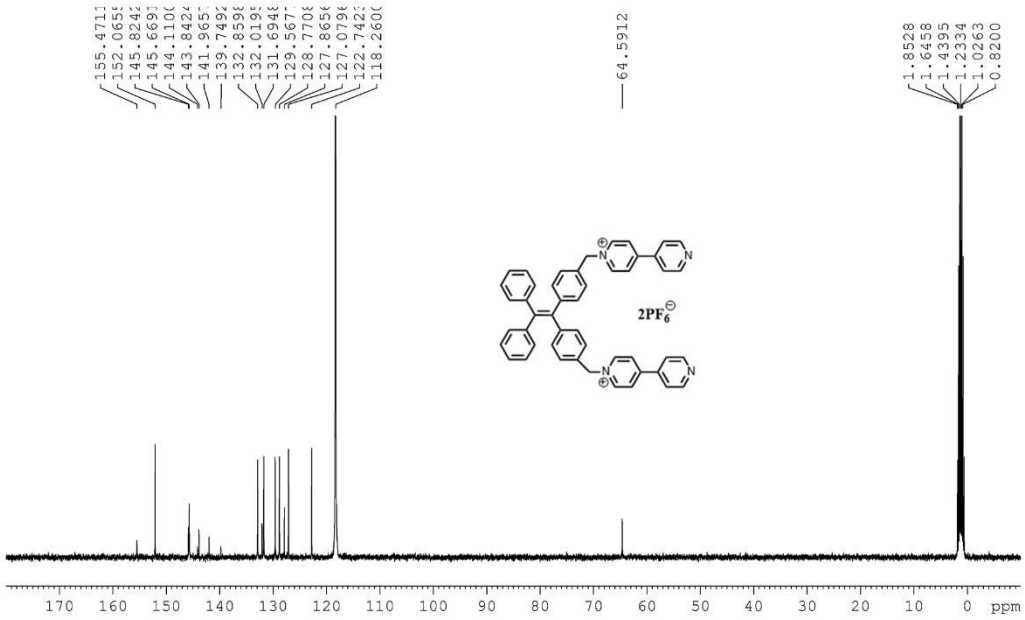

Figure S7. ^{13}C NMR spectrum recorded (100 MHz, CD_3CN, RT) for **4**•$2PF_6^-$.

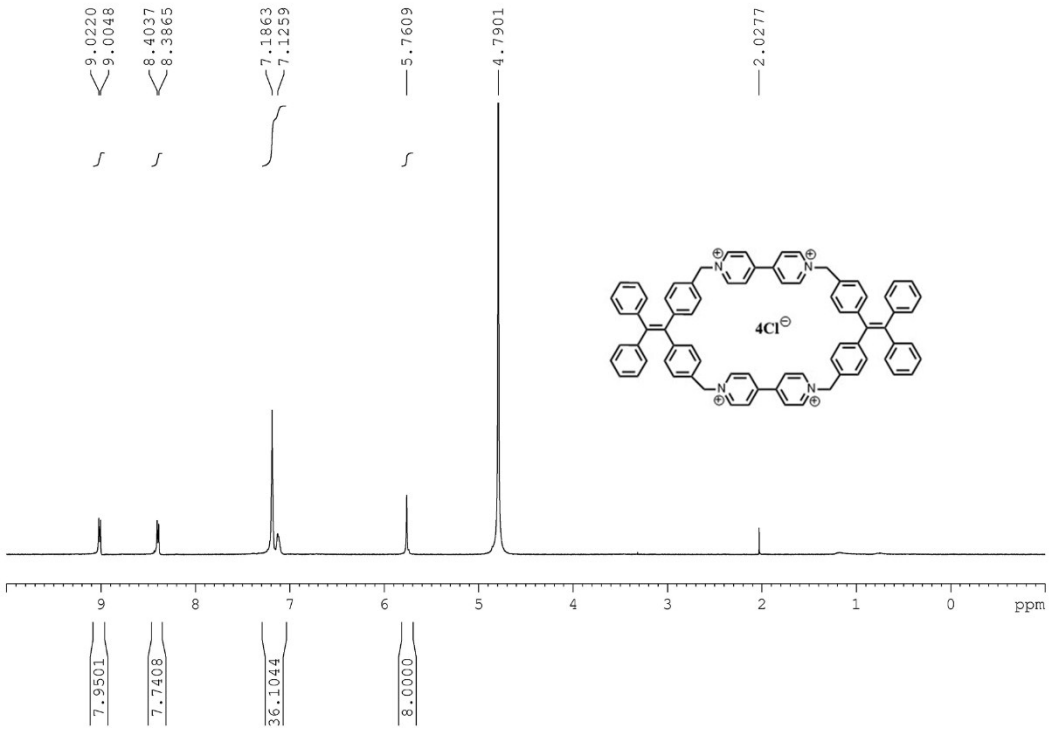

Figure S8. ^{1}H NMR spectrum recorded (400 MHz, D_2O, RT) for **2**•$4Cl^-$.

View Article Online
DOI: 10.1039/C9CC00599D

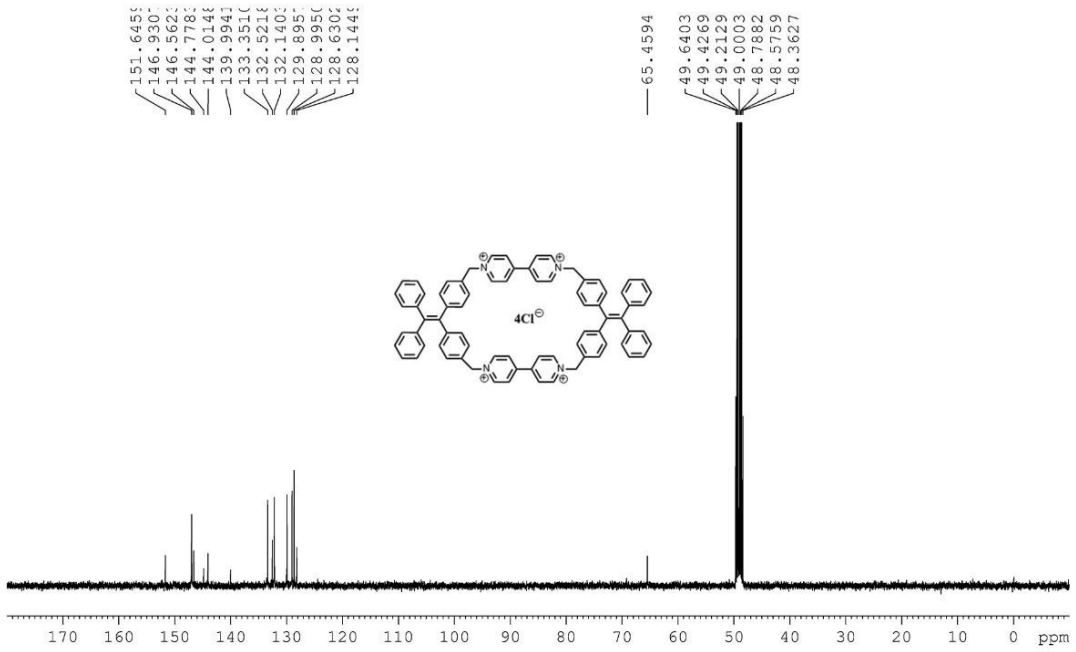

Figure S9. ^{13}C NMR spectrum recorded (100 MHz, CD_3OD, RT) for **2**•4Cl^-.

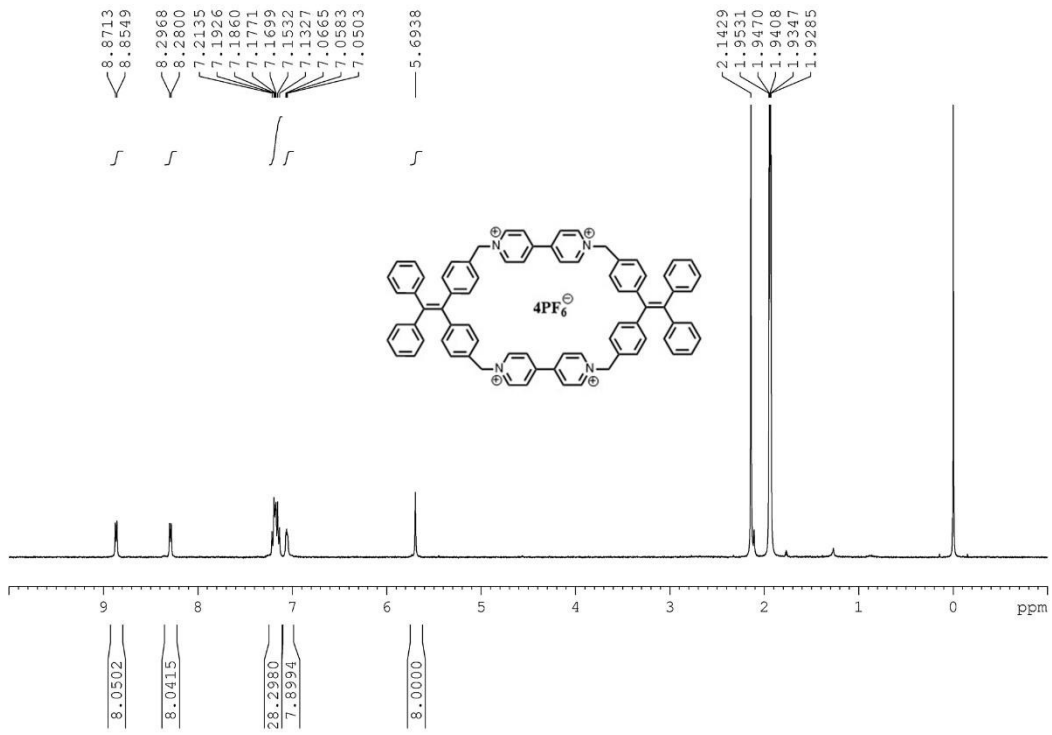

Figure S10. ^{1}H NMR spectrum recorded (400 MHz, CD_3CN, RT) for **2**•4PF_6^-.

View Article Online
DOI: 10.1039/C9CC00599D

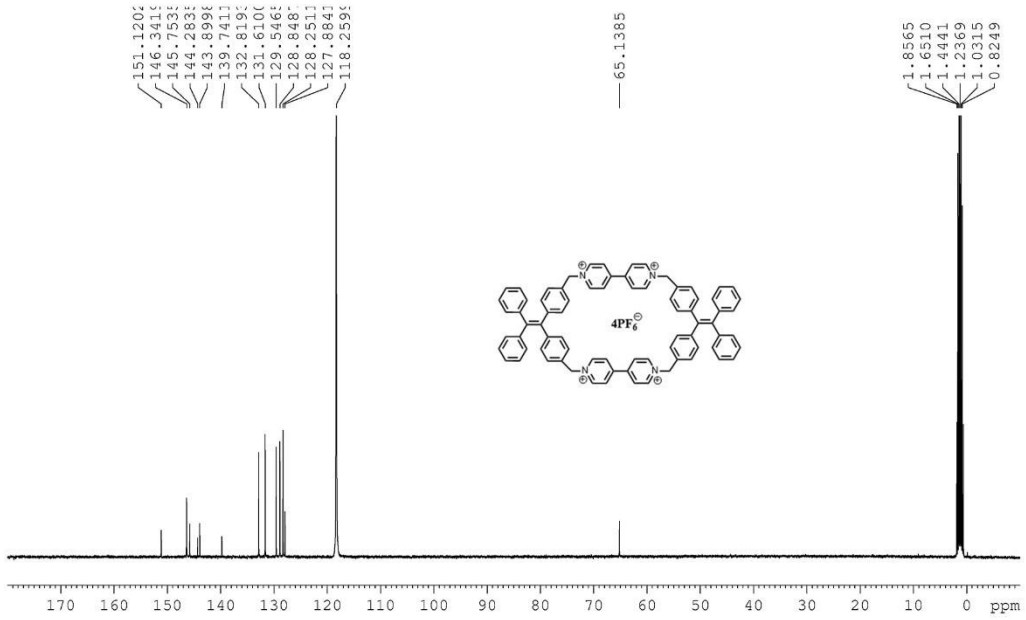

Figure S11. ^{13}C NMR spectrum recorded (100 MHz, CD_3CN, RT) for **2**•4PF_6^-.

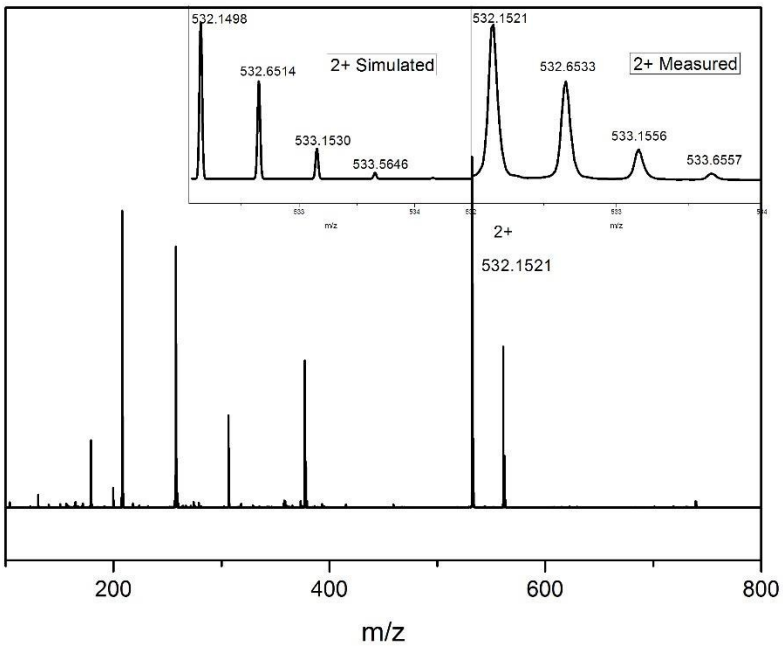

Figure S12. ESI-MS spectrum of **1**•4PF_6^- in CH_3CN. Expansions confirm the expect m/z spacing of 0.5 for the 2^+ ion.

View Article Online
DOI: 10.1039/C9CC00599D

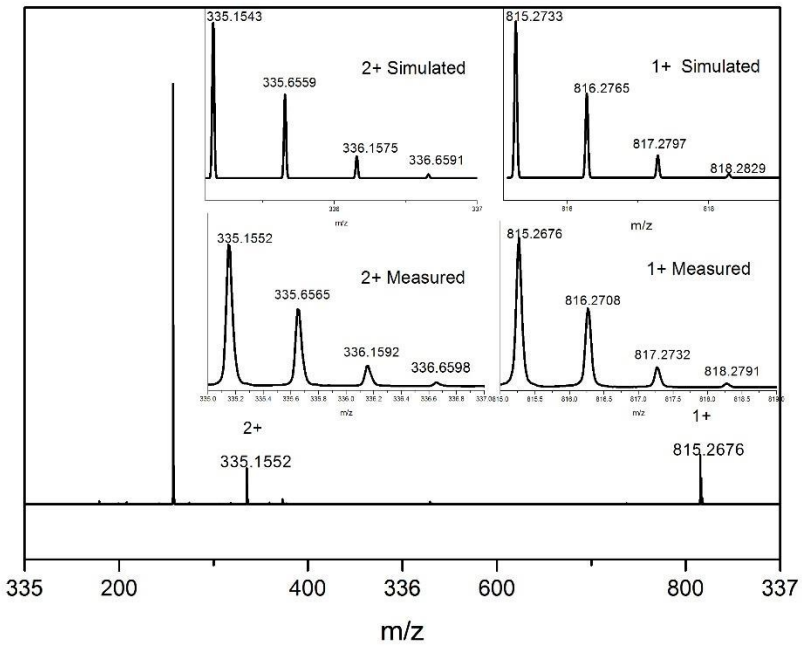

Figure S13. ESI-MS spectrum of **4**•2PF_6^- in CH_3CN. Expansions confirm the expect m/z spacing of 0.5 for the 2^+ ion and 1 for the 1^+ ion.

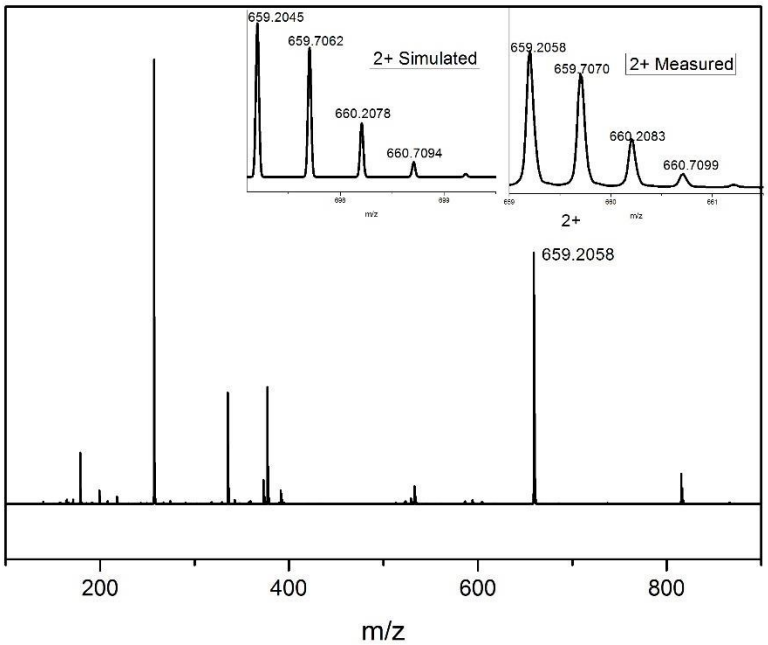

Figure S14. ESI-MS spectrum of **2**•4PF_6^- in CH_3CN. Expansions confirm the expect m/z spacing of 0.5 for the 2^+ ion.

View Article Online
DOI: 10.1039/C9CC00599D

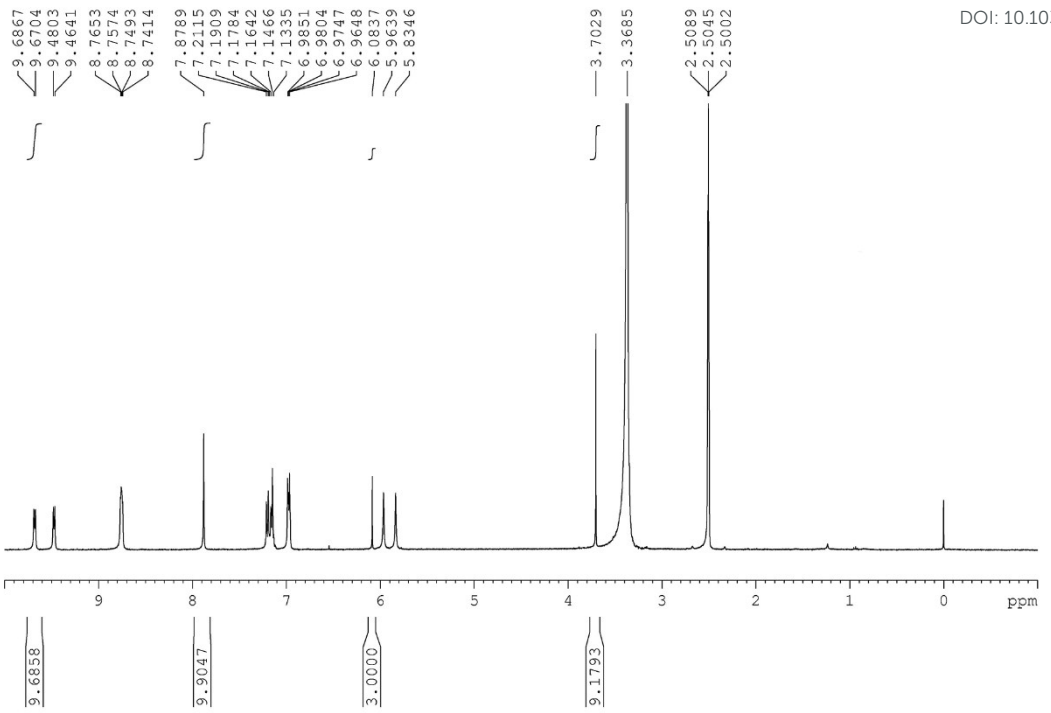

Figure S15. ^{1}H NMR of **1**•4Cl^{-} (400 MHz, DMSO-d_6), 20 mM (20 μL) 1,3,5-trimethoxy-benzen as internal reference. The solubility of **1**•4Cl^{-} (20 μL D_2O solution was dried in high vacuum) was calculated to be 48.98 mM (an average value of two sets of data).

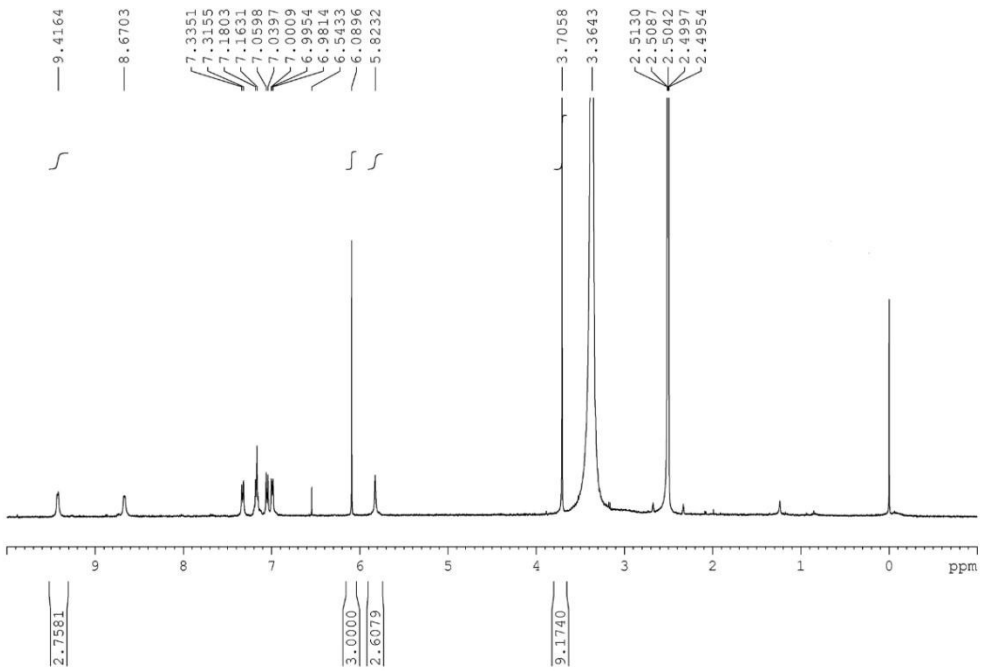

Figure S16. ^{1}H NMR of **2**•4Cl^{-} (400 MHz, DMSO-d_6), 20 mM (20 μL) 1,3,5-trimethoxy-benzen as internal reference. The solubility of **2**•4Cl^{-} (40 μL D_2O solution

was dried in high vacuum) was calculated to be 3.36 mM (an average value of two sets of data).

Table S1. **Crystal Data and Structure Refinement for Cyclophane 1•4PF_6^- and 2•4PF_6^-**

Parameters	**Cyclophane 1•4PF_6^-**	**Cyclophane 2•4PF_6^-**
Empirical formula	$C_{57.50}H_{48.50}Cl_{3.50}F_{24}N_4P_4$	$C_{108}H_{140}F_{24}N_4O_8P_4$
Formula weight	1499.46	2202.11
Temperature (K)	153(2)	153(2)
Wavelenghth (Å)	0.71073	0.71073
Crystal system	Monoclinic	Orthorhombic
Space group	*P* $2_1/c$	*C m c a*
a, (Å)	28.8044(17)	39.900(11)
b, (Å)	13.8129(8)	9.539(3)
c, (Å)	17.8677(10)	26.857(8)
α, (°)	90	90
β, (°)	91.3700(10)	90
γ, (°)	90	90
V (Å^3)	7107.0(7)	10222(5)
Z	4	4
ρ_{calcd} (g/cm^3)	1.401	1.431
μ (mm^{-1})	0.339	0.178
F(000)	3028	4624
Crystal size (mm^3)	0.250×0.200×0.200	0.250×0.250×0.200
θ range for data collection (°)	2.280 to 25.242	1.828 to 25.387
Limiting indices	$-30 \le h \le 34$ $-16 \le k \le 16$ $-18 \le l \le 21$	$-47 \le h \le 45$ $-11 \le k \le 11$ $-32 \le l \le 32$
Reflections collected	79616/13052	45361 / 4749
Refinement method	Full-matrix least-squares on F^2	Full-matrix least-squares on F^2
Data/restraints/parameters	13052/1587/903	4749/486/309
Goodness-of-fit[c]	1.078	1.084
*R*1,[a] *wR*2[b] ($I > 2\sigma(I)$)	0.0998, 0.2686	0.0729, 0.2589
*R*1,[a] *wR*2[b] (all data)	0.1145, 0.2799	0.0900, 0.2750
Largest diff. peak and hole, e Å^{-3}	0.880 and -1.062	0.306 and -0.444
CCDC	1870620	1870621

[a]$R1 = \Sigma||F_o|-|F_c||/\Sigma|F_o|$. [b]$wR2 = [\Sigma[w(F_o^2-F_c^2)^2]/\Sigma[w(F_o^2)^2]]$.
[c]Quality-of-fit = $[\Sigma[w(F_o^2-F_c^2)^2]/(N_{obs}-N_{params})]^{½}$, based on all data.

View Article Online
DOI: 10.1039/C9CC00599D

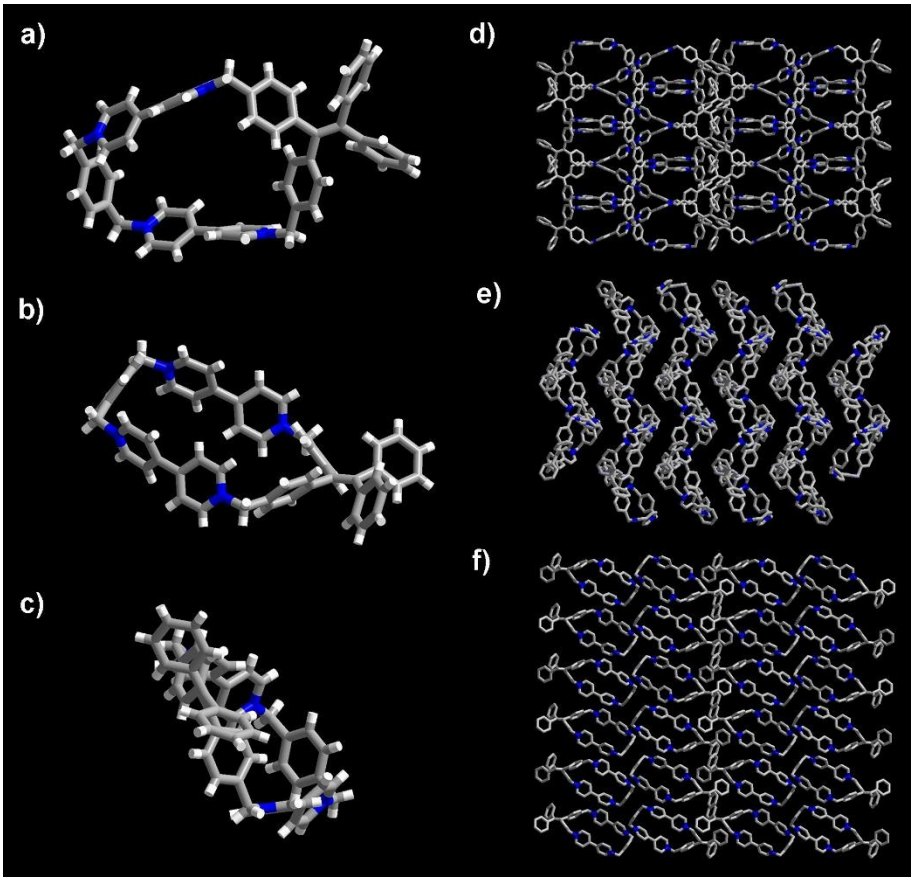

Figure S17. Solid-state (super)structures of cyclophane **1**•4PF_6^- obtained from single-crystal X-ray crystallography. a) top view, b) front view and c) side view of cyclophane **1**•4PF_6^-**.** d) top view, e) side view and f) front view of molecular packing of cyclophane **1**•4PF_6^-. Color code: N, blue; C, gray; H, white. (The solvent molecules and PF_6^- pairs are omitted.)

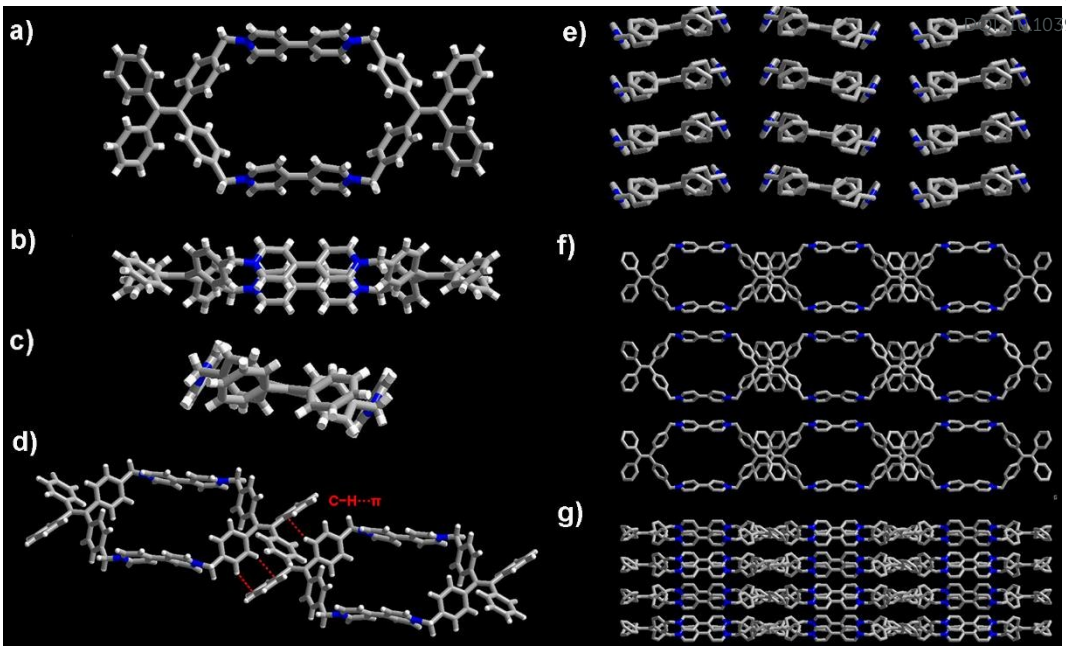

Figure S18. Solid-state (super)structures of cyclophane **2**•4PF_6^- obtained from single-crystal X-ray crystallography. a) front view, b) top view and c) side view of cyclophane **2**•4PF_6^-. d) neighboring **2**•4PF_6^- molecules contact with each other through C–H···π interactions. e) side view, f) front view and g) top view of molecular packing of cyclophane **2**•4PF_6^-. Color code: N, blue; C, gray; H, white. (The solvent molecules and PF_6^- pairs are omitted.)

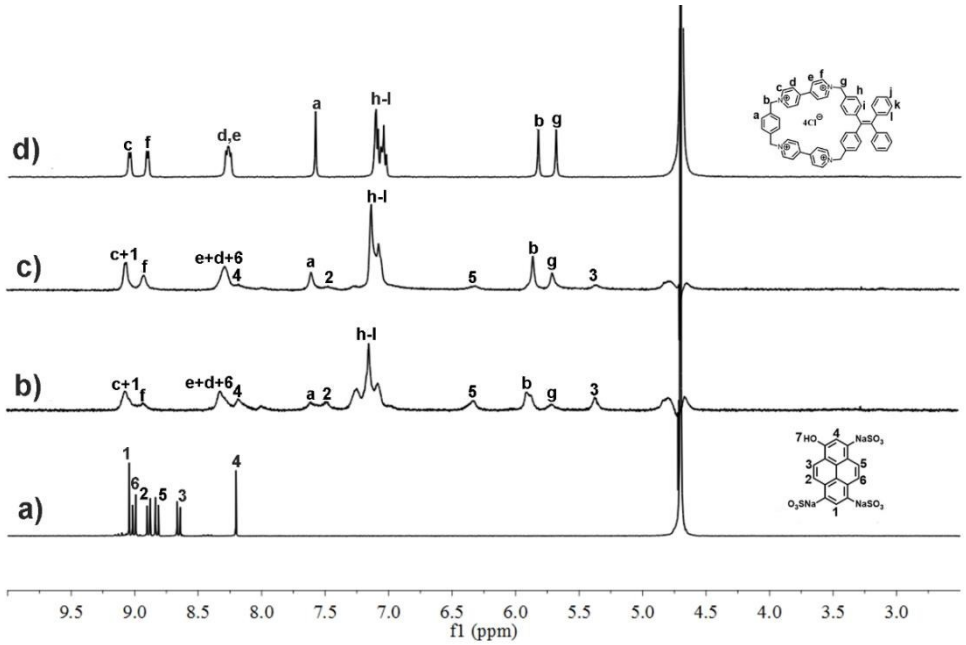

Figure S19. ^{1}H NMR spectra (400MHz, D_2O, phosphate buffer, pH = 7.4): a) HPTS

(0.4 mM); b) HPTS (0.4 mM) and **1**•4Cl$^-$ (0.4 mM); c) HPTS (0.4 mM) and **1**•4Cl$^-$ (0.8 mM); d) **1**•4Cl$^-$ (0.4 mM) at 298K.

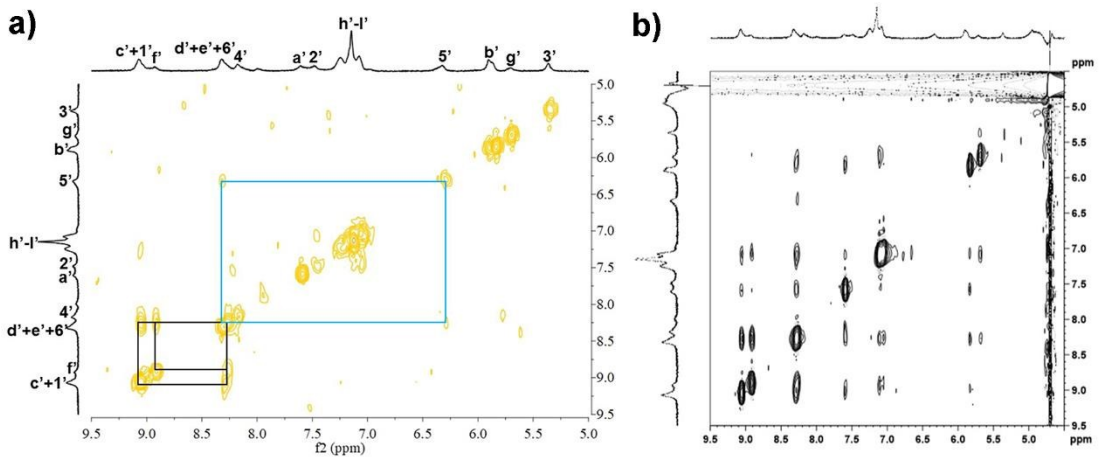

Figure S20. a) COSY and b) NOSEY ^{1}H NMR spectrum recorded (400 MHz, D_2O, 298 K) for **1**•4Cl$^-$ (0.4 mM) with HPTS (0.4 mM).

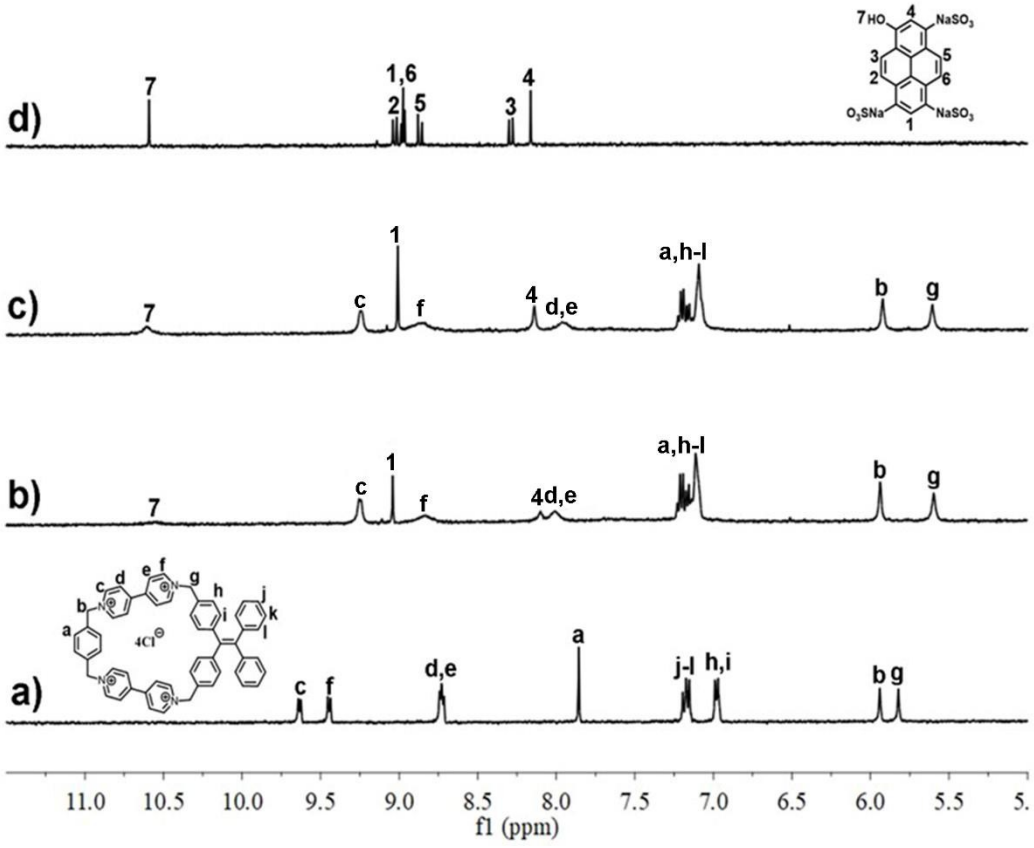

Figure S21. ^{1}H NMR spectra (400MHz, DMSO-d_6): a) **1**•4Cl$^-$ (0.4 mM); b) **1**•4Cl$^-$ (0.4 mM) and HPTS (0.4 mM); c) **1**•4Cl$^-$ (0.4 mM) and HPTS (0.8 mM); d) HPTS (0.4 mM)**.**

View Article Online
DOI: 10.1039/C9CC00599D

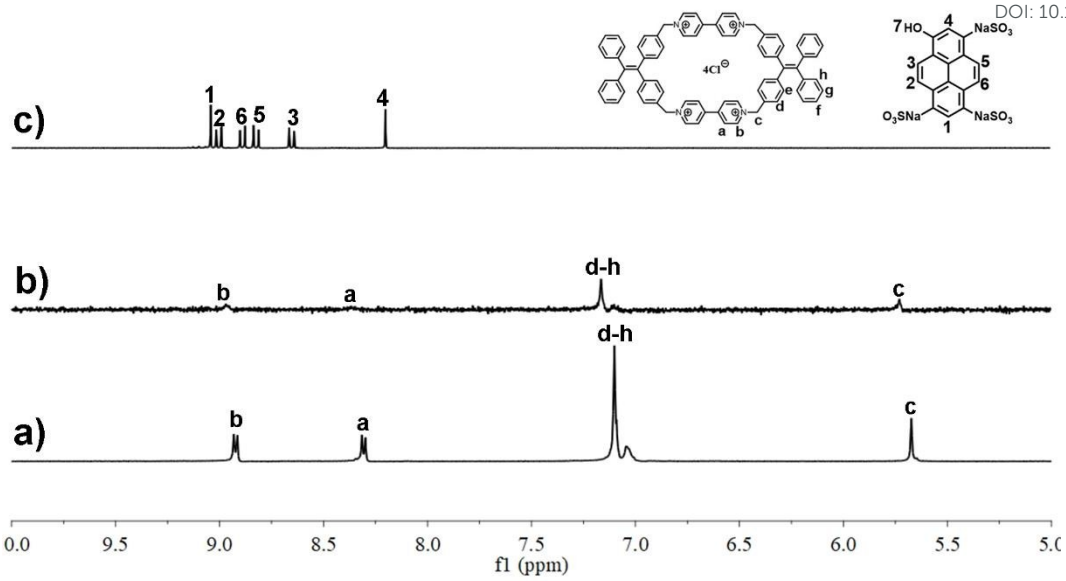

Figure S22. ^{1}H NMR spectra (400MHz, D_2O, phosphate buffer, pH=7.4): a) **2**•4Cl$^-$ (0.4 mM); b) **2**•4Cl$^-$ (0.4 mM) and HPTS (0.4 mM); c) HPTS (0.4 mM) at 298K.

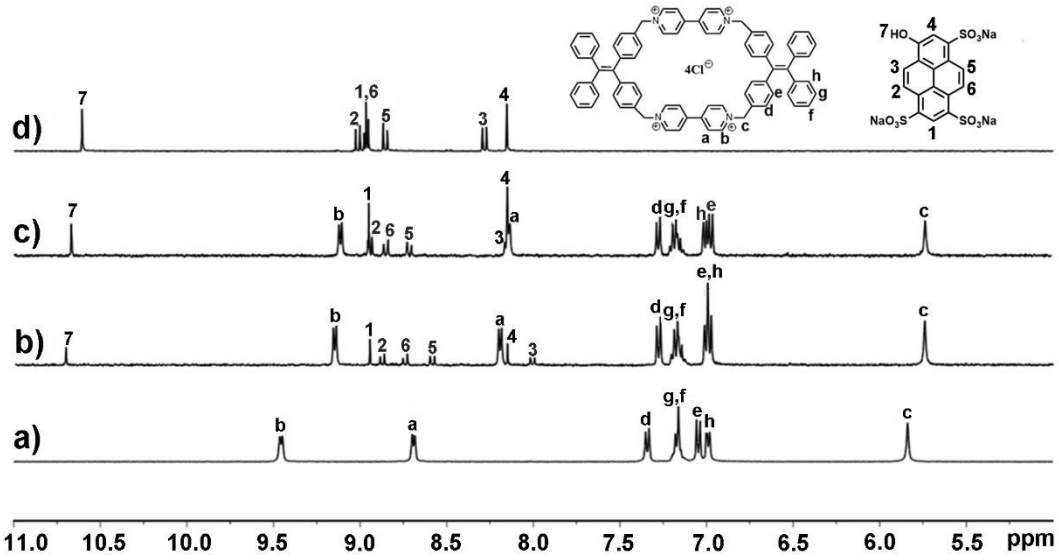

Figure S23. ^{1}H NMR spectra (400 MHz, DMSO-d_6): a) **2**•4Cl$^-$ (0.4 mM); b) **2**•4Cl$^-$ (0.4 mM) and HPTS (0.4 mM); c) **2**•4Cl$^-$ (0.4 mM) and HPTS (0.8 mM); d) HPTS (0.4 mM)**.**

View Article Online
DOI: 10.1039/C9CC00599D

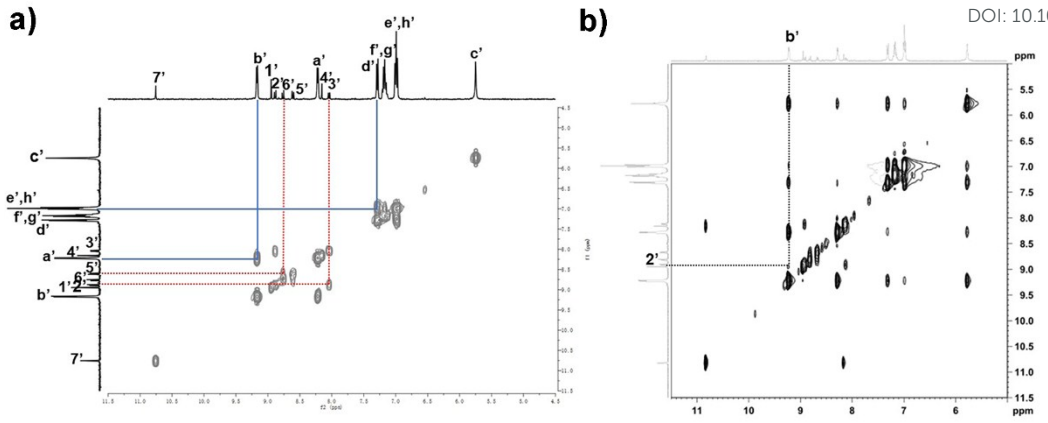

Figure S24. a) COSY and b) NOSEY ^{1}H NMR spectrum recorded (400 MHz, DMSO-d_6, 298 K) for **2**•4Cl^{-} (1.0 mM) with HPTS (1.0 mM).

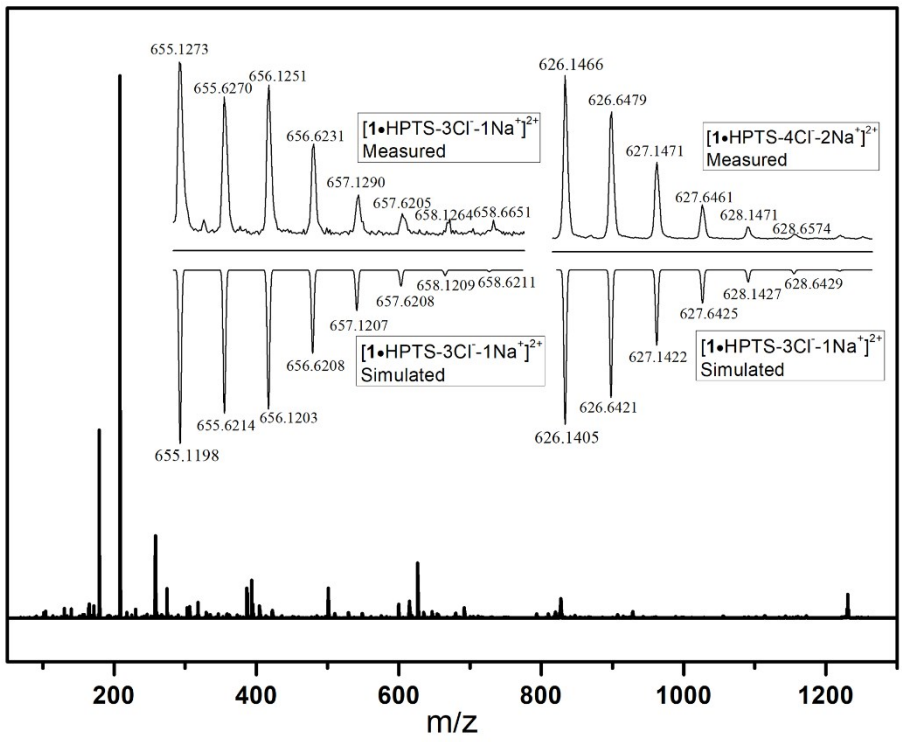

Figure S25. ESI-MS spectrum of **1**•HPTS.

View Article Online
DOI: 10.1039/C9CC00599D

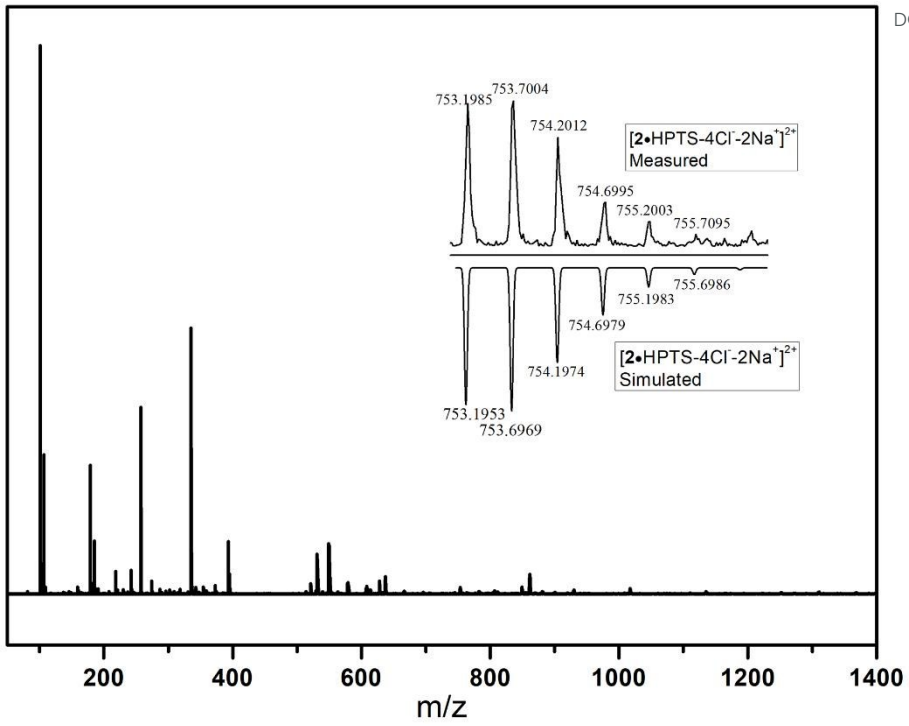

Figure S26. ESI-MS spectrum of **2**•HPTS.

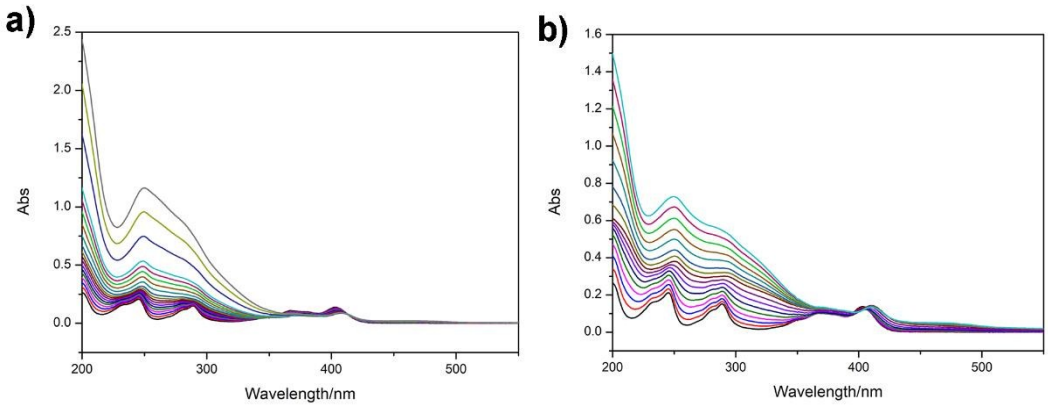

Figure S27. UV-vis absorption of HPTS (5 μmol) in phosphate buffer (pH = 7.4) upon addition of a) **1**•4Cl$^-$ and b) **2**•4Cl$^-$.

View Article Online
DOI: 10.1039/C9CC00599D

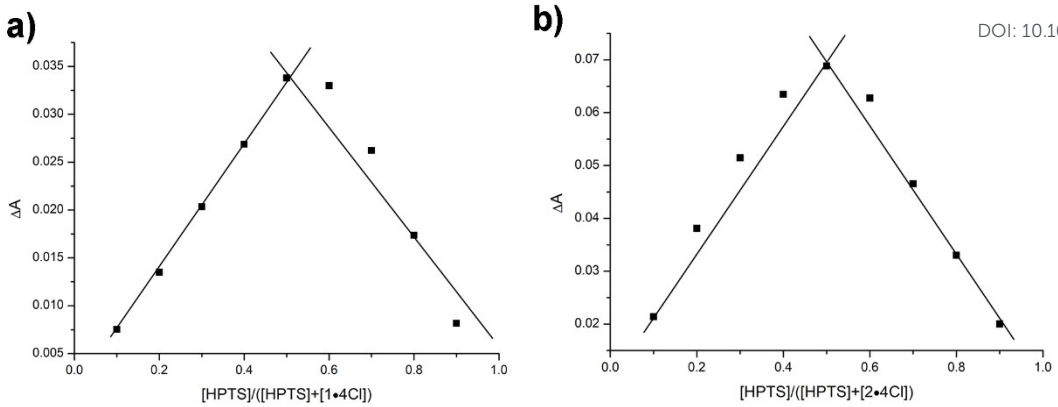

Figure S28. Job's plots obtained by recording the absorption a) at 349 nm for the solution of **1**•4Cl$^-$ and HPTS ([**1**•4Cl$^-$]+[HPTS] = 10 μmol) , b) at 403 nm for the solution of **2**•4Cl$^-$ and HPTS ([**2**•4Cl$^-$]+[HPTS] = 10 μmol) in phosphate buffer (pH = 7.4) at RT, confirming the 1:1 stoichiometry of both complexes.

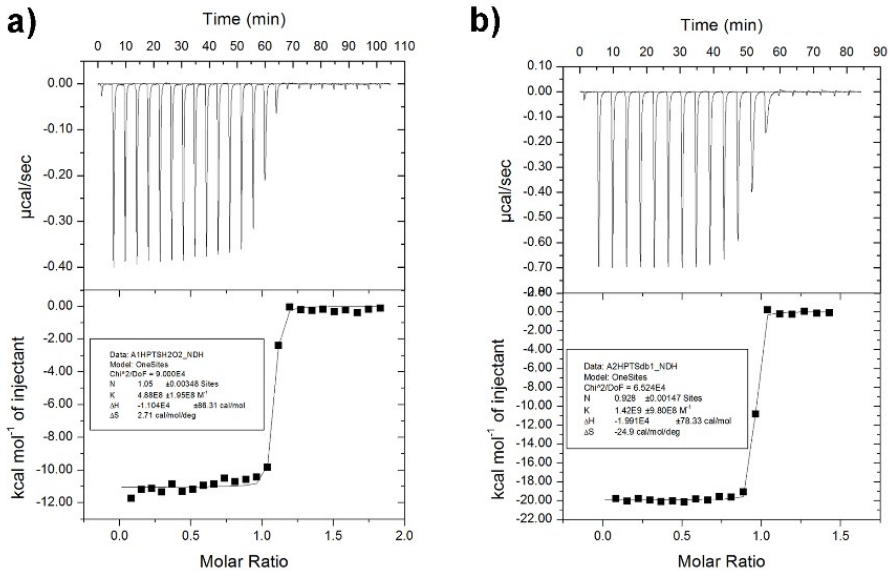

Figure S29. a) ITC titration of **1**•4Cl$^-$ (0.1 mM) with HPTS (0.01 mM) in phosphate buffer (pH = 7.4); b) ITC titration of **2**•4Cl$^-$ (0.1 mM) with HPTS (0.01 mM) in phosphate buffer (pH = 7.4).

View Article Online
DOI: 10.1039/C9CC00599D

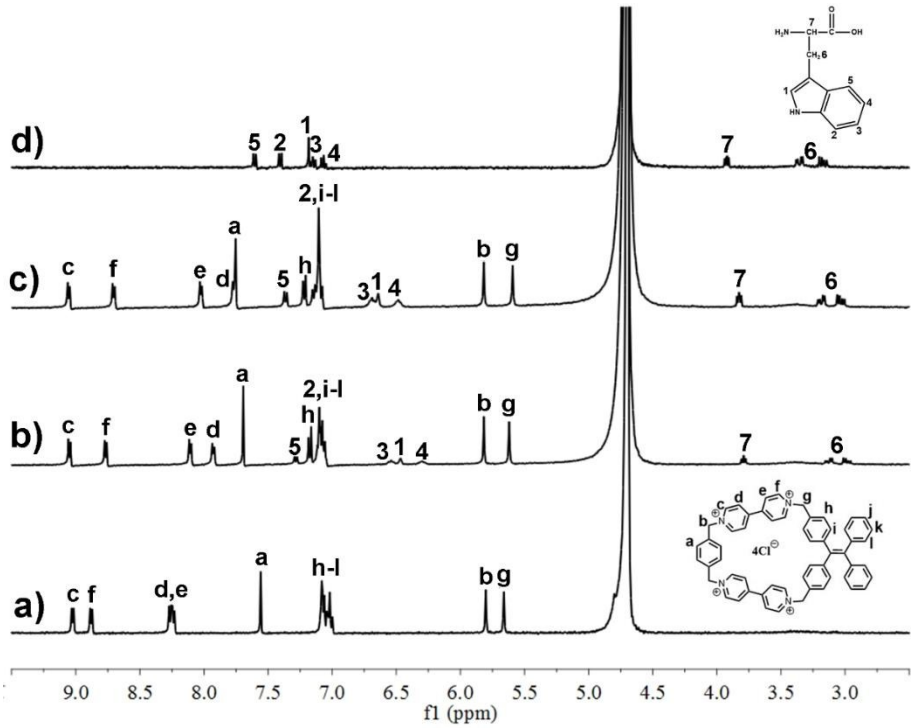

Figure S30. ^{1}H NMR spectra (400MHz, D_2O, phosphate buffer, pH = 7.4): a) **1**•4Cl$^-$ (0.4 mM); b) **1**•4Cl$^-$ and tryptophan (0.4 mM); c) **1**•4Cl$^-$ and tryptophan (0.8 mM); d) tryptophan (0.4 mM) at 298K.

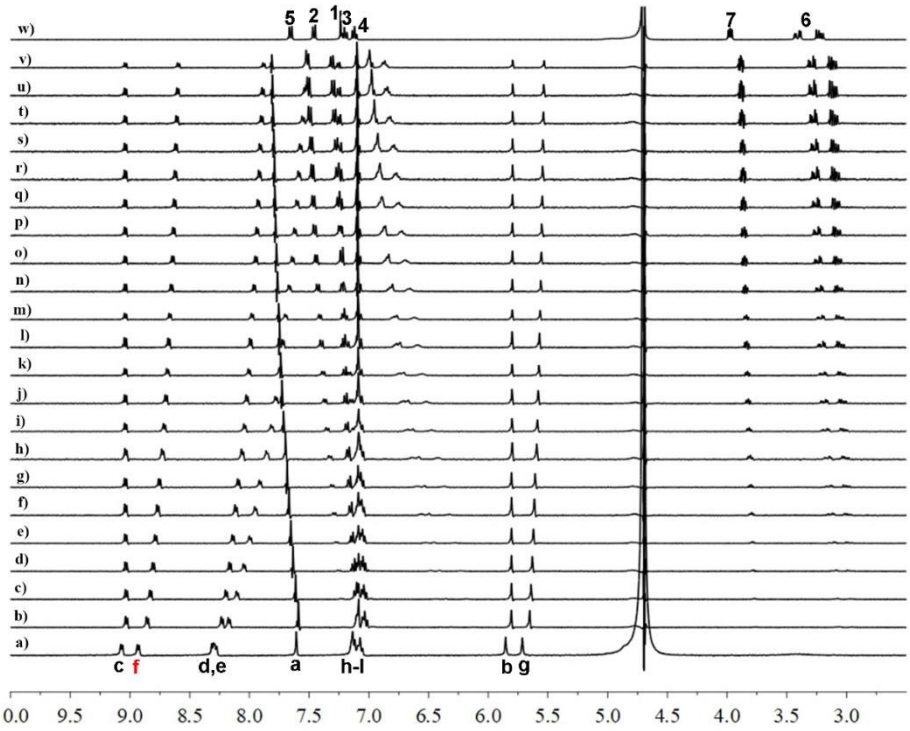

Figure S31. ^{1}H NMR spectra (400 MHz, D_2O, phosphate buffer, pH = 7.4, 298 K) of **1**•4Cl$^-$ at a concentration of 0.40 mM upon the addition of tryptophan**:** a) 0.00 mM, b)

0.08 mM, c) 0.16 mM, d) 0.24 mM, e) 0.32 mM, f) 0.40 mM, g) 0.48 mM, h) 0.60 mM, i) 0.72 mM, j) 0.84 mM, k) 0.96 mM, l) 1.08 mM, m) 1.20 mM, n) 1.40 mM, o) 1.60 mM, p) 1.80 mM, q) 2.00 mM, r) 2.20 mM, s) 2.40 mM, t) 2.80 mM, u) 3.20 mM, v) 3.60 mM, w) 4.00 mM.

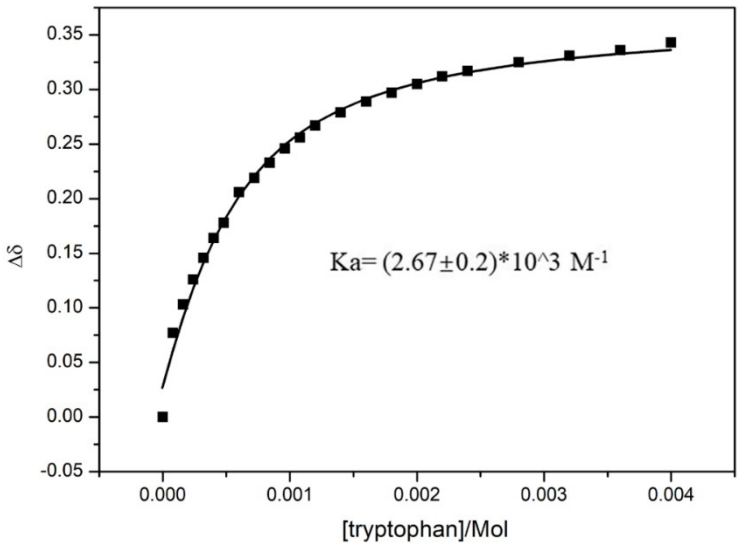

Figure S32. Non-linear fitting curve of the chemical shift changes of H_f of **1**•4Cl^- versus the concentration of tryptophan.

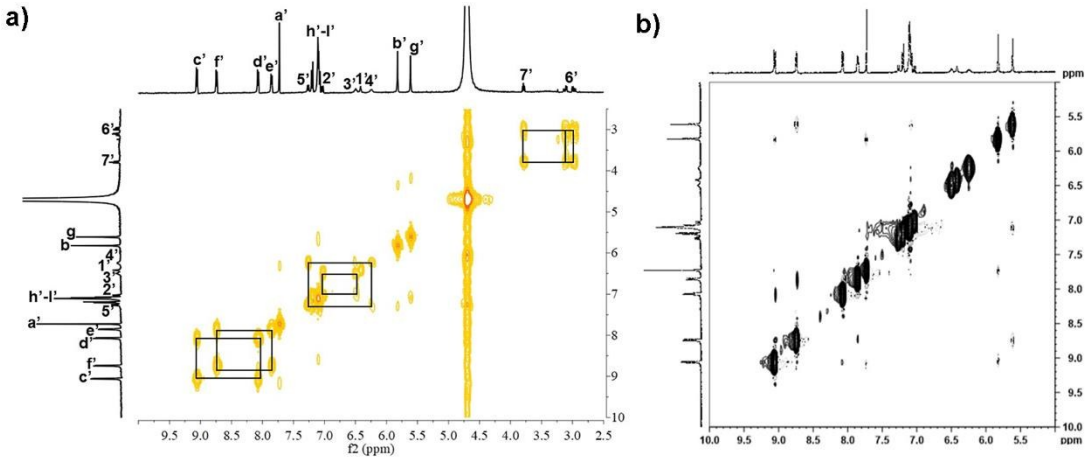

Figure S33. a) COSY and b) NOESY ^{1}H NMR spectrum recorded (400 MHz, D_2O, 298 K) for **1**•4Cl^- (0.4mM) with tryptophan (0.4 mM).

View Article Online
DOI: 10.1039/C9CC00599D

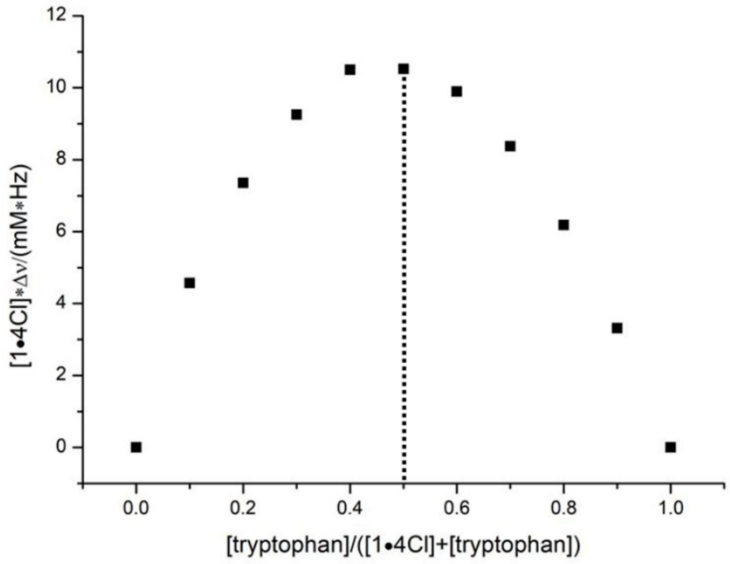

Figure S34. ^{1}H-NMR spectral Job-plots (400MHz, D_2O, phosphate buffer, pH = 7.4, 10 mM) corresponding to the binding between **1**•4Cl^{-} and tryptophan ([**1**•4Cl^{-}] + [tryptophan] = 5×10^{-4} mM). The maximum values are determined to be 0.5 at such an overall concentration and this finding is consistent a 1:1 (host:guest) binding stoichiometry.

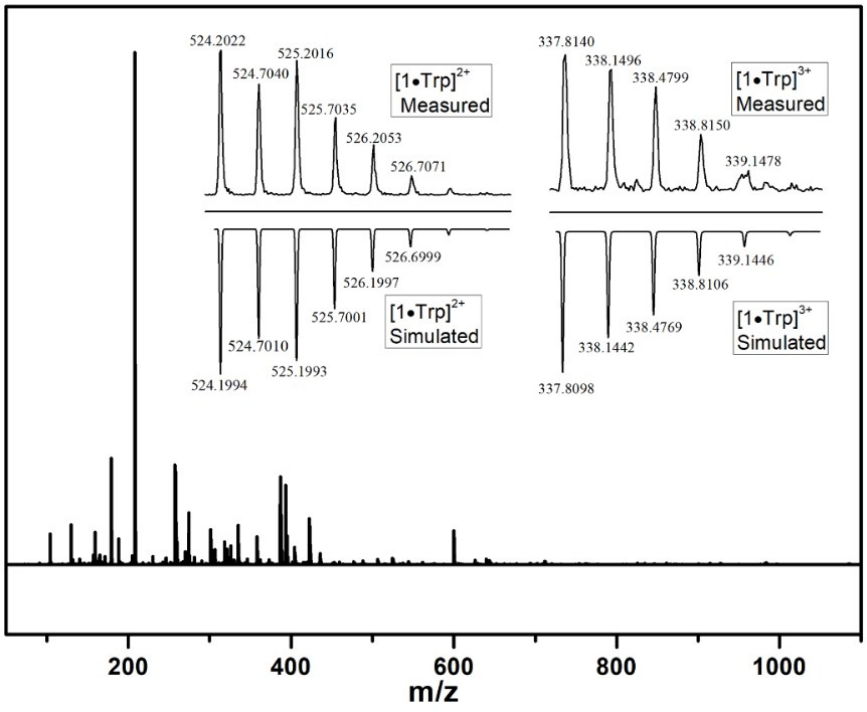

Figure S35. ESI-MS spectrum of **1**•Trp.

View Article Online
DOI: 10.1039/C9CC00599D

The method of the recognition sensitivity:

The recognition sensitivity (i.e. the detection limits) of host for guests were determined by UV-vis experiments in phosphate buffer (10 mmol, pH = 7.4). With different concentrations of 2 μL guests (Trp and ATP) solution (0, 2, 4, 6, 8, 10 μmol) were added into 2.4 mL host (1•4Cl^-) while keeping the host concentration constant (10 μmol) in all the samples. And UV-vis absorption of host-guest solution was measured after mixing homogeneously. Next, the difference ΔA between the different host-guest mixtures and host of absorption values in a certain wavelength was taken, and the linear fitting between ΔA and the corresponding guest concentration can be conducted ([guest] as the x-axis, ΔA as the y-axis). When y = 0, the obtained x value is the detection limits of guest that the lowest concentration of the guest can be detected by host.

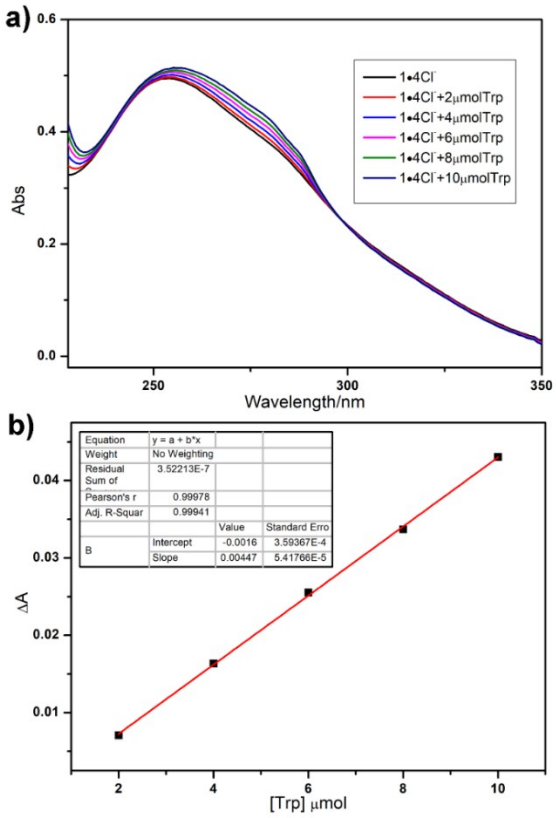

Figure S36. (a) UV-vis absorption of the **1**•4Cl^- and **1**•Trp in phosphate buffer (10 mmol, pH = 7.4) at 298K; (b) A plot of the difference of the absorption intensity ΔA at 280 nm versus the concentration of Trp. Linear Equation: y = 0.00447x - 0.0016, R^2 = 0.99941; y = 0， x = 0.36 μmol.

View Article Online
DOI: 10.1039/C9CC00599D

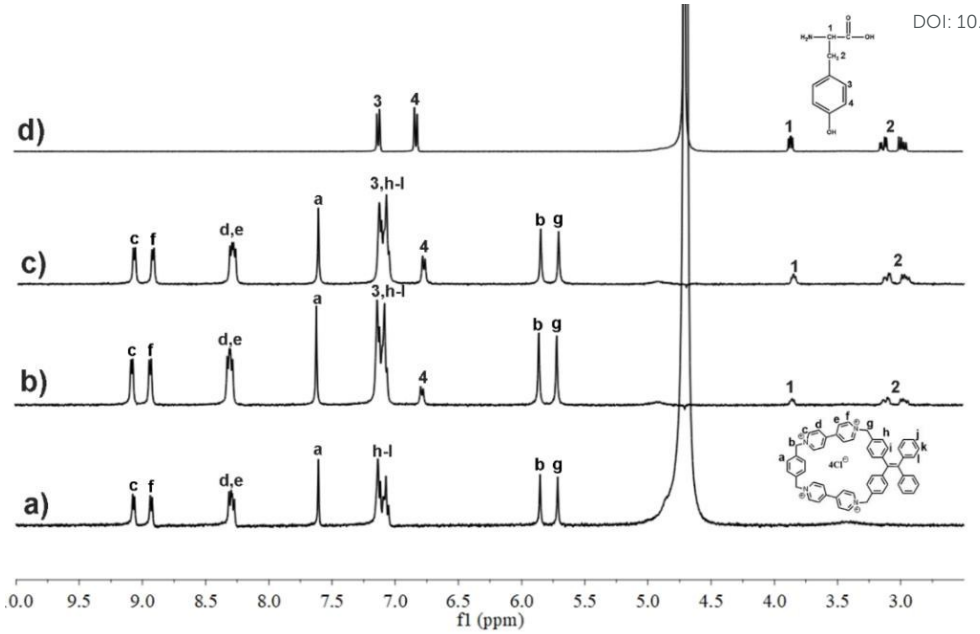

Figure S37. ^{1}H NMR spectra (400MHz, D_2O, phosphate buffer, pH=7.4): a) **1**•4Cl^- (0.4 mM); b) **1**•4Cl^- and tyrosine (0.4 mM); c) **1**•4Cl^- and tyrosine (0.8 mM); d) tyrosine (0.4 mM) at 298K.

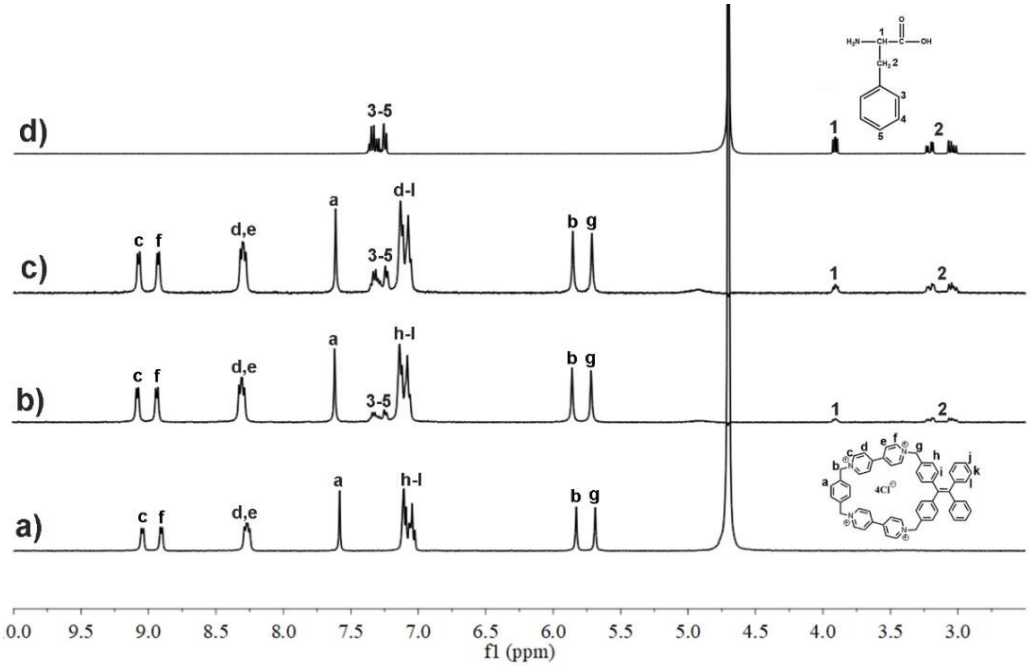

Figure S38. ^{1}H NMR spectra (400MHz, D_2O, phosphate buffer, pH=7.4): a) **1**•4Cl^- (0.4 mM); b) **1**•4Cl^- and phenylalanine (0.4 mM); c) **1**•4Cl^- (0.4 mM) and phenylalanine (0.8 mM); d) phenylalanine (0.4 mM) at 298K.

View Article Online
DOI: 10.1039/C9CC00599D

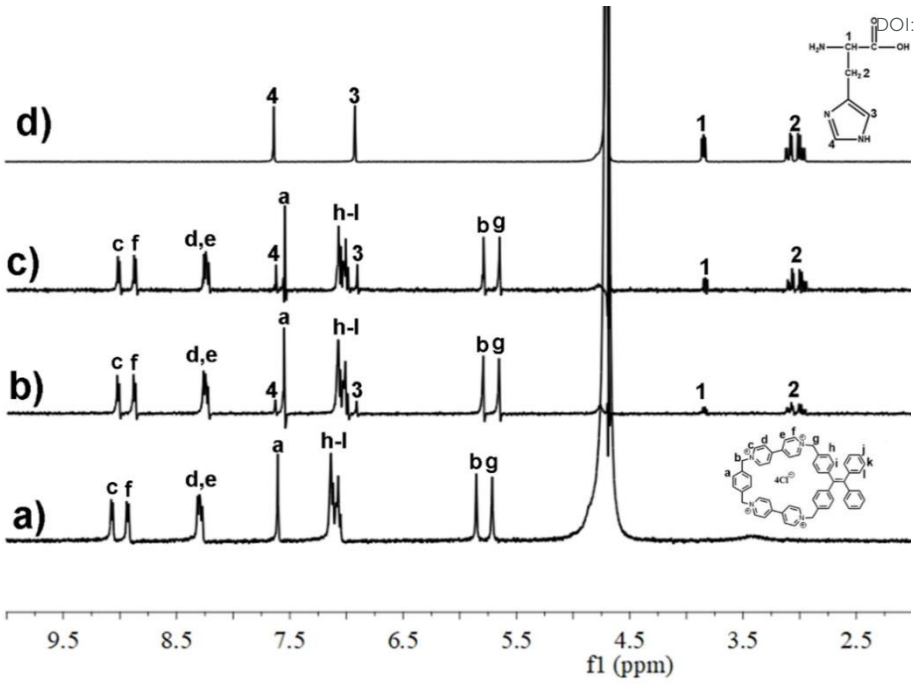

Figure S39. ^{1}H NMR spectra (400MHz, D_2O, phosphate buffer, pH=7.4): a) **1**•4Cl^- (0.4 mM); b) **1**•4Cl^- and histidine (0.4 mM); c) **1**•4Cl^- and histidine (0.8 mM); d) histidine (0.4 mM) at 298K.

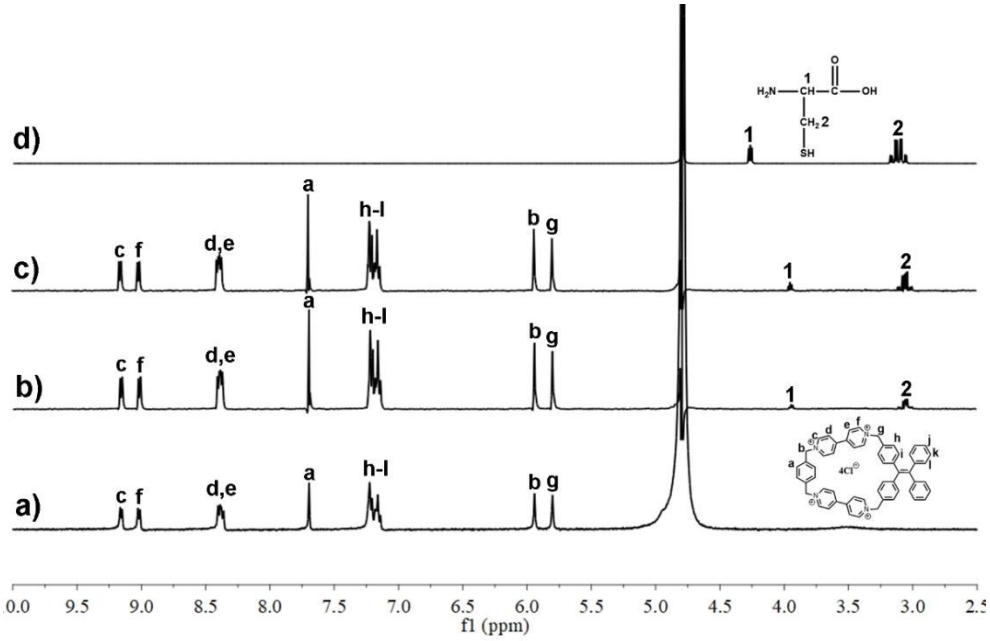

Figure S40. ^{1}H NMR spectra (400MHz, D_2O, phosphate buffer, pH=7.4): a) **1**•4Cl^- (0.4 mM); b) **1**•4Cl^- and cysteine (0.4 mM); c) **1**•4Cl^- and cysteine (0.8 mM); d) cysteine (0.4 mM) at 298K.

View Article Online
DOI: 10.1039/C9CC00599D

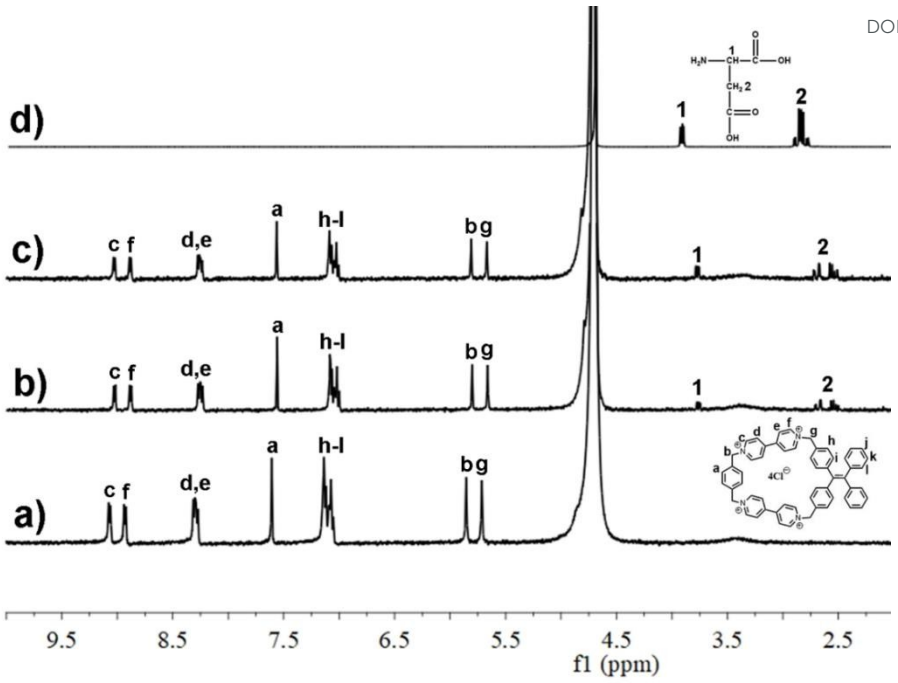

Figure S41. ^{1}H NMR spectra (400MHz, D_2O, phosphate buffer, pH=7.4): a) **1**•4Cl$^-$ (0.4 mM); b) **1**•4Cl$^-$ and aspartic acid (0.4 mM); c) **1**•4Cl$^-$ and aspartic acid (0.8 mM); d) aspartic acid (0.4 mM) at 298K.

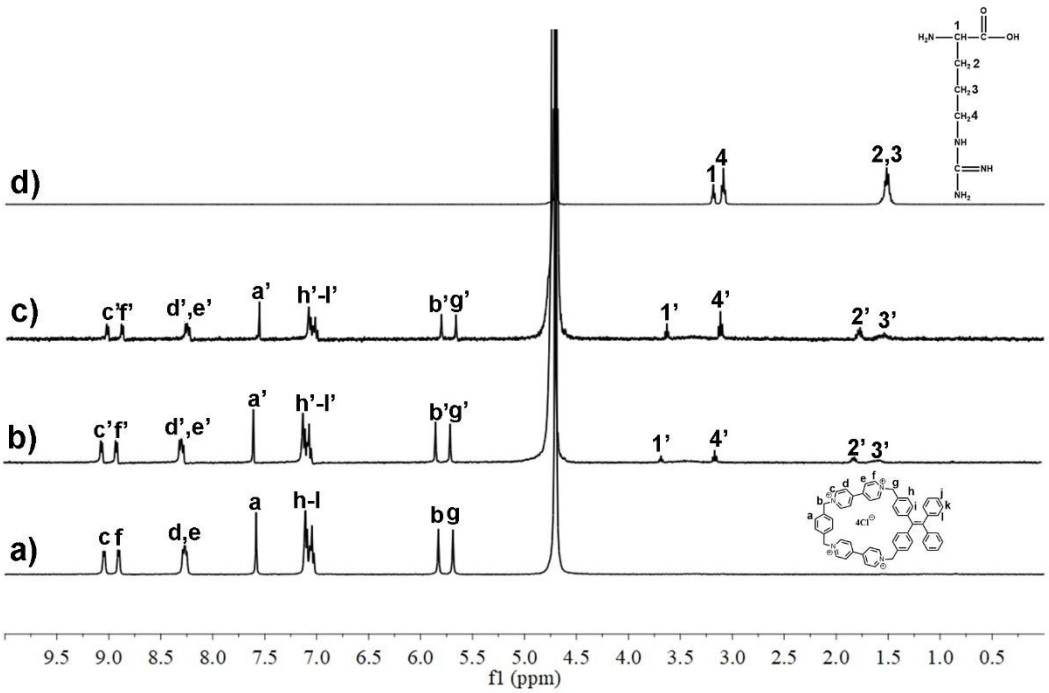

Figure S42. ^{1}H NMR spectra (400MHz, D_2O, phosphate buffer, pH=7.4): a) **1**•4Cl$^-$ (0.4 mM); b) **1**•4Cl$^-$ and arginine (0.4 mM); c) **1**•4Cl$^-$ and arginine (0.8 mM); d) arginine (0.4 mM) at 298K.

View Article Online
DOI: 10.1039/C9CC00599D

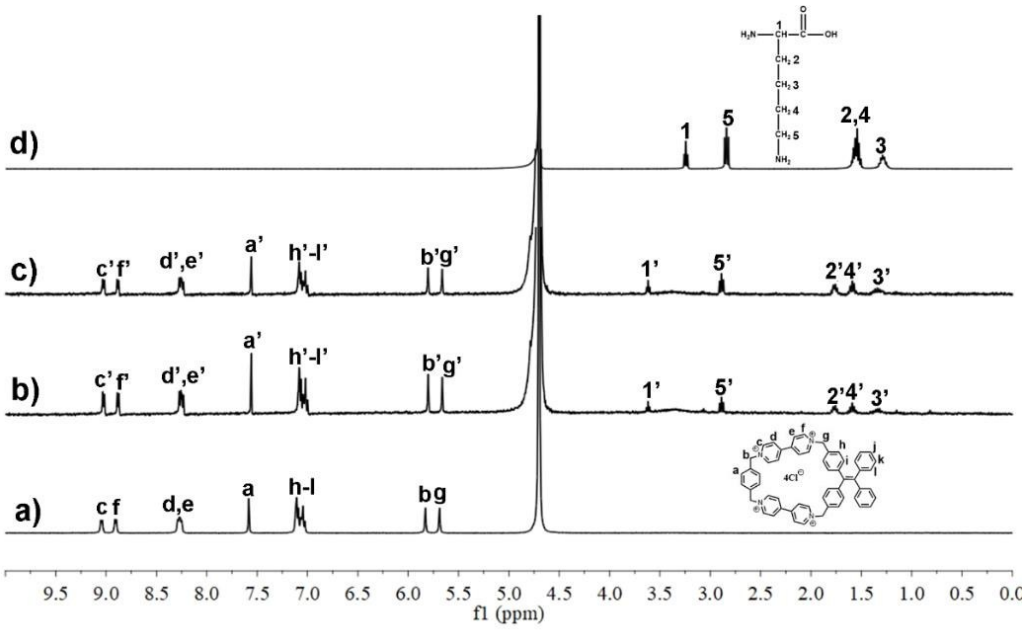

Figure S43. ^{1}H NMR spectra (400MHz, D_2O, phosphate buffer, pH=7.4): a) **1**•4Cl$^-$ (0.4 mM); b) **1**•4Cl$^-$ and lysine (0.4 mM); c) **1**•4Cl$^-$ and lysine (0.8 mM); d) lysine (0.4 mM) at 298K.

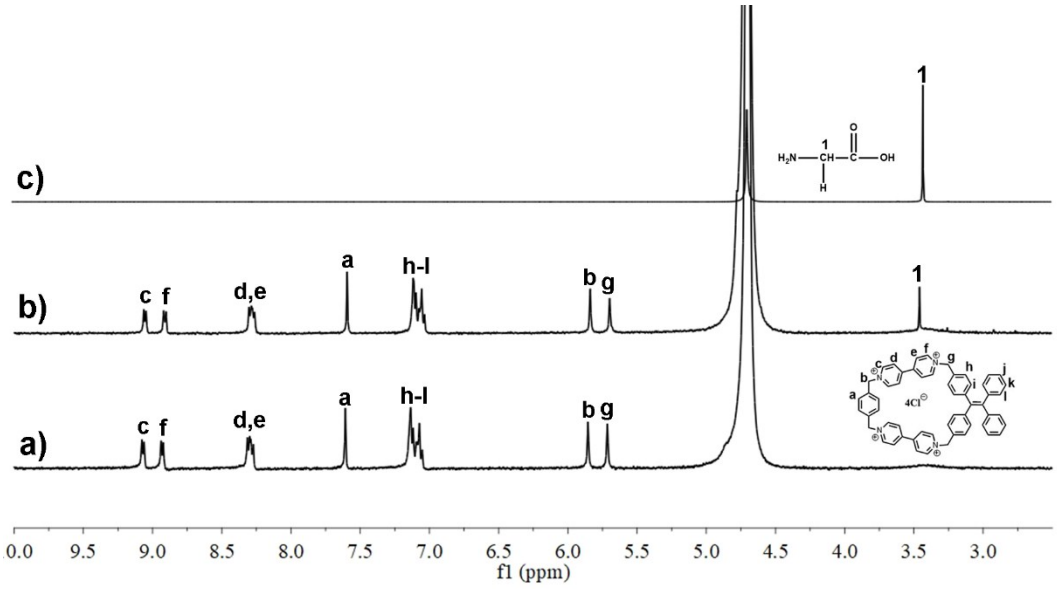

Figure S44. ^{1}H NMR spectra (400MHz, D_2O, phosphate buffer, pH=7.4): a) **1**•4Cl$^-$ (0.4 mM); b) **1**•4Cl$^-$ and glycine (0.4 mM); c) **1**•4Cl$^-$ (0.4 mM) at 298K.

View Article Online
DOI: 10.1039/C9CC00599D

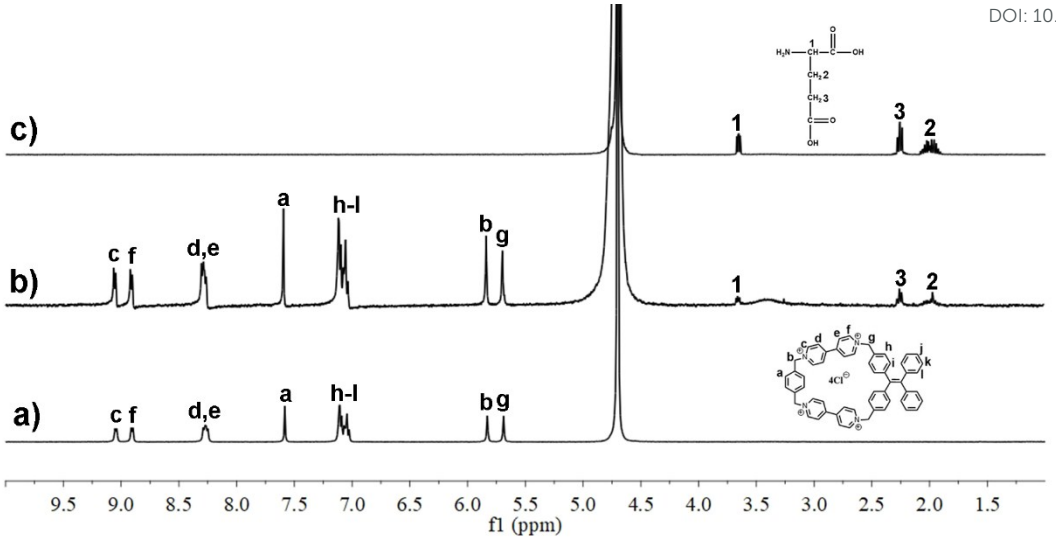

Figure S45. ^{1}H NMR spectra (400MHz, D_2O, phosphate buffer, pH=7.4): a) **1**•4Cl$^-$ (0.4 mM); b) **1**•4Cl$^-$ and glutamate (0.4 mM); c) glutamate (0.4 mM) at 298K.

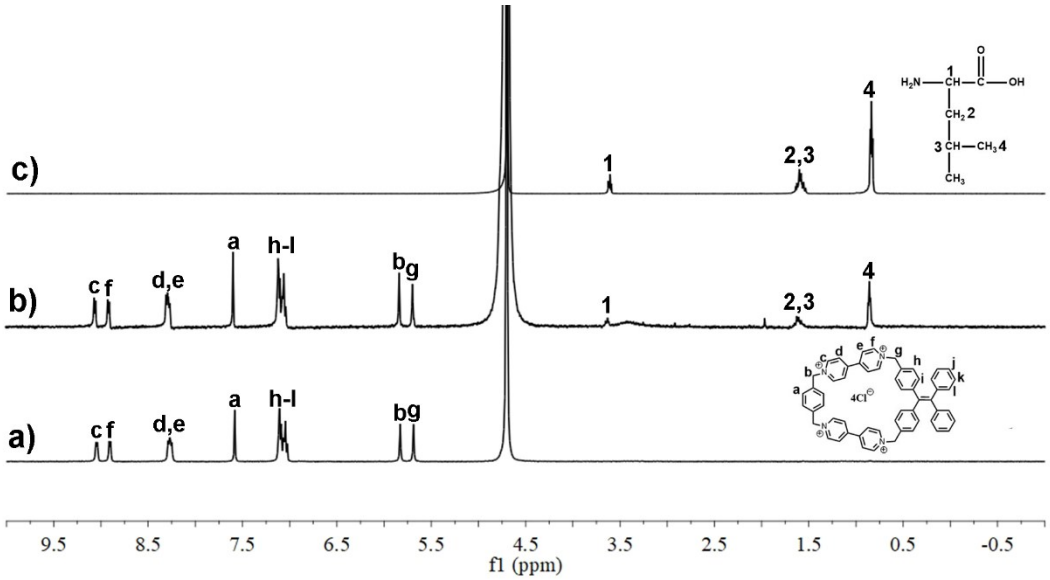

Figure S46. ^{1}H NMR spectra (400MHz, D_2O, phosphate buffer, pH=7.4): a) **1**•4Cl$^-$ (0.4 mM); b) **1**•4Cl$^-$ and leucine (0.4 mM); c) leucine (0.4 mM) at 298K.

View Article Online
DOI: 10.1039/C9CC00599D

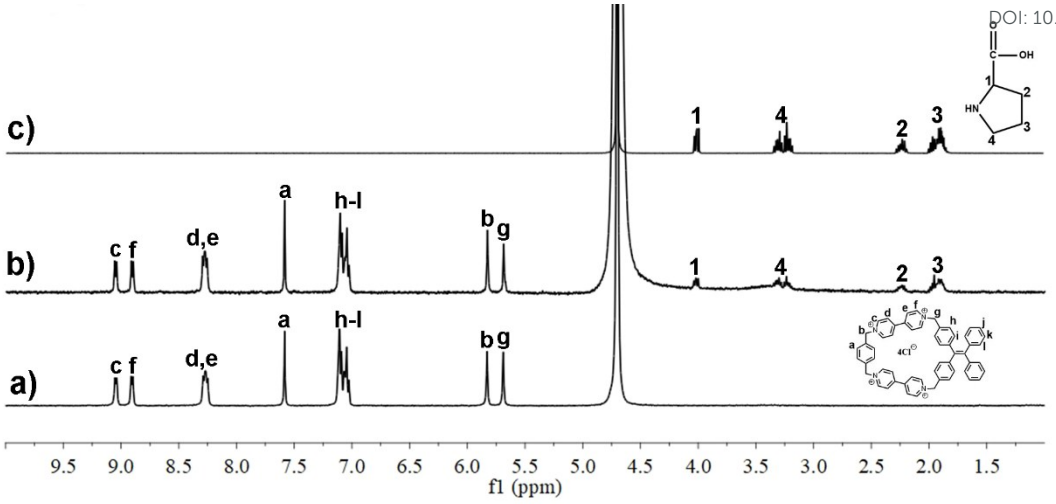

Figure S47. ^{1}H NMR spectra (400MHz, D_2O, phosphate buffer, pH=7.4): a) **1**•4Cl$^-$ (0.4 mM); b) **1**•4Cl$^-$ and proline (0.4 mM); c) proline (0.4 mM) at 298K.

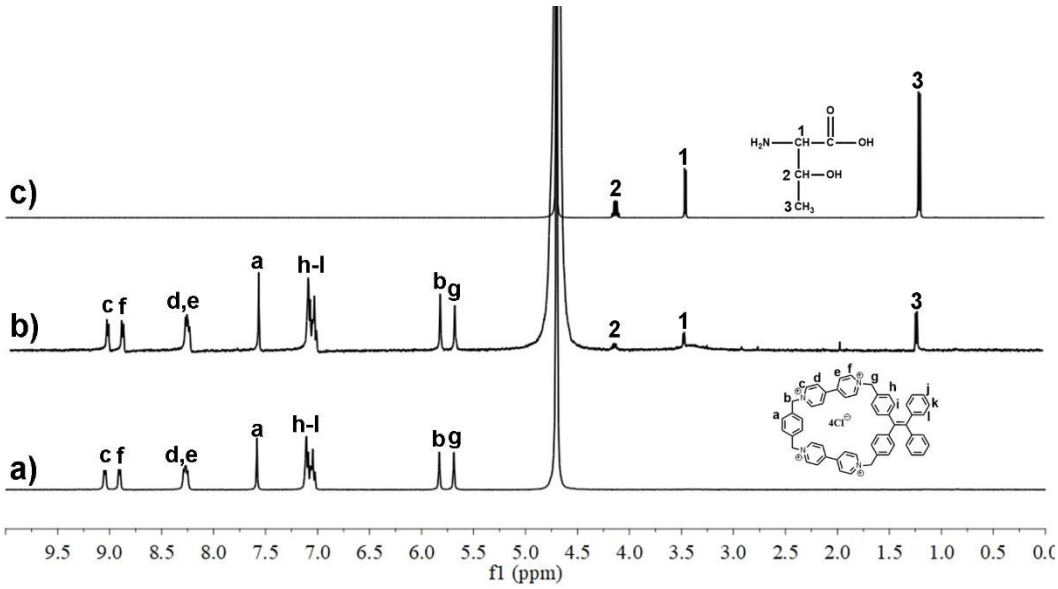

Figure S48. ^{1}H NMR spectra (400MHz, D_2O, phosphate buffer, pH=7.4): a) **1**•4Cl$^-$ (0.4 mM); b) **1**•4Cl$^-$ and threonine (0.4 mM); c) threonine (0.4 mM) at 298K.

View Article Online
DOI: 10.1039/C9CC00599D

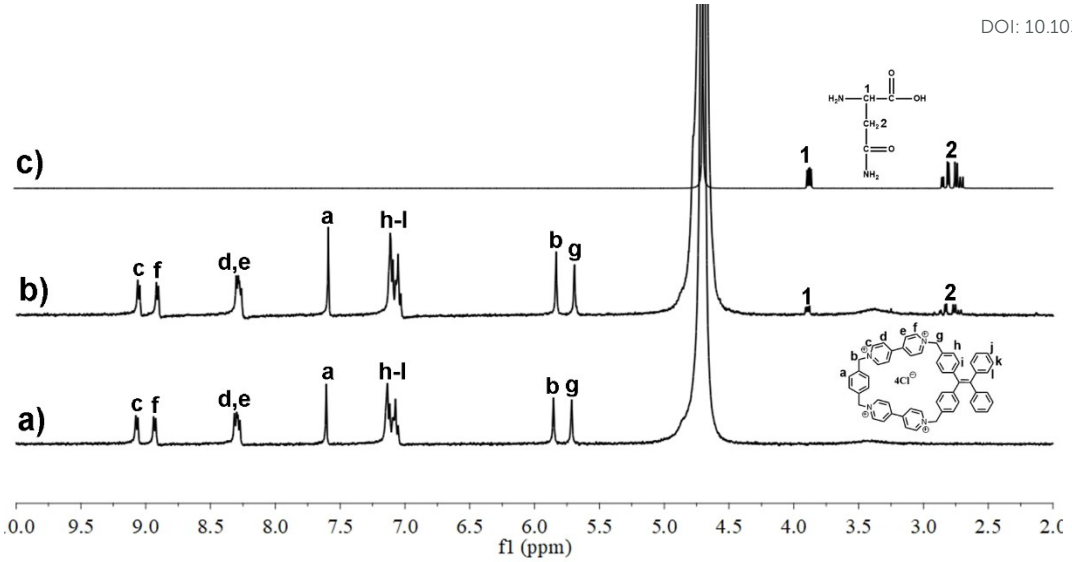

Figure S49. ^{1}H NMR spectra (400MHz, D_2O, phosphate buffer, pH=7.4): a) **1**•4Cl$^-$ (0.4 mM); b) **1**•4Cl$^-$ and asparaginate (0.4 mM); c) asparaginate (0.4 mM) at 298K.

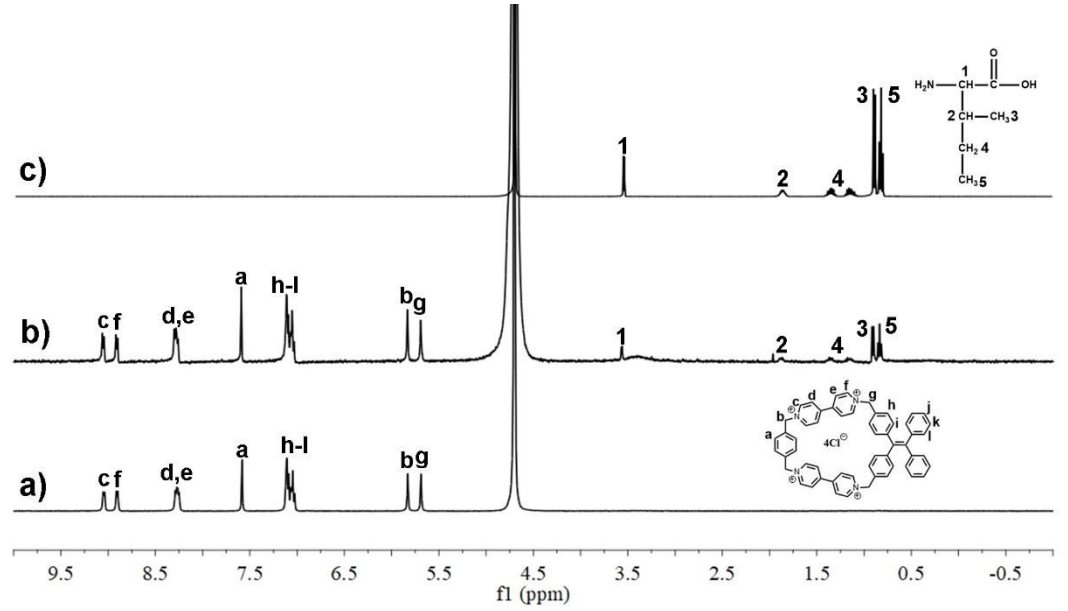

Figure S50. ^{1}H NMR spectra (400MHz, D_2O, phosphate buffer, pH=7.4): a) **1**•4Cl$^-$ (0.4 mM); b) **1**•4Cl$^-$ and isoleucine (0.4 mM); c) isoleucine (0.4 mM) at 298K.

View Article Online
DOI: 10.1039/C9CC00599D

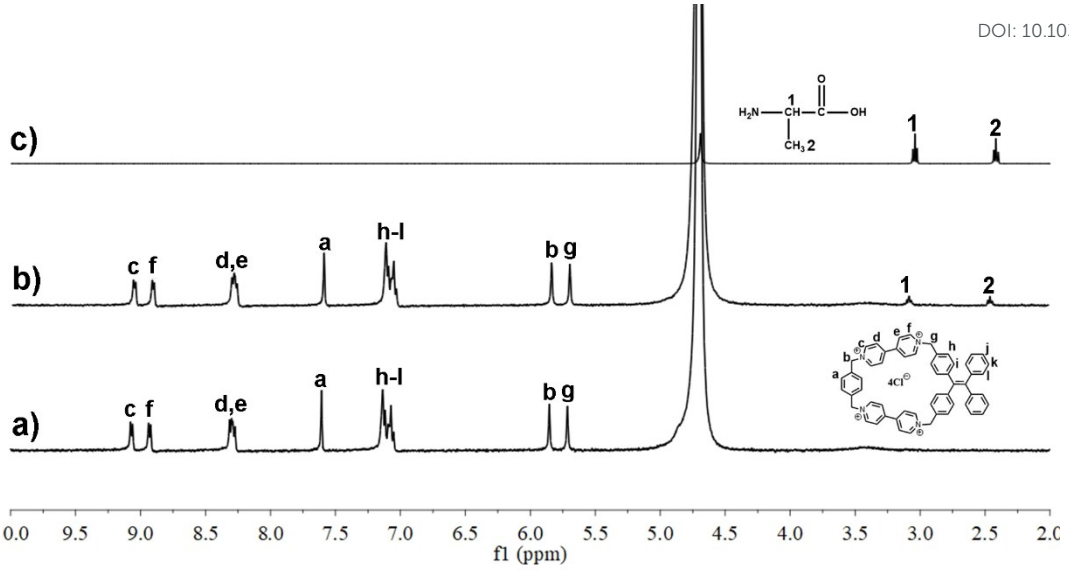

Figure S51. ^{1}H NMR spectra (400MHz, D_2O, phosphate buffer, pH=7.4): a) **1**•4Cl$^-$ (0.4 mM); b) **1**•4Cl$^-$ and alanine (0.4 mM); c) alanine (0.4 mM) at 298K.

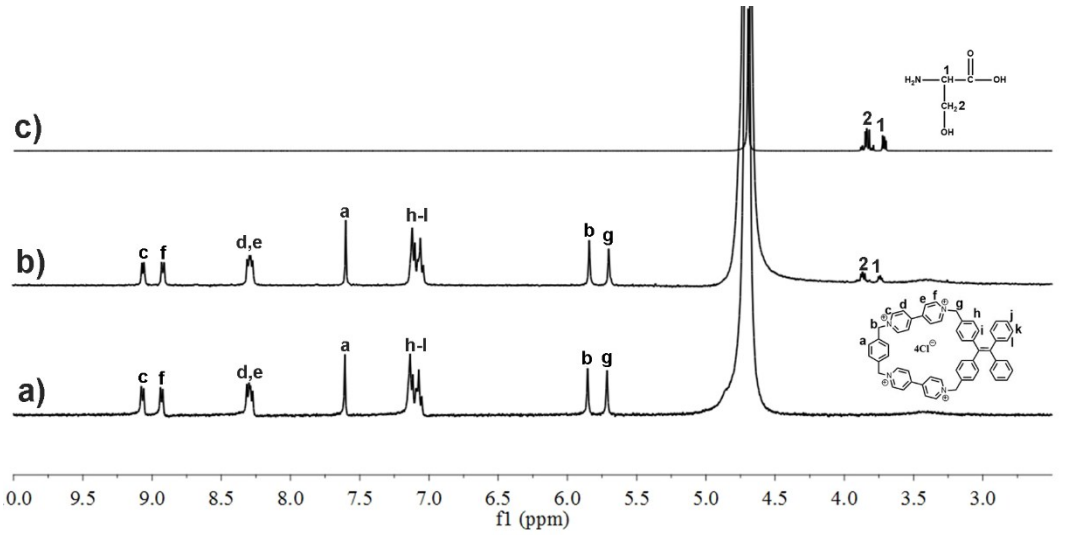

Figure S52. ^{1}H NMR spectra (400MHz, D_2O, phosphate buffer, pH=7.4): a) **1**•4Cl$^-$ (0.4 mM); b) **1**•4Cl$^-$ and serine (0.4 mM); c) serine (0.4 mM) at 298K.

View Article Online
DOI: 10.1039/C9CC00599D

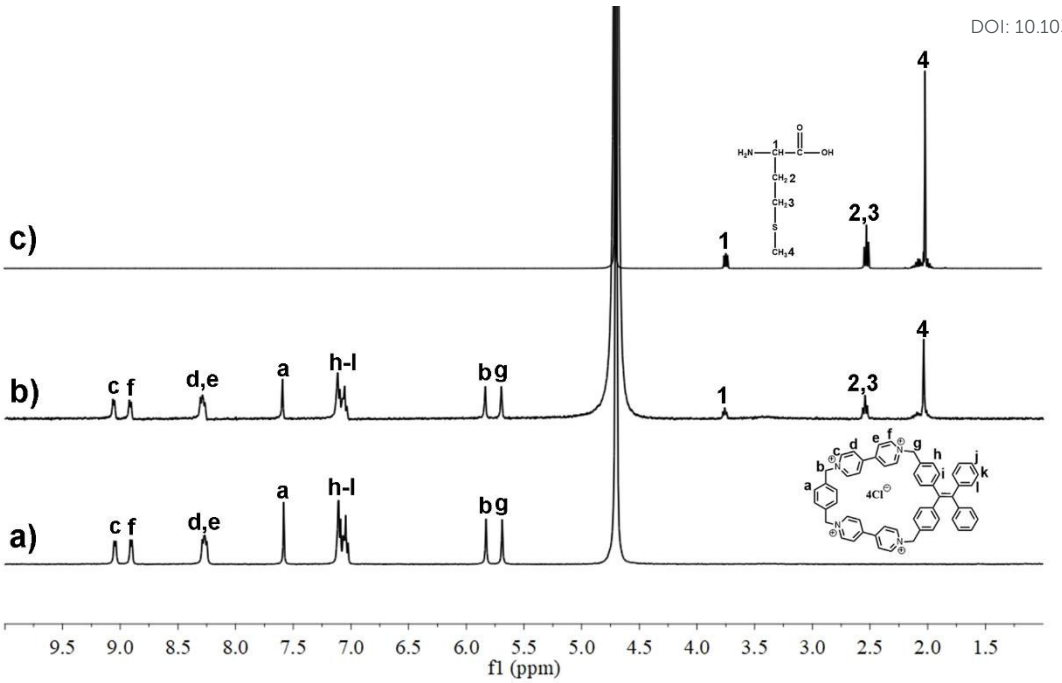

Figure S53. ^{1}H NMR spectra (400MHz, D_2O, phosphate buffer, pH=7.4): a) **1**•4Cl$^-$ (0.4 mM); b) **1**•4Cl$^-$ and methionine (0.4 mM); c) methionine (0.4 mM) at 298K.

Figure S54. ^{1}H NMR spectra (400MHz, D_2O, phosphate buffer, pH=7.4): a) **1**•4Cl$^-$ (0.4 mM); b) **1**•4Cl$^-$ and glutamine (0.4 mM); c) glutamine (0.4 mM) at 298K.

View Article Online
DOI: 10.1039/C9CC00599D

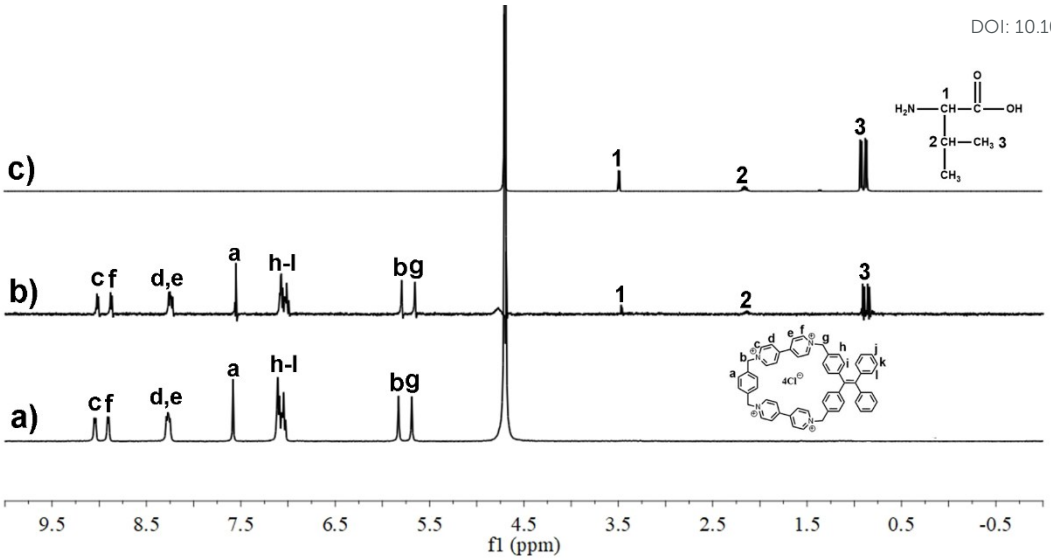

Figure S55. ^{1}H NMR spectra (400MHz, D_2O, phosphate buffer, pH=7.4): a) **1**•4Cl^- (0.4 mM); b) **1**•4Cl^- and valine (0.4 mM); c) valine (0.4 mM) at 298K.

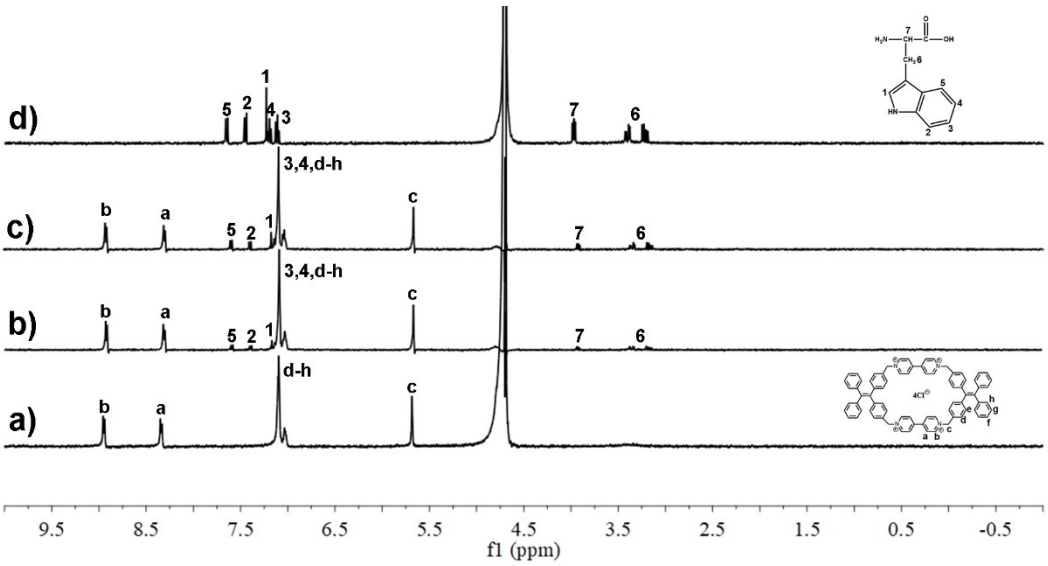

Figure S56. ^{1}H NMR spectra (400MHz, D_2O, phosphate buffer, pH=7.4): a) **2**•4Cl^- (0.4 mM); b) **2**•4Cl^- and tryptophan (0.4 mM); c) **2**•4Cl^- and tryptophan (0.8 mM); d) tryptophan (0.4 mM) at 298K.

View Article Online
DOI: 10.1039/C9CC00599D

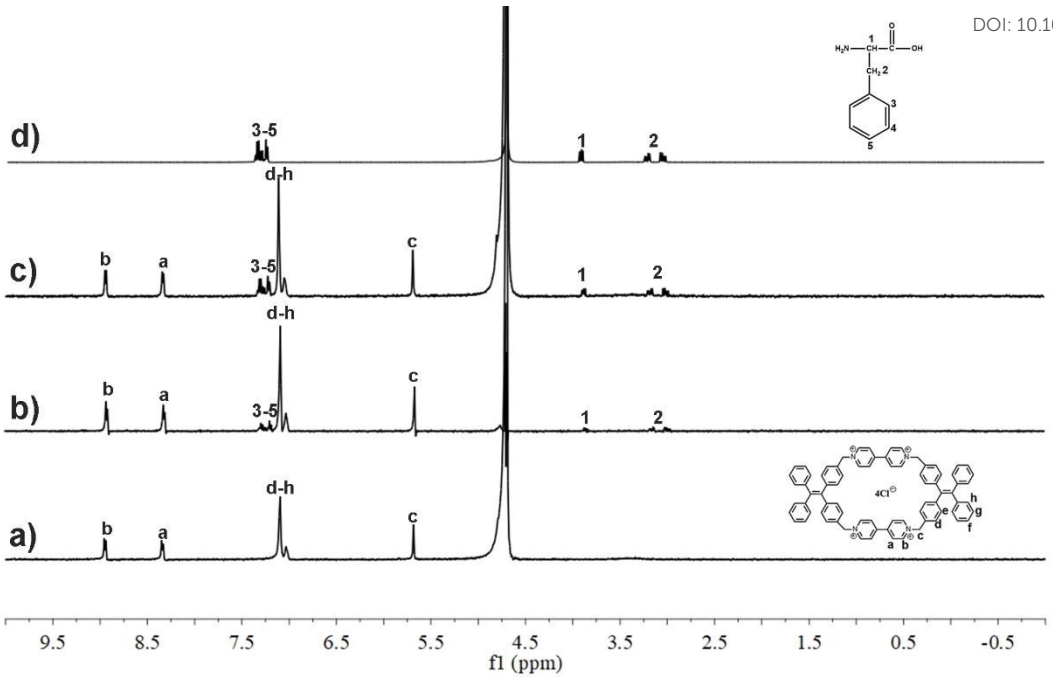

Figure S57. ^{1}H NMR spectra (400MHz, D_2O, phosphate buffer, pH=7.4): a) **2**•4Cl$^-$ (0.4 mM); b) **2**•4Cl$^-$ and phenylalanine (0.4 mM); c) **2**•4Cl$^-$ and phenylalanine (0.8 mM); d) phenylalanine (0.4 mM) at 298K.

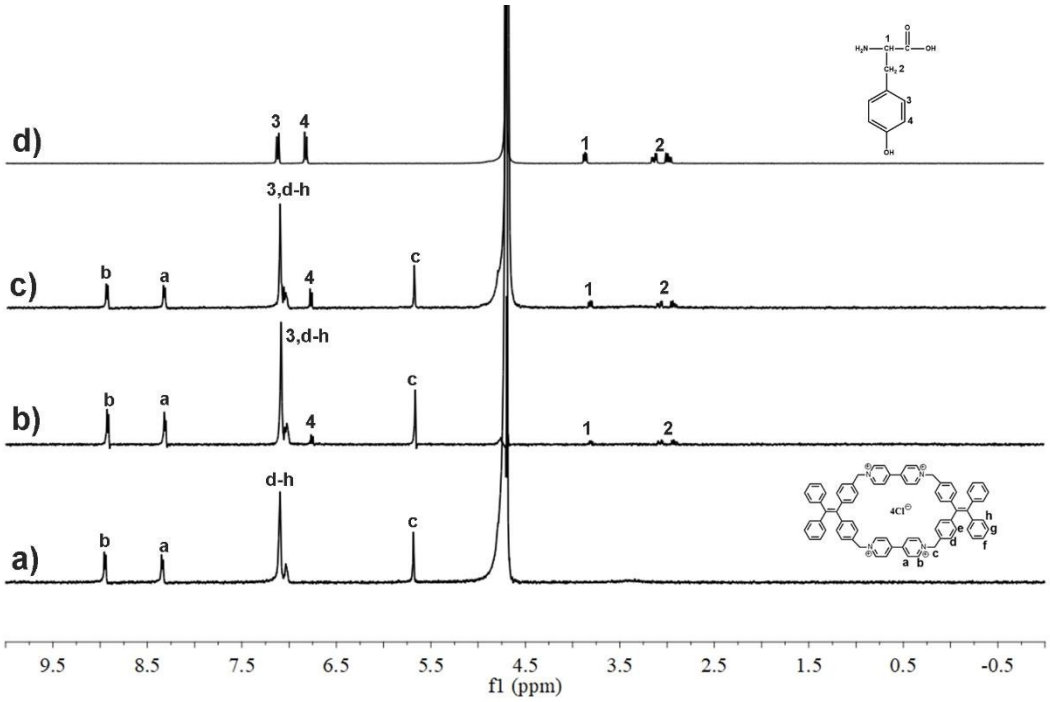

Figure S58. ^{1}H NMR spectra (400MHz, D_2O, phosphate buffer, pH=7.4): a) **2**•4Cl$^-$ (0.4 mM); b) **2**•4Cl$^-$ and tyrosine (0.4 mM); c) **2**•4Cl$^-$ and tyrosine (0.8 mM); d) tyrosine (0.4 mM) at 298K.

View Article Online
DOI: 10.1039/C9CC00599D

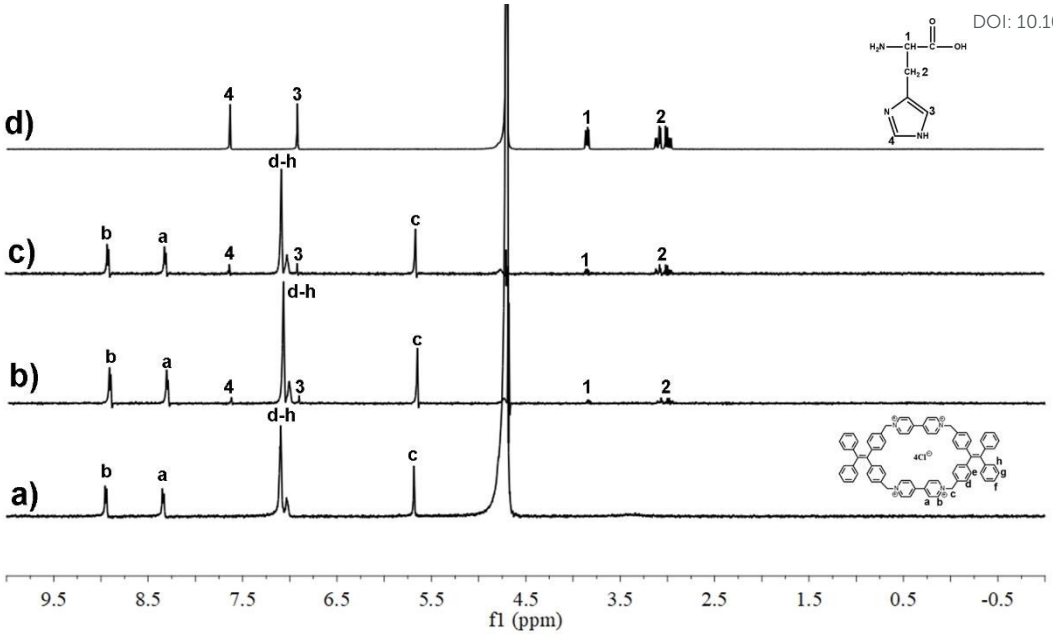

Figure S59. ^{1}H NMR spectra (400MHz, D_2O, phosphate buffer, pH=7.4): a) **2**•4Cl^- (0.4 mM); b) **2**•4Cl^- and histidine (0.4 mM); c) **2**•4Cl^- and histidine (0.8 mM); d) histidine (0.4 mM) at 298K.

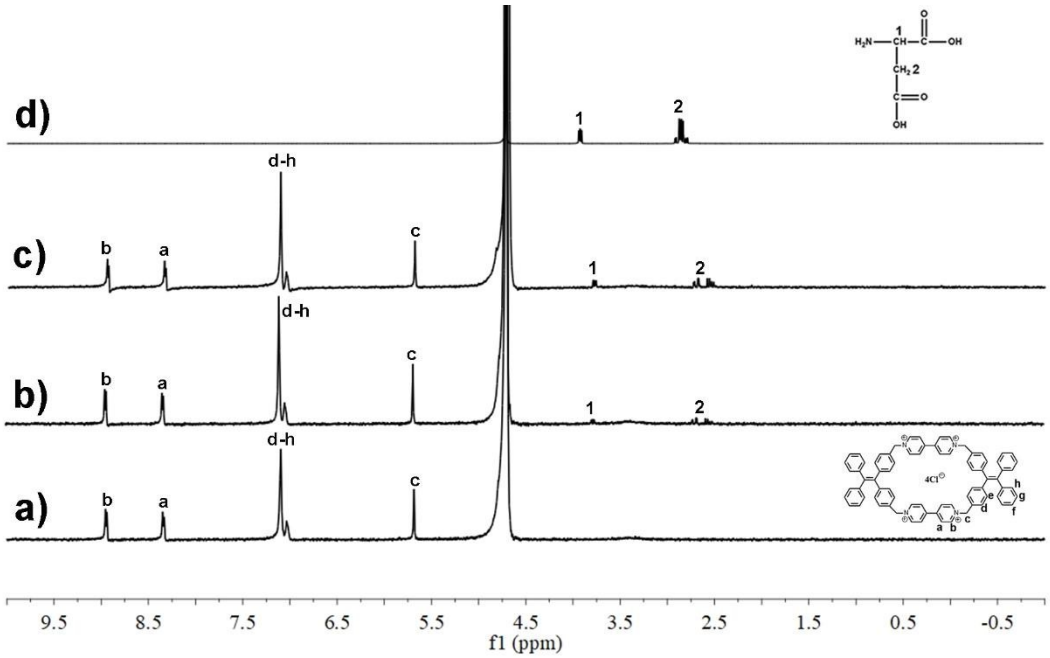

Figure S60. ^{1}H NMR spectra (400MHz, D_2O, phosphate buffer, pH=7.4): a) **2**•4Cl^- (0.4 mM); b) **2**•4Cl^- and aspartic acid (0.4 mM); c) **2**•4Cl^- and aspartic acid (0.8 mM); d) aspartic acid (0.4 mM) at 298K.

View Article Online
DOI: 10.1039/C9CC00599D

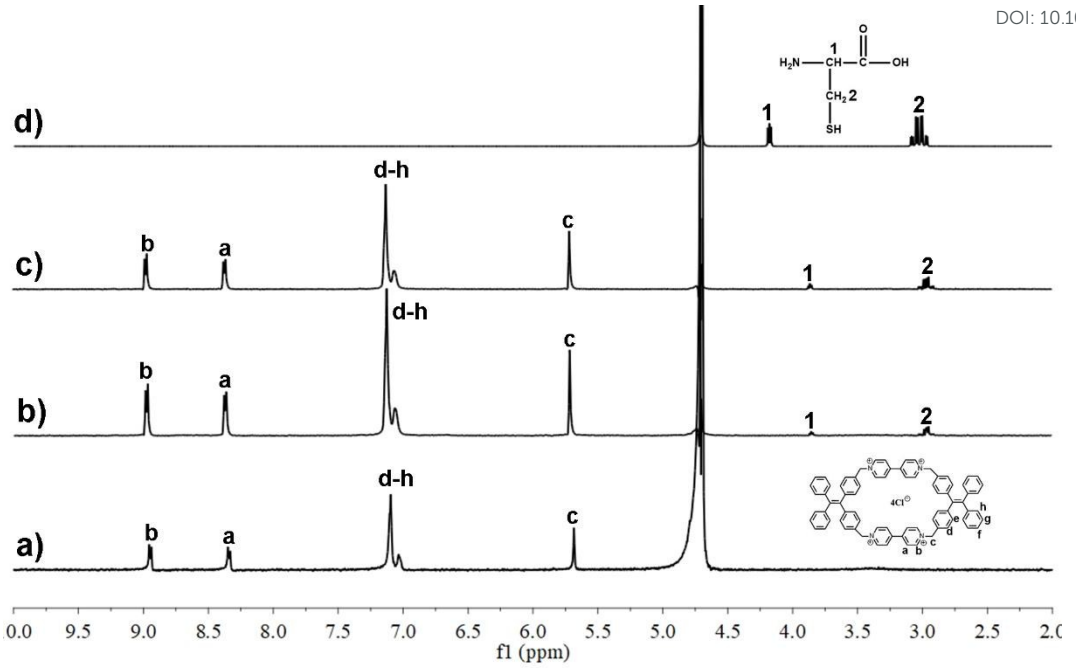

Figure S61. ^{1}H NMR spectra (400MHz, D_2O, phosphate buffer, pH=7.4): a) **2**•4Cl$^-$ (0.4 mM); b) **2**•4Cl$^-$ and cysteine (0.4 mM); c) **2**•4Cl$^-$ and cysteine (0.8 mM); d) cysteine (0.4 mM) at 298K.

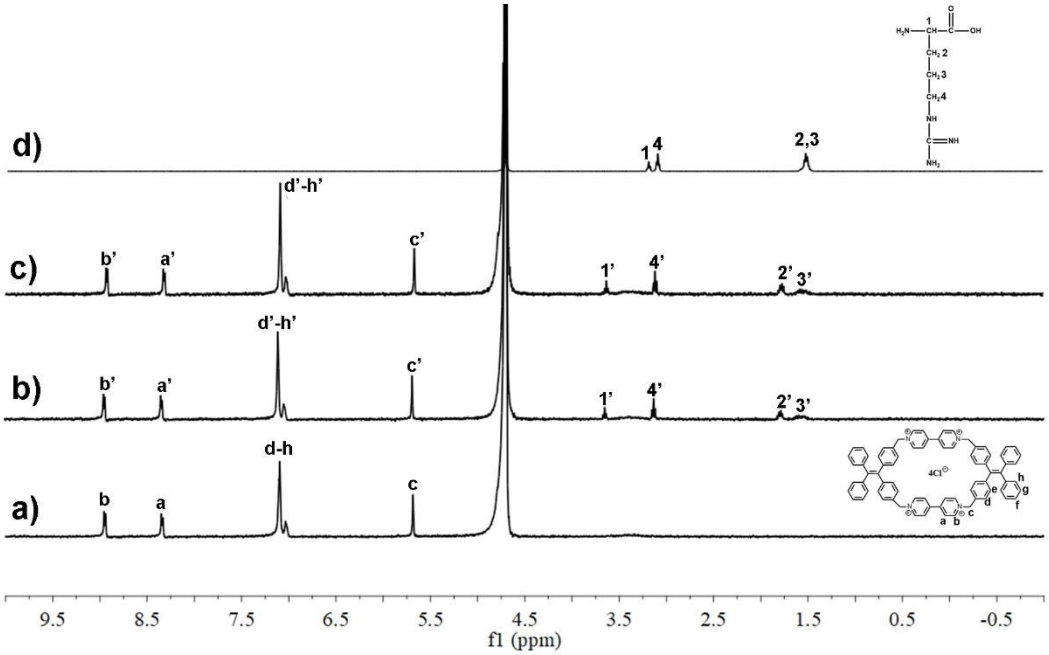

Figure S62. ^{1}H NMR spectra (400MHz, D_2O, phosphate buffer, pH=7.4): a) **2**•4Cl$^-$ (0.4 mM); b) **2**•4Cl$^-$ and arginine (0.4 mM); c) **2**•4Cl$^-$ and arginine (0.8 mM); d) arginine (0.4 mM) at 298K.

View Article Online
DOI: 10.1039/C9CC00599D

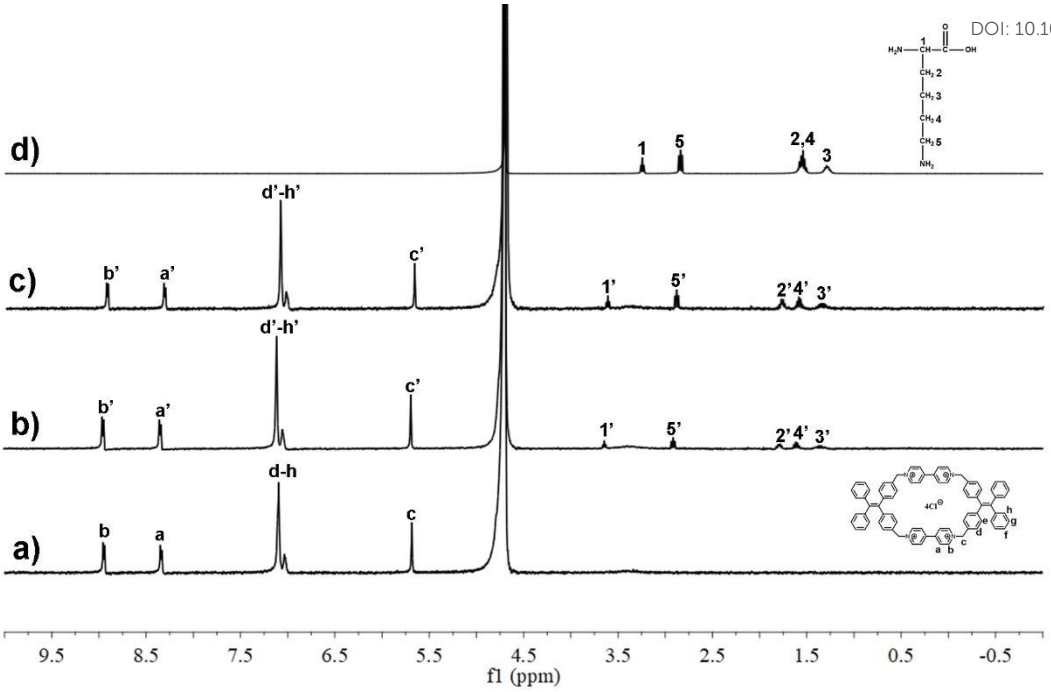

Figure S63. ^{1}H NMR spectra (400MHz, D_2O, phosphate buffer, pH=7.4): a) **2**•4Cl$^-$ (0.4 mM); b) **2**•4Cl$^-$ and lysine (0.4 mM); c) **2**•4Cl$^-$ and lysine (0.8 mM); d) lysine (0.4 mM) at 298K.

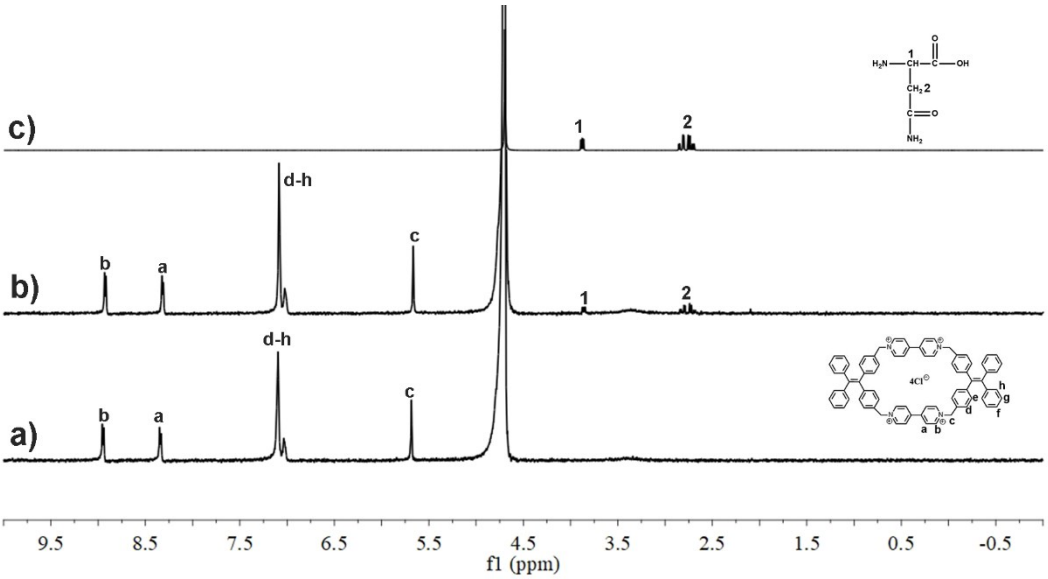

Figure S64. ^{1}H NMR spectra (400MHz, D_2O, phosphate buffer, pH=7.4): a) **2**•4Cl$^-$ (0.4 mM); b) **2**•4Cl$^-$ and asparaginate (0.4 mM); c) asparaginate (0.4 mM) at 298K.

View Article Online
DOI: 10.1039/C9CC00599D

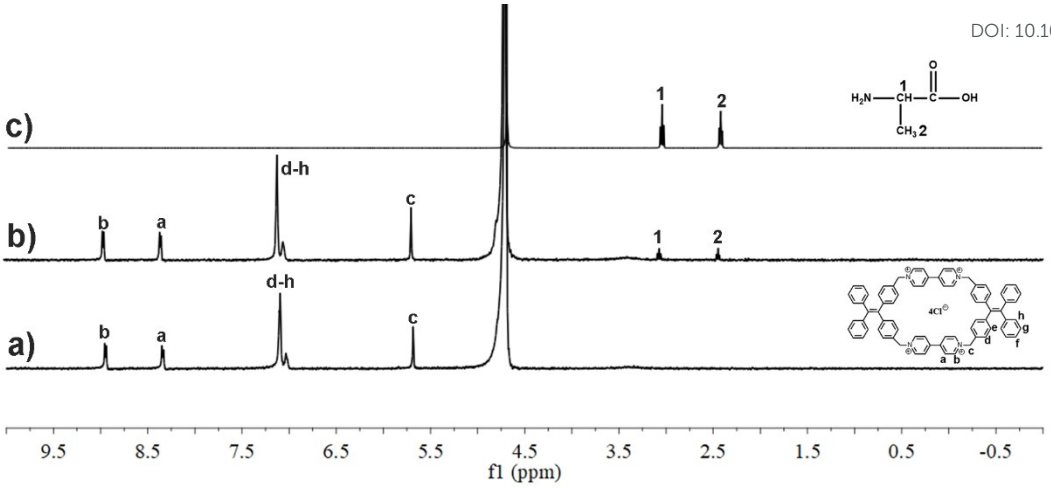

Figure S65. ^{1}H NMR spectra (400MHz, D_2O, phosphate buffer, pH=7.4): a) **2**•4Cl$^-$ (0.4 mM); b) **2**•4Cl$^-$ and alanine (0.4 mM); c) alanine (0.4 mM) at 298K.

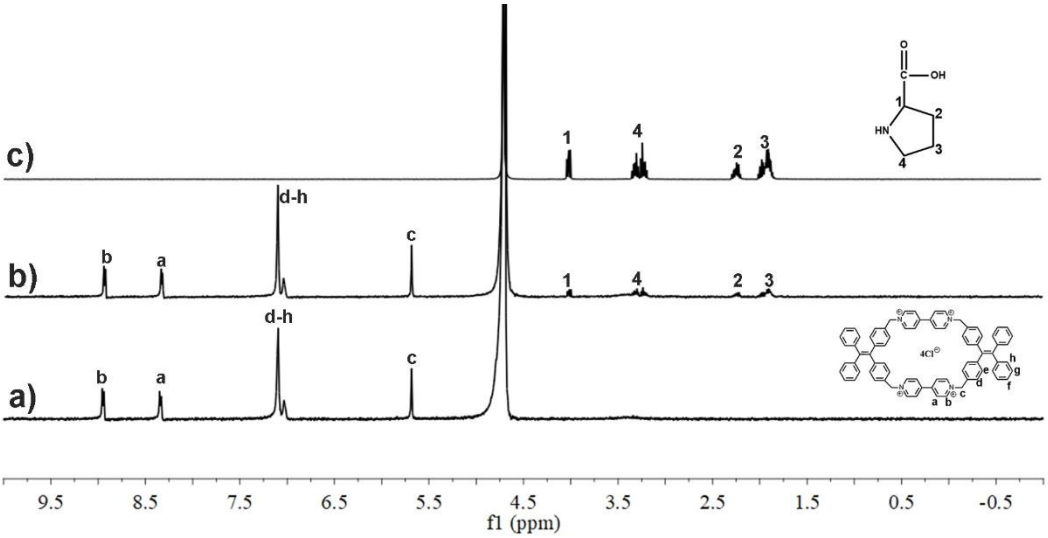

Figure S66. ^{1}H NMR spectra (400MHz, D_2O, phosphate buffer, pH=7.4): a) **2**•4Cl$^-$ (0.4 mM); b) **2**•4Cl$^-$ and proline (0.4 mM); c) proline (0.4 mM) at 298K.

View Article Online
DOI: 10.1039/C9CC00599D

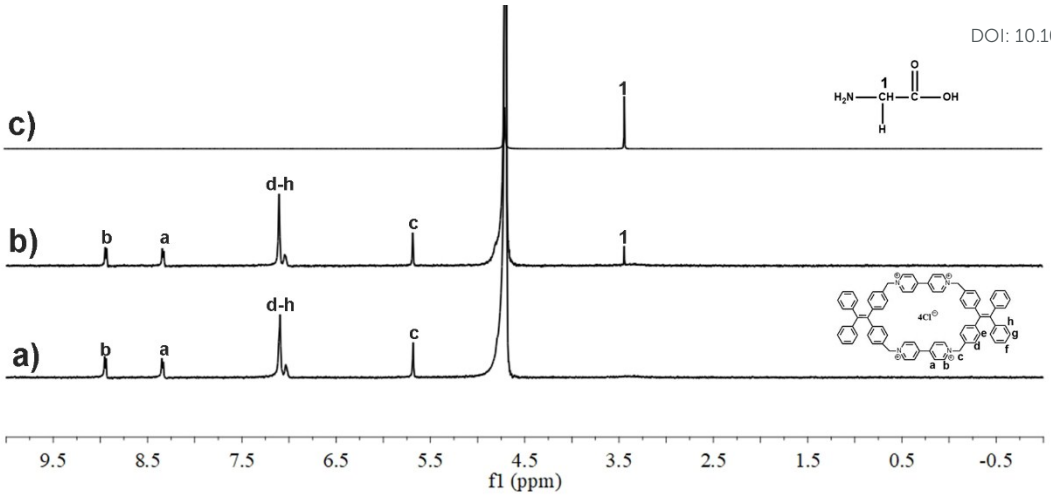

Figure S67. ^{1}H NMR spectra (400MHz, D_2O, phosphate buffer, pH=7.4): a) **2**•4Cl$^-$ (0.4 mM); b) **2**•4Cl$^-$ and glycine (0.4 mM); c) glycine (0.4 mM) at 298K.

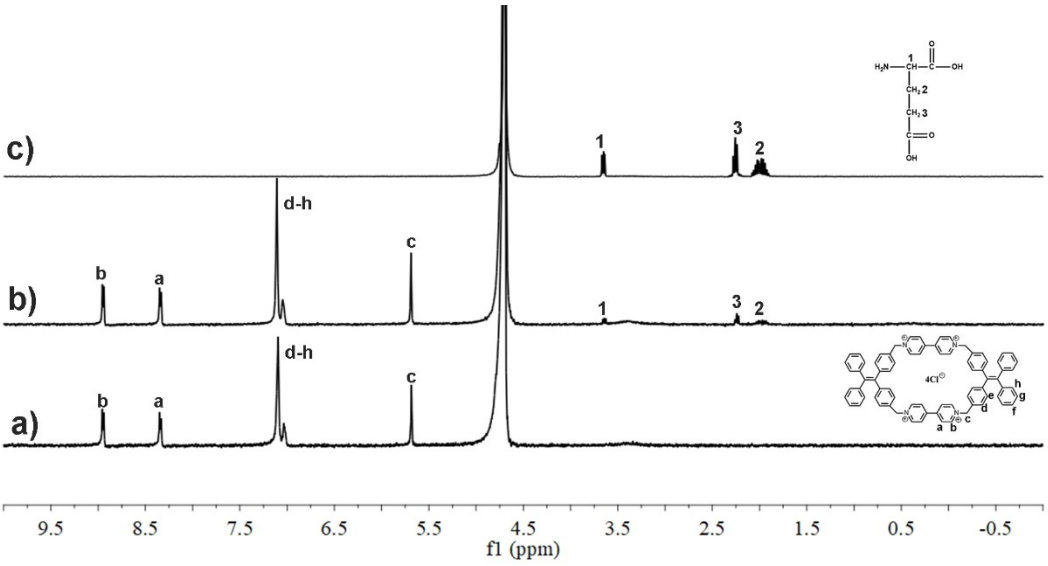

Figure S68. ^{1}H NMR spectra (400MHz, D_2O, phosphate buffer, pH=7.4): a) **2**•4Cl$^-$ (0.4 mM); b) **2**•4Cl$^-$ and glutamine (0.4 mM); c) glutamine (0.4 mM) at 298K.

View Article Online
DOI: 10.1039/C9CC00599D

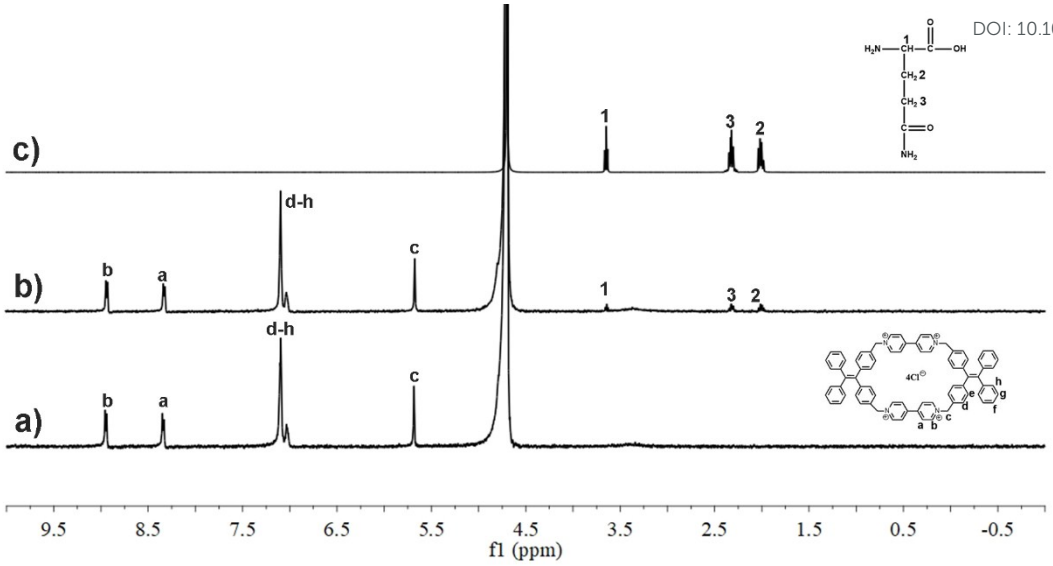

Figure S69. ^{1}H NMR spectra (400MHz, D_2O, phosphate buffer, pH=7.4): a) **2**•4Cl^- (0.4 mM); b) **2**•4Cl^- and glutamic acid (0.4 mM); c) glutamic acid (0.4 mM) at 298K.

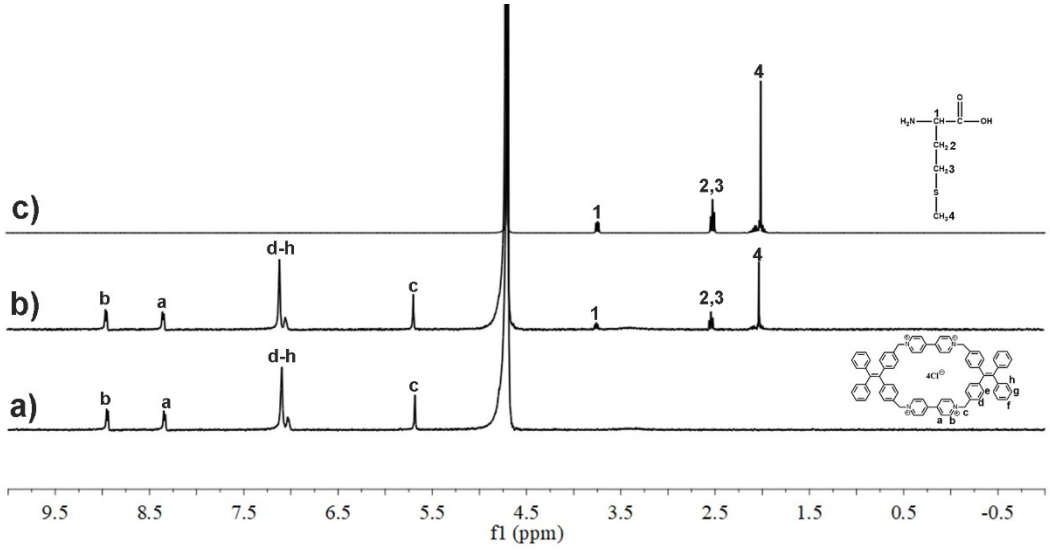

Figure S70. ^{1}H NMR spectra (400MHz, D_2O, phosphate buffer, pH=7.4): a) **2**•4Cl^- (0.4 mM); b) **2**•4Cl^- and methionine (0.4 mM); c) methionine (0.4 mM) at 298K.

View Article Online
DOI: 10.1039/C9CC00599D

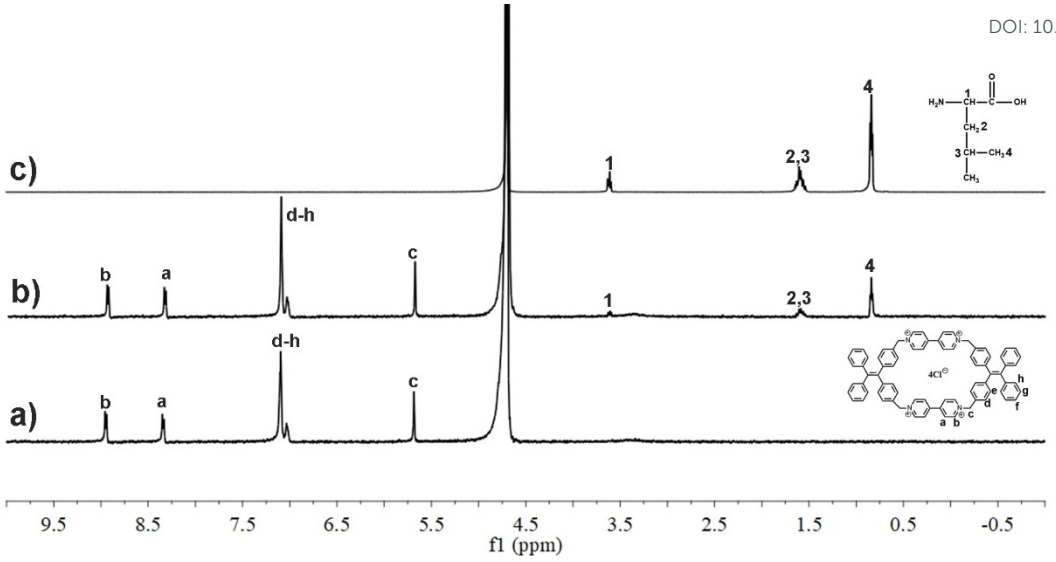

Figure S71. ^{1}H NMR spectra (400MHz, D_2O, phosphate buffer, pH=7.4): a) **2**•4Cl$^-$ (0.4 mM); b) **2**•4Cl$^-$ and leucine (0.4 mM); c) leucine (0.4 mM) at 298K.

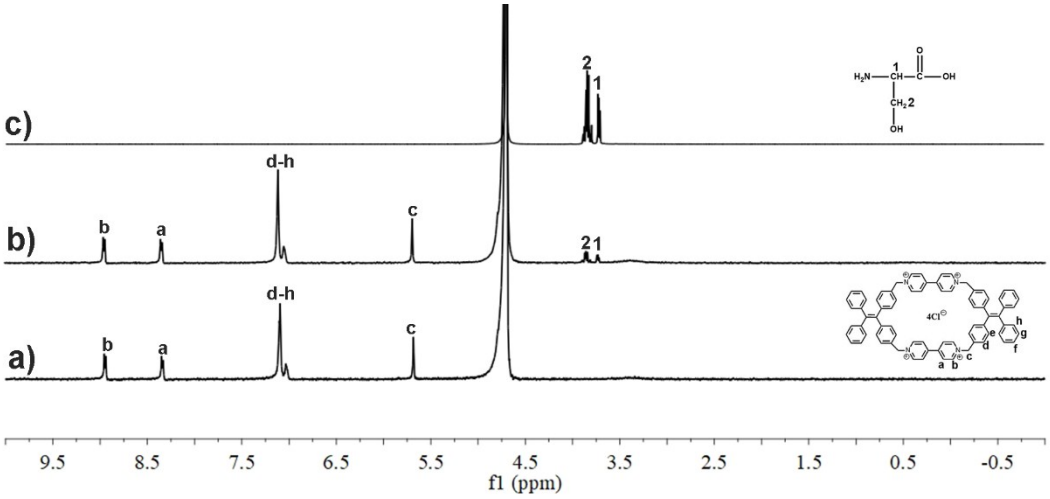

Figure S72. ^{1}H NMR spectra (400MHz, D_2O, phosphate buffer, pH=7.4): a) **2**•4Cl$^-$ (0.4 mM); b) **2**•4Cl$^-$ and serine (0.4 mM); c) serine (0.4 mM) at 298K.

View Article Online
DOI: 10.1039/C9CC00599D

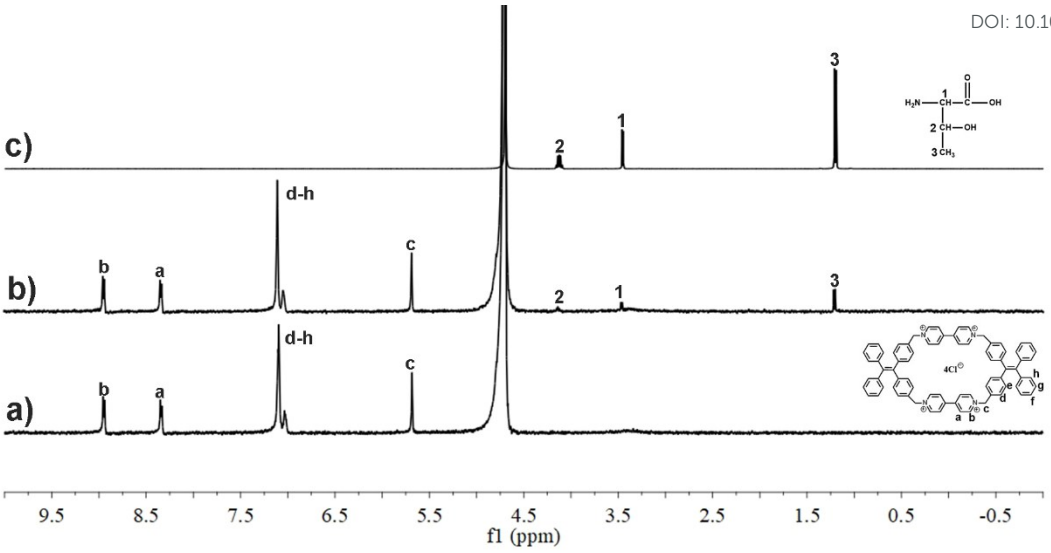

Figure S73. ^{1}H NMR spectra (400MHz, D_2O, phosphate buffer, pH=7.4): a) **2**•4Cl$^-$ (0.4 mM); b) **2**•4Cl$^-$ and threonine (0.4 mM); c) threonine (0.4 mM) at 298K.

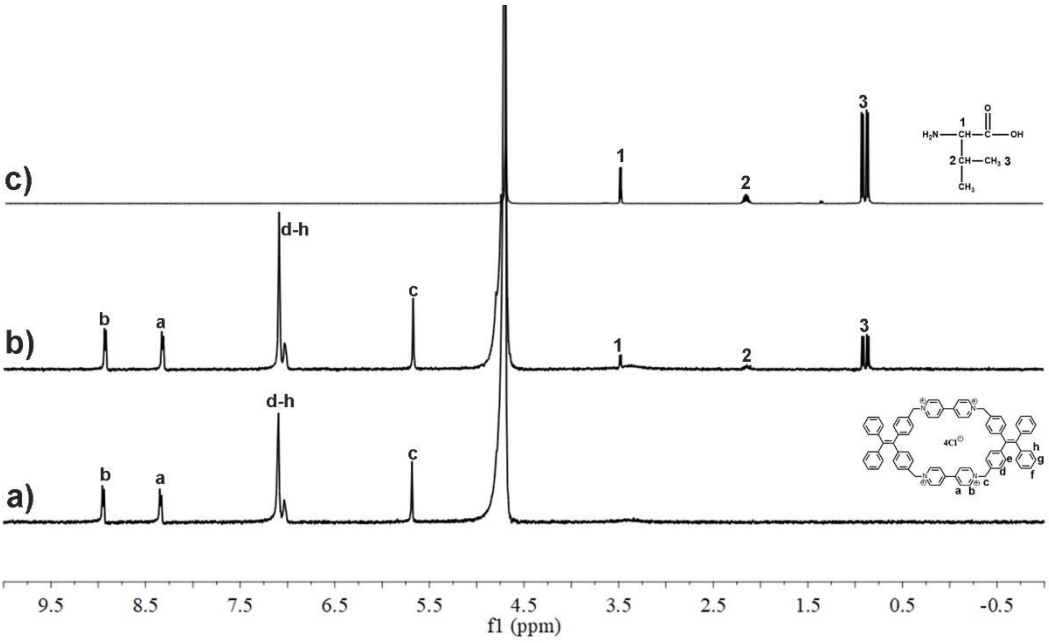

Figure S74. ^{1}H NMR spectra (400MHz, D_2O, phosphate buffer, pH=7.4): a) **2**•4Cl$^-$ (0.4 mM); b) **2**•4Cl$^-$ and valine (0.4 mM); c) valine (0.4 mM) at 298K.

View Article Online
DOI: 10.1039/C9CC00599D

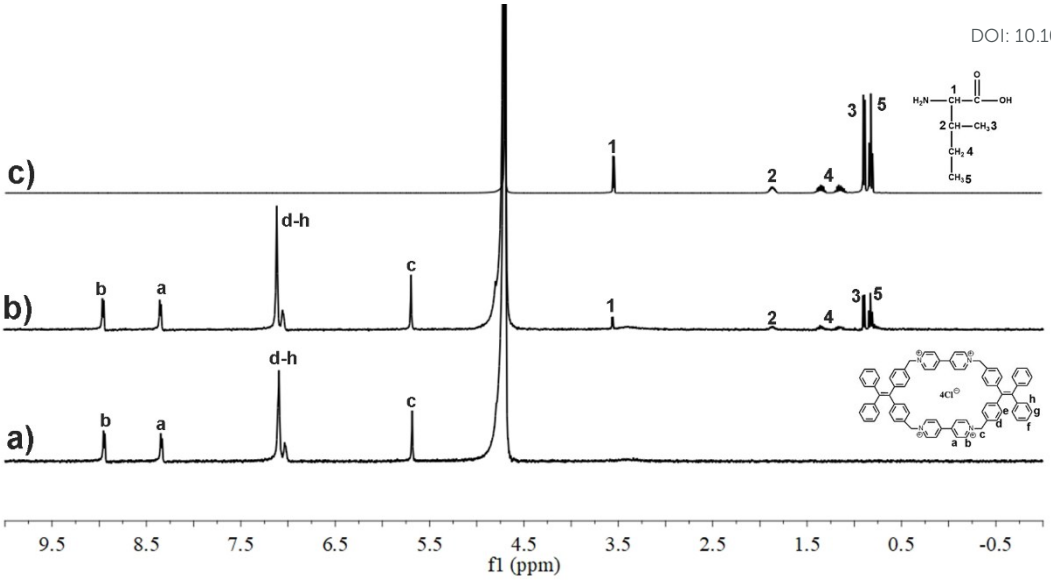

Figure S75. ^{1}H NMR spectra (400MHz, D_2O, phosphate buffer, pH=7.4): a) **2**•4Cl$^-$ (0.4 mM); b) **2**•4Cl$^-$ and isoleucine (0.4 mM); c) isoleucine (0.4 mM) at 298K.

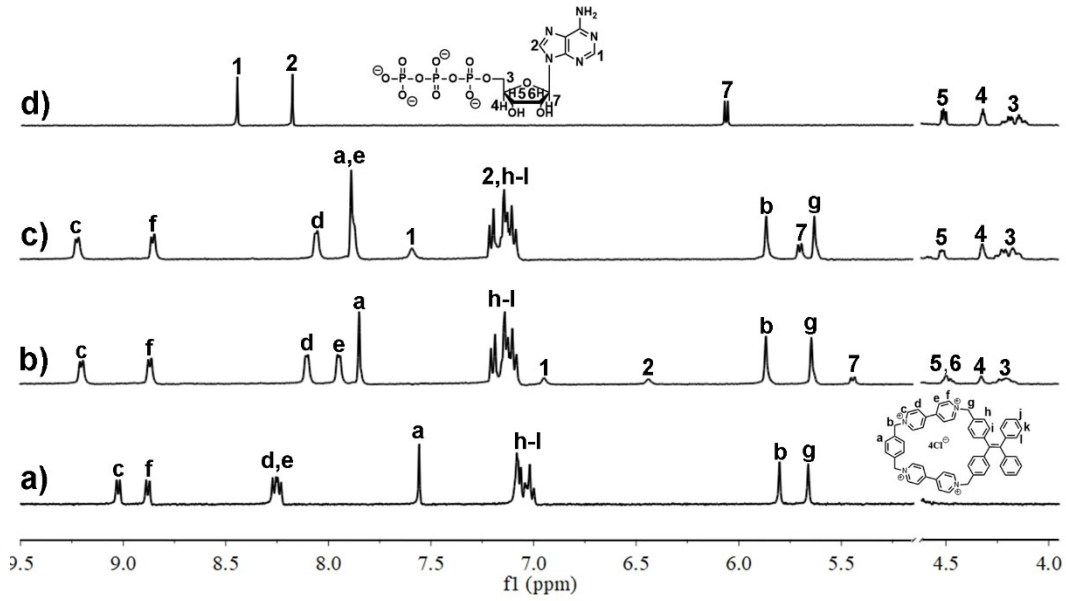

Figure S76. ^{1}H NMR spectra (400MHz, D_2O, phosphate buffer, pH=7.4): a) **1**•4Cl$^-$ (0.4 mM); b) **1**•4Cl$^-$ and ATP (0.4 mM); c) **1**•4Cl$^-$ and ATP (0.8 mM); d) ATP (0.4 mM) at 298K.

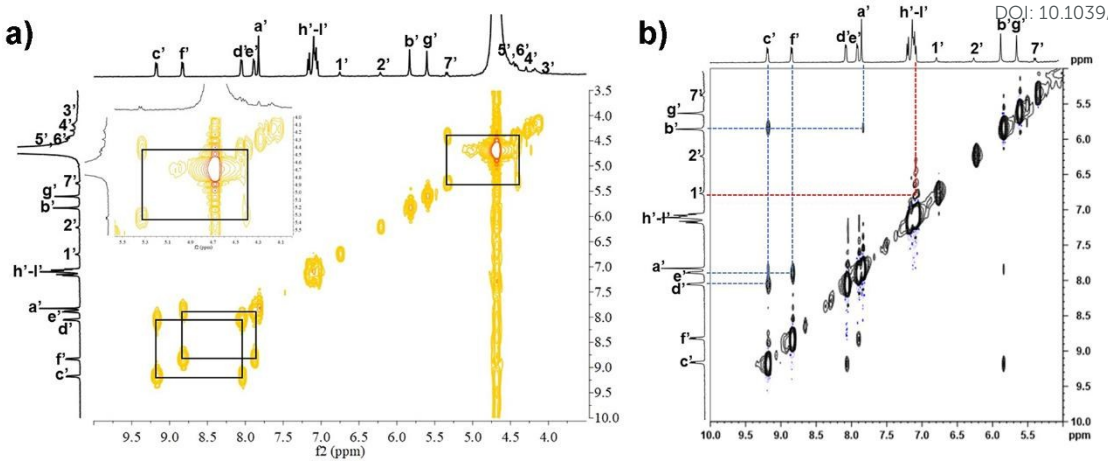

Figure S77. COSY and NOESY ^{1}H NMR spectrum recorded (400 MHz, D_2O, phosphate buffer, pH = 7.4, 298 K) for **1**•4Cl$^-$ (0.5mM) with ATP (0.5 mM).

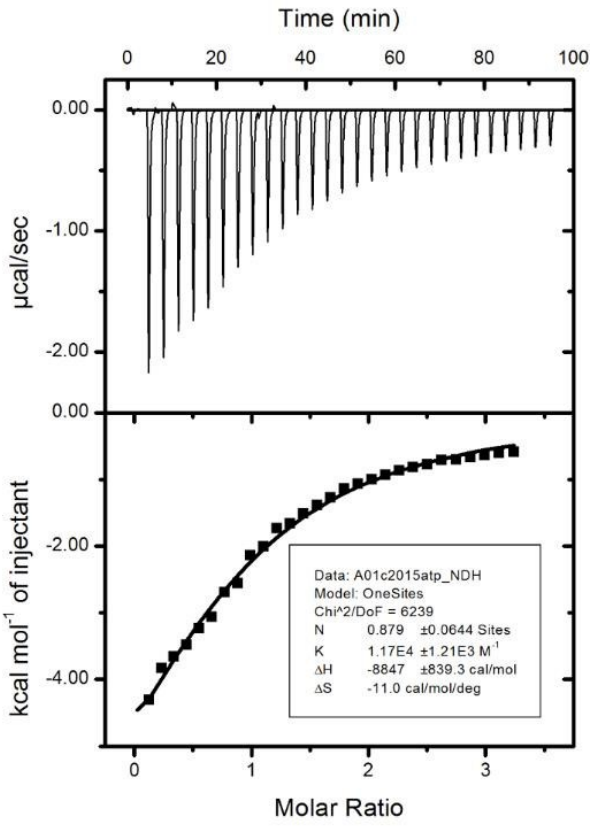

Figure S78. ITC titration of **1**•4Cl$^-$ (0.1 mM) with ATP (1.5 mM) in phosphate buffer (pH = 7.4).

View Article Online
DOI: 10.1039/C9CC00599D

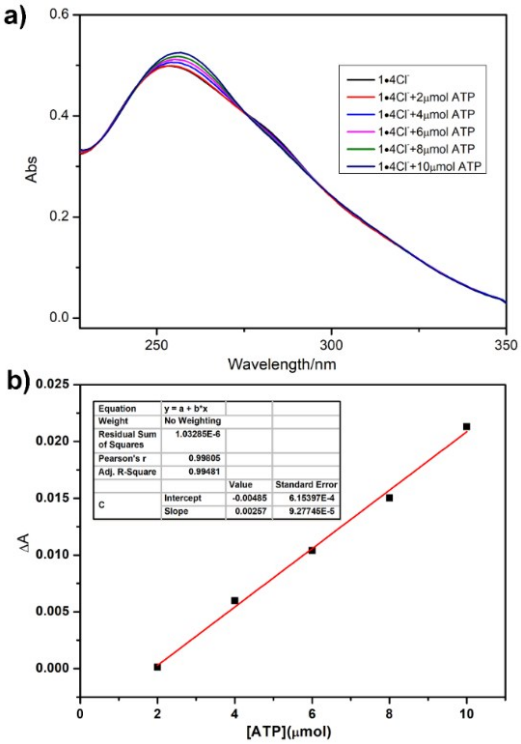

Figure S79. (a) UV-vis absorption of **1**•4Cl⁻ and **1**•ATP in phosphate buffer (10 mmol, pH=7.4) at 298K; (b) A plot of the difference of the absorption intensity ΔA at 253 nm verasus the concentration of ATP. Linear Equation: y= 0.00257x - 0.00485，R^2 = 0.99481; y = 0，x =1.89 μmol.

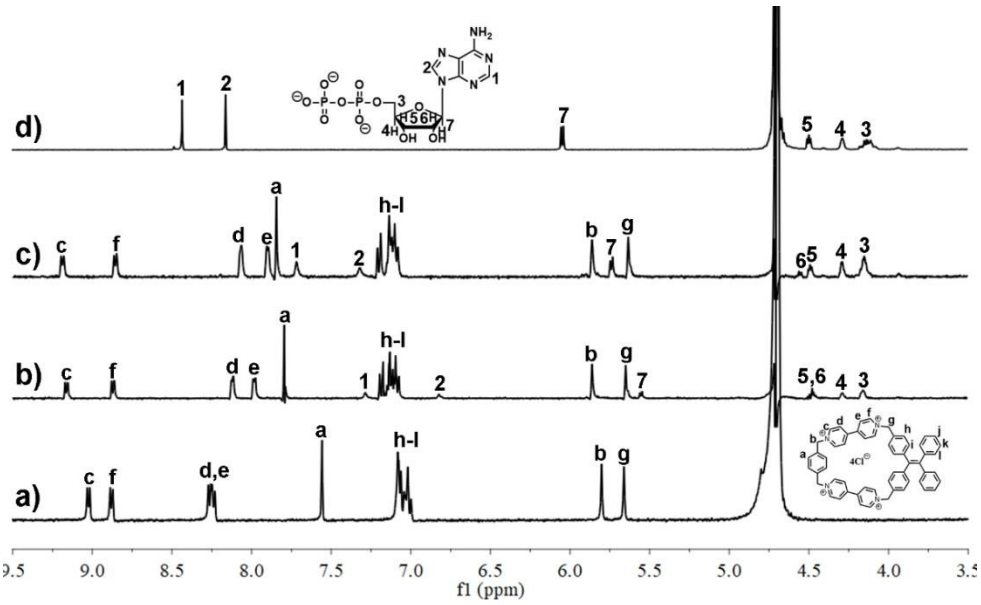

Figure S80. ^{1}H NMR spectra (400MHz, D_2O, phosphate buffer, pH=7.4): a) **1**•4Cl⁻ (0.4 mM); b) **1**•4Cl⁻ and ADP (0.4 mM); c) **1**•4Cl⁻ and ADP (0.8 mM); d) ADP (0.4 mM) at 298K.

View Article Online
DOI: 10.1039/C9CC00599D

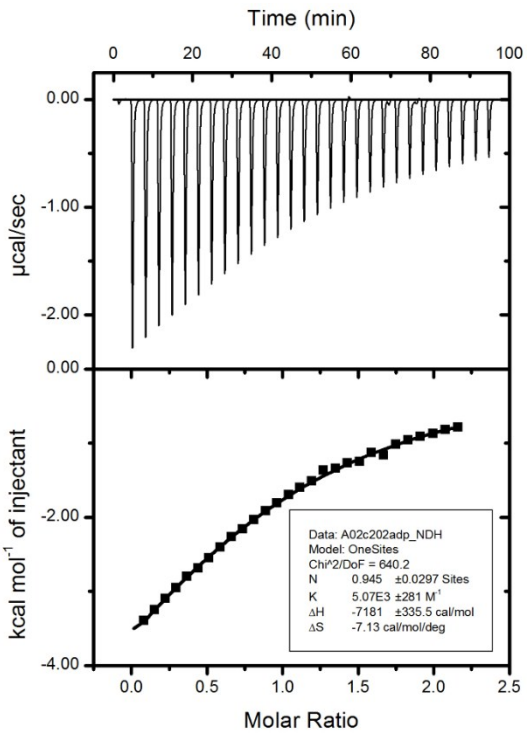

Figure S81. ITC titration of **1**•4Cl$^-$ (0.2 mM) with ADP (2.0 mM) in phosphate buffer (pH = 7.4).

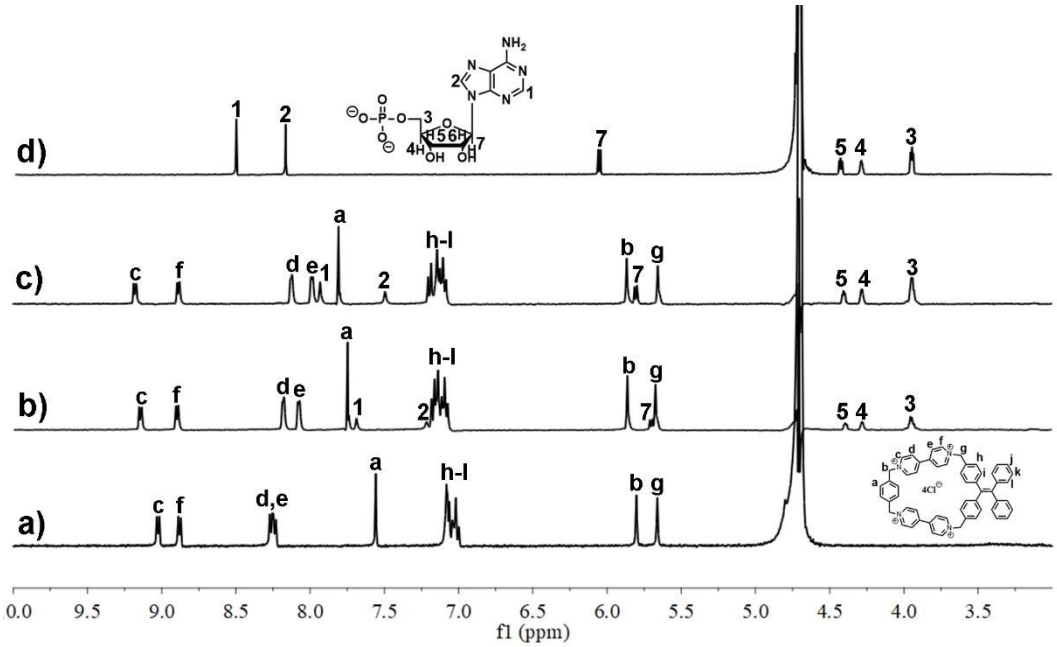

Figure S82. ^{1}H NMR spectra (400MHz, D_2O, phosphate buffer, pH=7.4): a) **1**•4Cl$^-$ (0.4 mM); b) **1**•4Cl$^-$ and AMP (0.4 mM); c) **1**•4Cl$^-$ and AMP (0.8 mM); d) AMP (0.4 mM) at 298K.

View Article Online
DOI: 10.1039/C9CC00599D

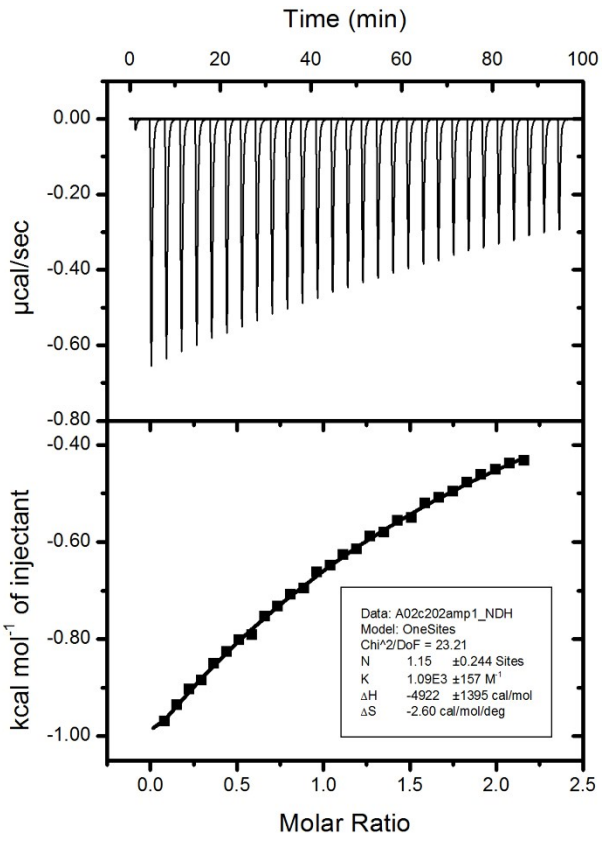

Figure S83. ITC titration of **1**•4Cl$^-$ (0.2 mM) with AMP (2.0 mM) in phosphate buffer (pH = 7.4).

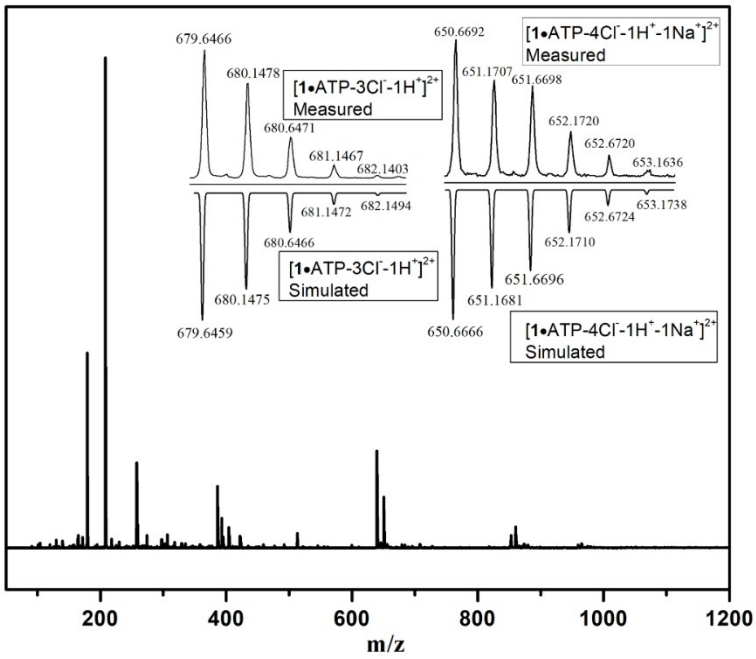

Figure S84. ESI-MS spectrum of **1**•ATP.

View Article Online
DOI: 10.1039/C9CC00599D

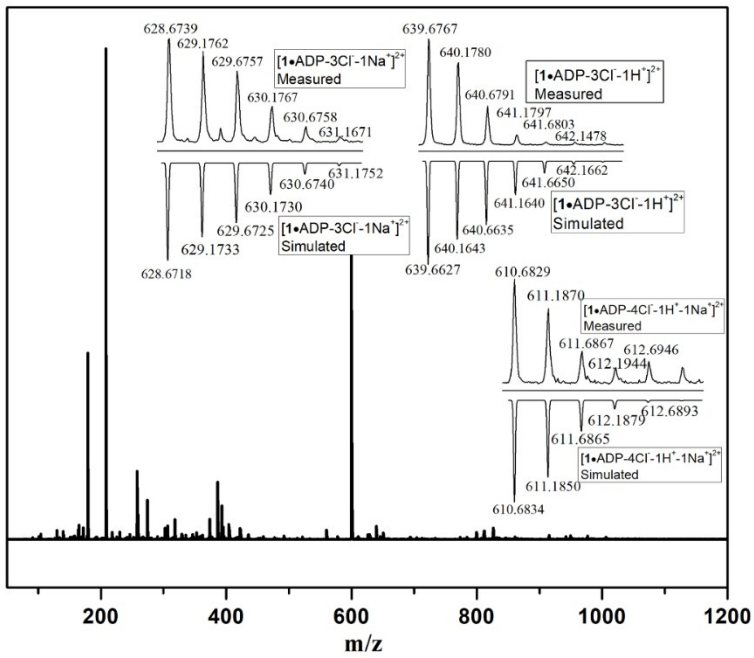

Figure S85. ESI-MS spectrum of **1**•ADP.

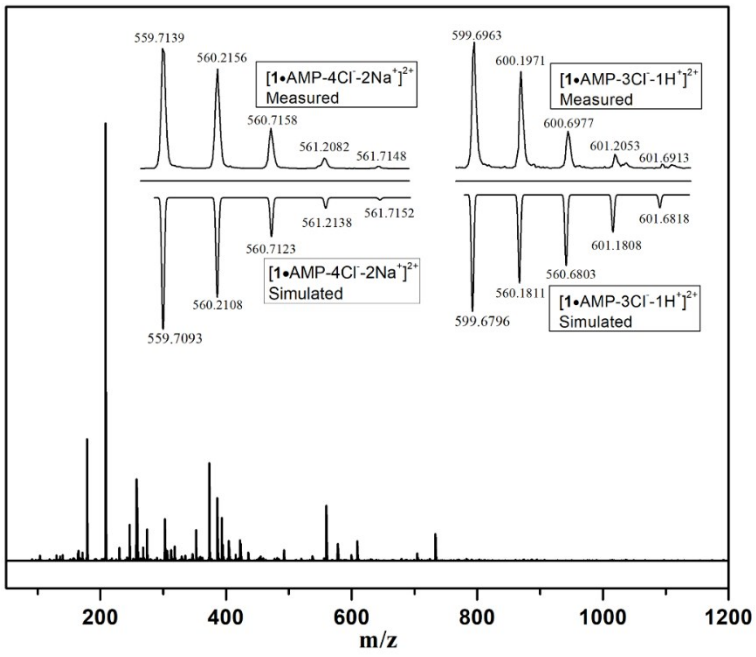

Figure S86. ESI-MS spectrum of **1**•AMP.

View Article Online
DOI: 10.1039/C9CC00599D

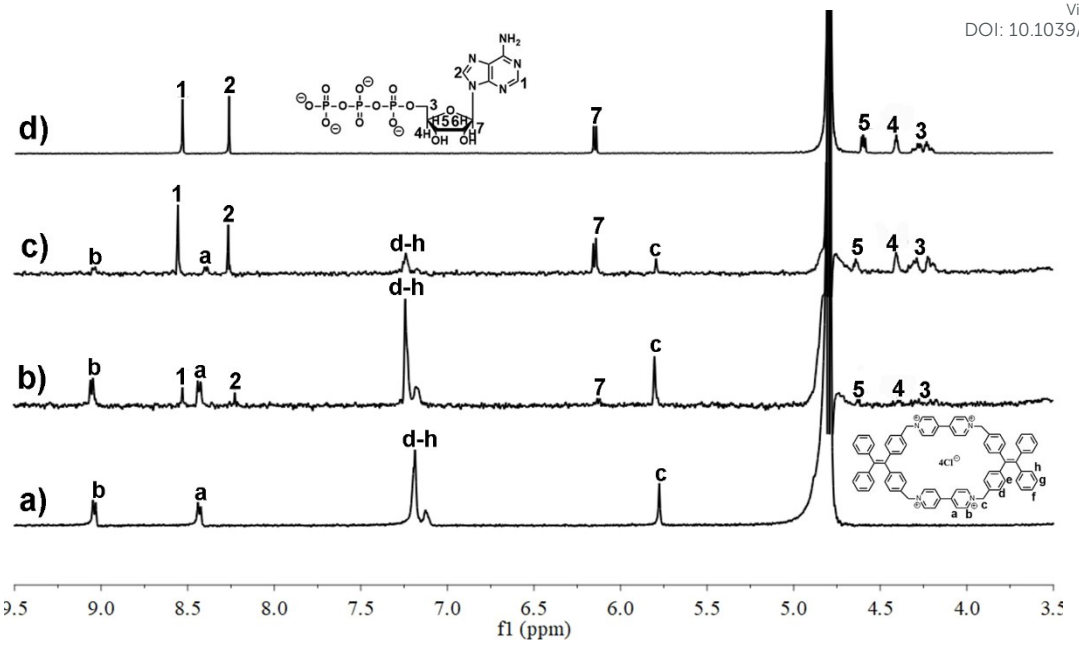

Figure S87. ^{1}H NMR spectra (400MHz, D_2O, phosphate buffer, pH=7.4): a) **2**•4Cl$^-$ (0.4 mM); b) **2**•4Cl$^-$ and ATP (0.4 mM); c) **2**•4Cl$^-$ and ATP (0.8 mM); d) ATP (0.4 mM) at 298K.

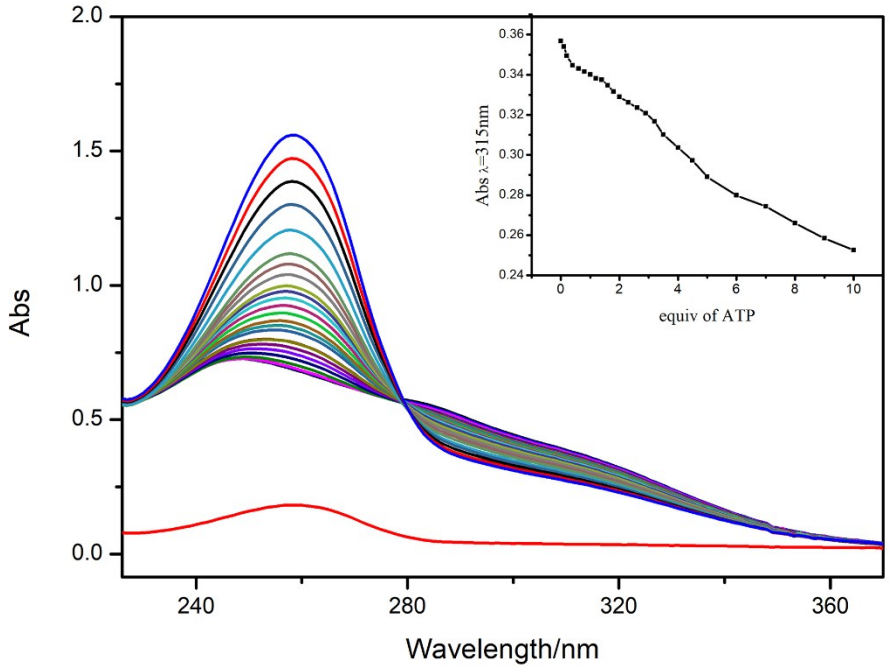

Figure S88. UV-vis absorption of **2**•4Cl$^-$ (10μmol) in phosphate buffer (pH = 7.4) upon addition of ATP. The inset shows a plot of absorbance intensity at 315 nm versus the equiv. of ATP.

View Article Online
DOI: 10.1039/C9CC00599D

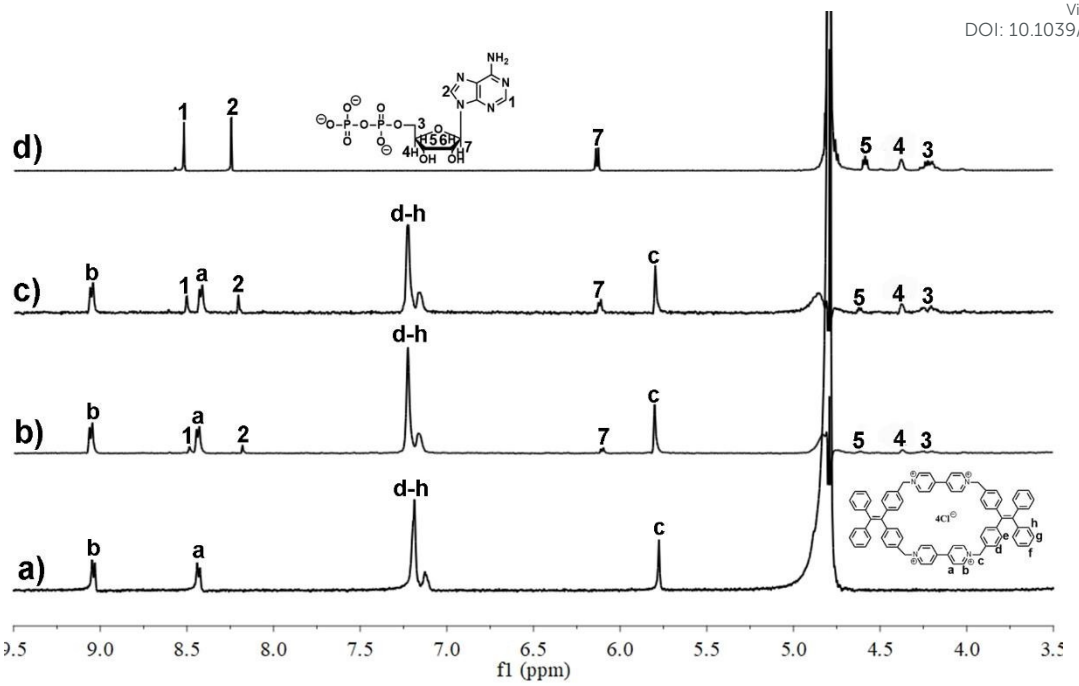

Figure S89. ^{1}H NMR spectra (400MHz, D_2O, phosphate buffer, pH=7.4): a) **2**•4Cl$^-$ (0.1 mM); b) **2**•4Cl$^-$ and ADP (0.1 mM); c) **2**•4Cl$^-$ and ADP (0.2 mM); d) ADP (0.1 mM) at 298K.

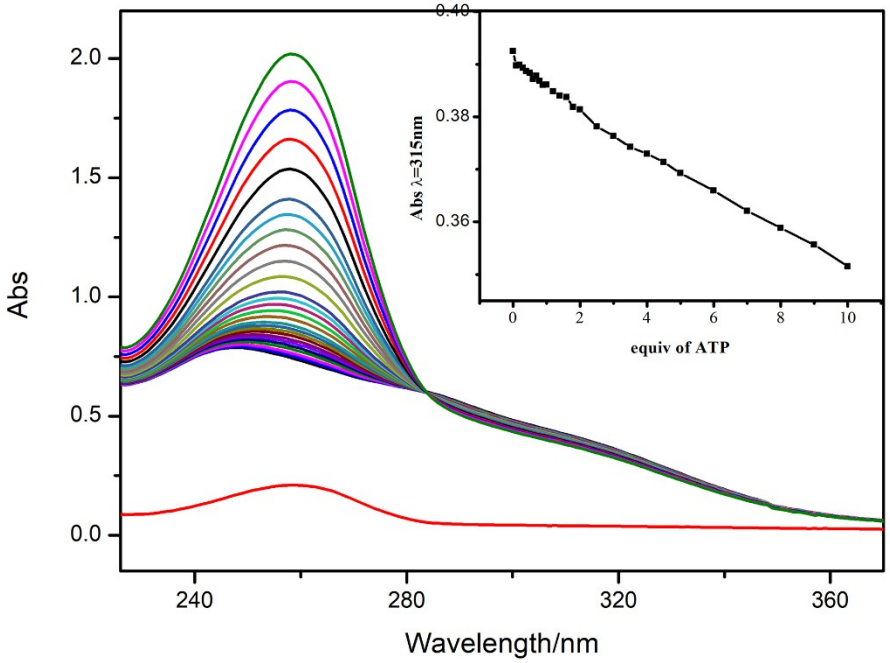

Figure S90. UV-vis absorption of **2**•4Cl$^-$ (10 μmol) in phosphate buffer (pH = 7.4) upon addition of ADP. The inset shows a plot of absorbance intensity at 315 nm versus the equiv. of ADP.

View Article Online
DOI: 10.1039/C9CC00599D

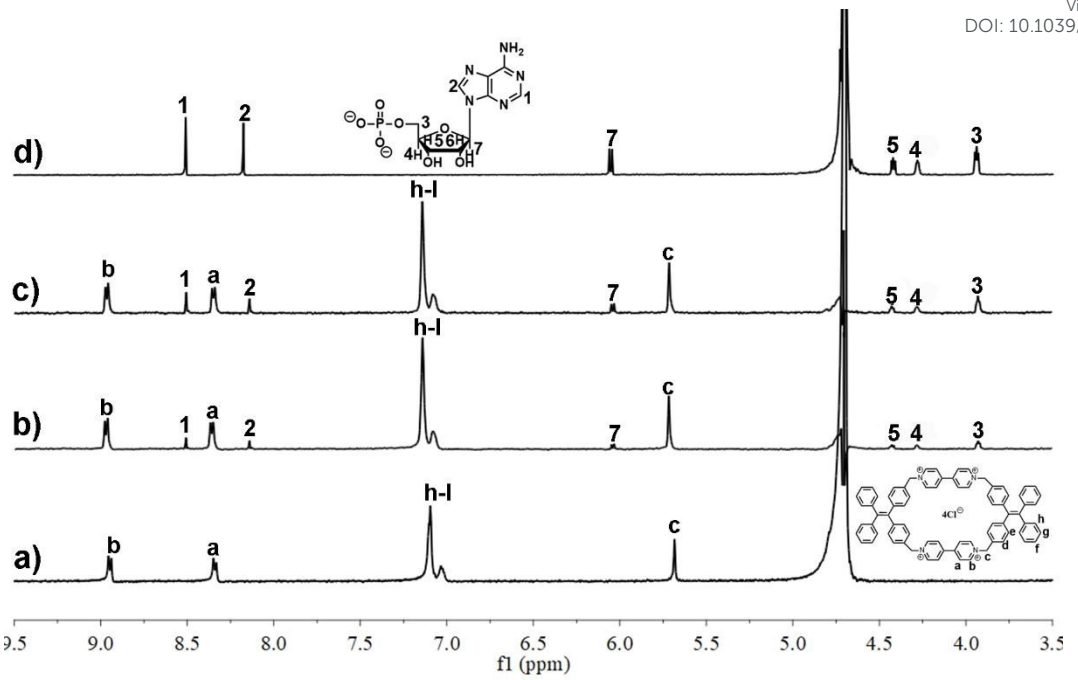

Figure S91. ^{1}H NMR spectra (400MHz, D_2O, phosphate buffer, pH=7.4): a) **2**•4Cl$^-$ (0.1 mM); b) **2**•4Cl$^-$ and AMP (0.1 mM); c) **2**•4Cl$^-$ and AMP (0.2 mM); d) AMP (0.1 mM) at 298K.

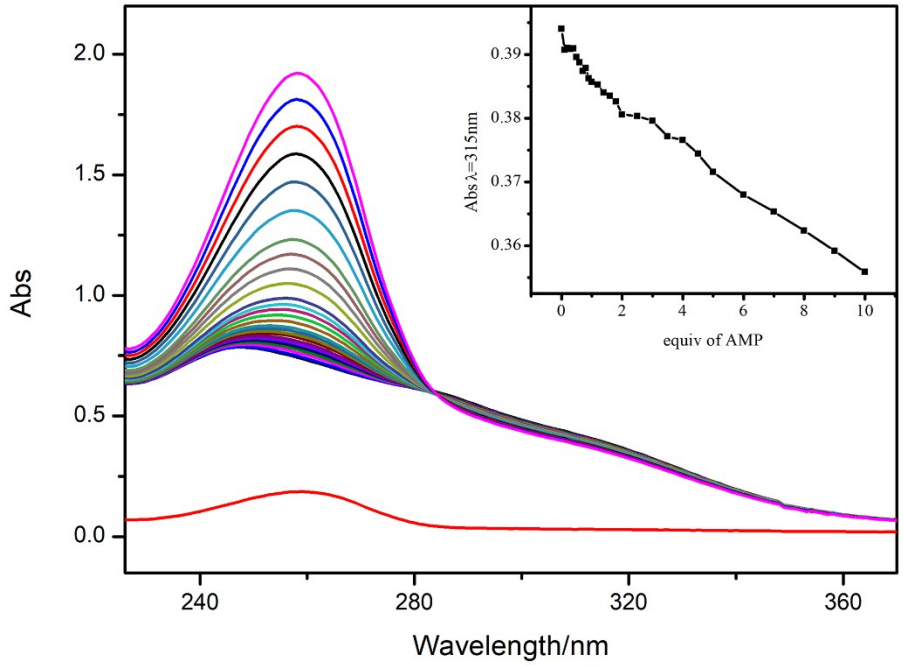

Figure S92. UV-vis absorption of **2**•4Cl$^-$ (10 μmol) in phosphate buffer (pH = 7.4) upon addition of AMP. The inset shows a plot of absorbance intensity at 315 nm versus the equiv. of AMP.